A PROGRESSION OF BUMPS IN THE LIGHT CURVES OF POPULATION II CEPHEIDS.

BY

SEAN P. A. LAWRENCE.

A Thesis Presented for the Degree of Master of Science at the University of St. Andrews.

January, 1985.

ABSTRACT

The published data of thirteen short-period population II Cepheid variable stars has been Fourier analysed to provide periods of pulsation for the stars. Light curves have been constructed and the possibility of the presence of a Hertzsprung progression in these stars has been investigated. Two approaches have been used. The first was a subjective discussion and the second an objective one. Both methods have indicated that a Hertzsprung progression does exist and the period of transition of bumps from descending to ascending branch has been found to be between 1.6 - 1.7 days.

A selection of published models have also been analysed using identical methods and good agreement has been found between theory and observation, a period of transition of bumps again occurring at a period of between 1.6 - 1.7 days for the models. A grid of linear models has also been constructed.

All Fourier analysis has been done using a harmonic analysis program written by the author and documented in this thesis.

I would like to dedicate this thesis to my parents, without whose help, I could never have even begun it.

DECLARATION

I hereby declare that the following Thesis is the result of work carried out by me, that the Thesis is my own composition, and that it has not previously been presented for a Higher Degree. The research was carried out at the University Observatory, St. Andrews.

Sean P.A. Lawrence.

CERTIFICATE.

I hereby certify that Sean P.A. Lawrence has spent four terms of research work in the University Observatory, St. Andrews, that he has fulfilled the conditions of Ordinance No. 51 (St. Andrews), and that he has qualified to submit the accompanying thesis in application for the Degree of Master of Science.

T.R. Carson.

ACKNOWLEDGEMENTS

I would like to thank my supervisor Dr. T.R. Carson, for his constant help, interest and valuable advice and Professor D.W.N. Stibbs, for assisting me in a supervisory capacity during my first term at the University Observatory. I would also like to thank Professor Stibbs for making the facilities at the University Observatory available to me.

Thanks are due to John Worrell, for allowing me to use his linear pulsation code, Ian Skillen, for valuable discussions and advice, and all the staff and research students at the University Observatory.

Last, but definitely not least, I would like to thank Veronica, for helping me to type this thesis, and for her immense help and support throughout, especially in the latter stages of writing.

CONTENTS

CHAPTER 1.

INTRODUCTION

In recent years, much work, both theoretical and observational, has been done on population I or classical Cepheids. Reviews of the literature show that these stars are young population I objects, yellow supergiants residing in the plane of the Galaxy. In comparison to this work, little has been done on the population II counterparts to the classical Cepheids; the W Virginis stars (periods 6 to about 50 days) and BL Herculis variables (periods 1 to 3 days). This work intends to give a theoretical account of the latter class of pulsating star, with particular emphasis being placed on the structure and shape of their light curves.

Chapter 2 gives a brief review of BL Herculis stars, describing their evolutionary status and properties. In chapter 3, we discuss the 613 UBV observations of Kwee and Diethelm (1984, hereafter KD). We then describe the light curves which have been constructed using these observations. Finally, there is a discussion of the Hertzsprung

progression and its possible existence in the stars of this survey.

Chapter 4 consists of two parts. The first is a summary of Fourier analysis, beginning with elementary ideas and continuing with a discussion of Fourier transforms and their application to discrete, non-equally spaced data. Fourier analysis provides us with very useful techniques for studying light variations in astronomy, whether it is the intrinsic variation in pulsating stars, or the extrinsic variations of eclipsing binary systems.

Not only does the theory allow us to model light curves of these stars using well-defined mathematical techniques, but it also enables us to find periods of pulsation of our stars.

The second part of chapter 4 involves a discussion of a harmonic analysis and period determination program written by the author. In brief, this involves fitting an Nth order Fourier series to the data of KD and finding the periods of the stars using a power spectrum and Fouriergram.

Recently, the analysis of Simon and Lee (1981) has indicated that the Fourier amplitudes and phases are related to the movement of bumps in the Hertzsprung progression and Gieren (1982) suggests that the parameter φ_{21}, in the notation of Simon and Lee, could also be of importance in determining the mode of pulsation of the single-mode Cepheids. The techniques of Simon and Lee also allow us to compare theoretical, non-linear models directly with the observed stars.

Chapter 5, therefore, contains a detailed discussion of the techniques of Simon and Lee and their application to the stars in KD. The results for our type II variables are then compared with similar results for classical Cepheids, which have been published by Simon and Lee. Finally in Chapter 5, we discuss the techniques as applied to the models of Carson and Stothers (1982, hereafter RCRS) and compare these with the observed stars.

Chapter 6 contains a summary of this thesis, conclusions and suggestions for further work in this field, some of which might give further insight into many of the problems which have been discussed in previous chapters.

There are four appendices, the first of which is a brief review of linear models which have been computed by the author, the second and third contain light curves of the observed stars of KD and the models of RCRS, respectively, and the fourth appendix contains the harmonic analysis program mentioned earlier.

CHAPTER 2.

EVOLUTIONARY STATUS AND PROPERTIES OF POPULATION II CEPHEIDS.

(2.1) Evolutionary Status.

Since the discovery of δ Cephei in 1784 by Goodricke, a great number of intrinsic variable stars have been discovered- over 25000 in our galaxy alone. In the first half of this century, the class of variable stars known as pulsating variables were broadly grouped into two subsets - the RR Lyrae variables and the classical Cepheids, these being further divided into the δ Cephei type stars and the W Virginis variables, the latter originally being thought of as a special case of the former, the difference being merely in the shape of the light curves.

At the 1952 International Astronomical Union Conference, however, Baade (1952) suggested that this classification scheme was in error and the W Virginis variables, previously thought of as being population I objects, were actually population II stars and at a very different evolutionary stage to the classical Cepheids. The

implications of this discovery on the distances of galaxies have been well discussed in the literature, and will not be gone into here (see, for example, Struve and Zeberg; 1962).

The classical Cepheids are known to be yellow supergiants, pulsating with periods between one and eighty days. Their progenitors are high mass stars which have exhausted their hydrogen-burning core and have reached the helium-core burning stage of stellar evolution. Because of their high mass, they do not undergo a helium flash, but enter the Cepheid instability strip after looping to the left from the supergiant region of the HR diagram, with the onset of core-helium burning.

By contrast with these population I Cepheids, the population II variables (or type II Cepheids as they are also called) are thought to have evolved from low to medium mass stars and to understand their evolutionary status, it will be necessary to briefly describe the properties of the red giant stars, since it is these which may ultimately become population II Cepheids.

Red giants are evolved stars which have moved upwards and to the right of the main sequence in the HR diagram. They have a degenerate helium core surrounded by a partially-degenerate helium shell and a shell of hydrogen-burning gas. This is all encompassed by a cool and very tenuous envelope of hydrogen, comprising about nine-tenths of the stellar radius. The degenerate core gradually contracts and the temperature rises. Eventually, it will become so hot that it can no longer remain degenerate and helium burning will begin. This stage of stellar evolution is associated with the explosive release of energy known as a helium flash.

By investigating the post red giant evolution of a grid of models with masses $0.65 \lesssim M/M_{\odot} \lesssim 1.0$, Schwarzschild and Härm (1970) have shown that certain stars will move rapidly to the left in the HR diagram and onto the horizontal branch (HB). It was known from previous calculations that a series of helium flashes occur in red giant stars due to the transition from core helium burning to helium shell burning (Schwarzschild and Härm, 1965; Weigert, 1966). Schwarzschild and Härm (1970) found, as did former investigators, that the majority of stars remained in the

red-giant branch; however, two of the model stars left the giant branch soon after one of the flashes and described a loop to the left and well into the Cepheid instability strip, each loop lasting about 10^3 years. They showed that about two flashes (and hence two loops) occur for each of these two stars about every 2×10^5 years. These calculations placed a reasonable fraction of a percent of red giants in the instability strip on their second time up the red-giant branch, this fraction being in good agreement with observation.

Later calculations by Kraft (1972) supported the theory of Schwarzschild and Harm and showed that not only will some stars evolve blueward towards the horizontal branch due to helium flashes on the giant branch, but also indicated that there were, in fact two types of population II Cepheids. He distinguishes between the "above the horizontal branch" (AHB) stars and the longer period "loop" Cepheids. Thus, the problem of the status of population II variables was carried even further, with the difficulty of distinguishing between AHB and "loop" Cepheids. Kraft suggested that the AHB objects are post-horizontal branch stars, being fed from the blue end of the HB by stars on their way to the

asymptotic giant branch, and are temporarily passing through the Cepheid instability strip.

Demers and Harris (1974) continue from Kraft with a discussion of "loop" Cepheids, suggesting that these are, in fact, W Virginis variables, and are post-AGB stars, having looped into the instability strip due to a series of helium flashes. Theories of stellar evolution indicate that the W Virginis stars are on their way to the white dwarf region of the HR diagram and the final stages of evolution. The AHB stars, on the other hand, are the BL Herculis stars and, as suggested by Kraft, are post-horizontal branch and are burning helium in their cores. Strength is added to this view, when Demers and Harris plot a colour-magnitude diagram (fig. 2.1) for a list of observed population II variables.

They find that there is a distinct separation into two groups. The first group contains variables with periods less than three days, lying below the second group, but above the horizontal branch. The second group, on the other hand, have periods greater than six days. They call the former group BL Herculis variables, and the latter the W Virginis stars. This argument is in good agreement with earlier comments by Kraft (1972), who suggested that a

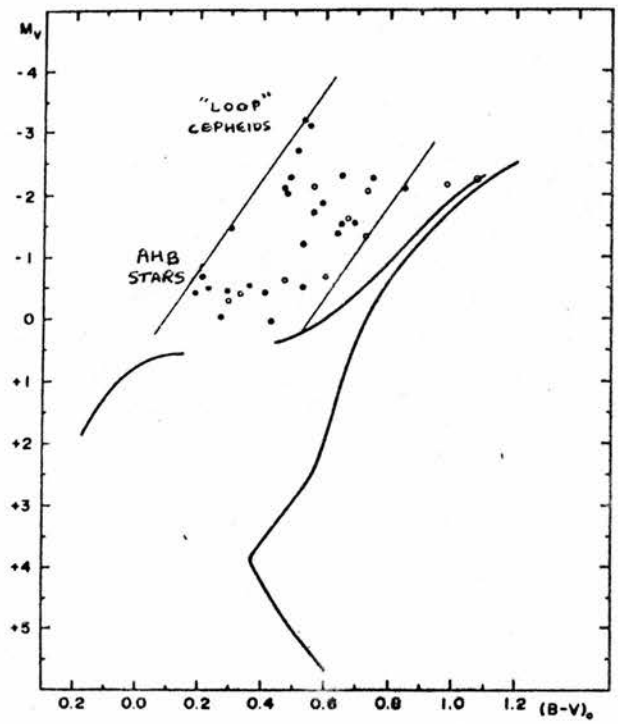

Fig. 2.1: Colour magnitude diagram for population II Cepheids. Field variables are denoted by open circles and cluster variables by dots.
(Figure 1 of Demers and Harris, 1974)

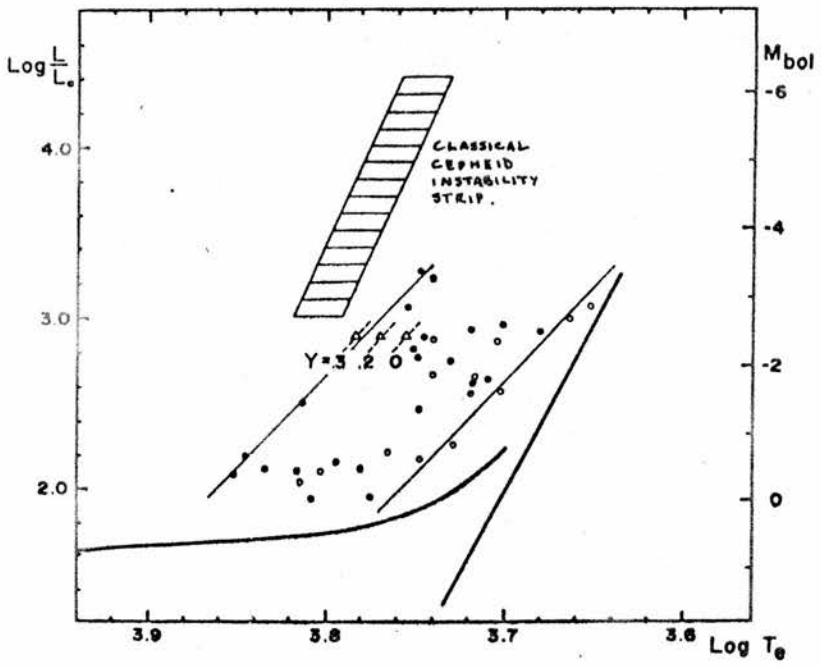

Fig. 2.2: Theoretical HR diagram for population II Cepheids. Blue edges are shown for theoretical models using three helium abundances.
(Figure 2 of Demers and Harris, 1974)

change in the galactic abundance of AHB stars occurs at around four days, where the numbers drop considerably. At periods greater than about seven days, the AHB stars become very scarce and the "loop" Cepheids increase in numbers. These comments are confirmed by Sweigart and Gross (1976) and Smith et al. (1978), who suggest that there are few, if any, BL Herculis stars with periods greater than about six days, and few, if any, W Virginis variables with periods less than six days. Smith et al. take $0.9 \leqslant P \leqslant 3.0$ days for all BL Herculis stars.

Since this thesis is concerned with population II variables with periods between one and three days, it may be concluded that it is only BL Herculis stars which are of interest here and their properties will be discussed below.

(2.2) Properties of the Type II Cepheids.

(2.2.1) Masses.

The range of masses of population II variables were originally constrained by evolution theory. It has been known for some time that if a star is to evolve onto the

horizontal branch, its mass must be less than $0.8M_{\odot}$; otherwise, the star will remain on the red giant branch, until it moves into the white-dwarf region of the HR diagram (Iben, 1972). A reduction of mass will make the star move blueward and, in fact, if $M \lesssim 0.5M_{\odot}$, the star will not return to the red giant branch at all (Gingold, 1976; Sweigart and Gross, 1976) and hence will not enter the instability strip.

The evolution of a star onto the horizontal branch depends mainly on its mass and chemical composition. For fixed core mass and lower total mass, the evolution on the giant branch is more rapid and the motion in the HR diagram will be further blueward towards the helium-burning main sequence than for a star of higher mass. CSV state that if our current theories of stellar evolution are correct, then the masses must certainly be constrained within the bounds of $0.4 \lesssim M/M_{\odot} \lesssim 0.8$, the lower limit representing the possible mass of the helium-burning core in stars about to undergo the helium flash, and the upper limit the mass of stars at the main-sequence turn-off in globular clusters. Petersen (1981) examined the bump masses of BL Herculis variables and concluded that all BL Herculis stars have

practically the same mass ($\sim 0.5M_{\odot}$), although his analysis is somewhat simplified.

More recent investigators seem to confirm this view. For example, Hodson, Cox and King (1982, hereafter HCK) have computed models using two masses of $0.75M_{\odot}$ and $0.55M_{\odot}$, whilst Wallerstein and Cox (1984) use theoretical masses of between $0.5M_{\odot}$ and $0.75M_{\odot}$ for normal population II stars.

This brief review of literature seems to indicate that the masses can be confined to $0.5 \leqslant M/M_{\odot} \leqslant 0.8$ and the models which are discussed in appendix 1 will have masses in this range.

(2.2.2)Temperatures and Luminosities.

Due to the distances of the type II Cepheids from the solar neighbourhood and their relatively low apparent magnitudes as compared to, for example, the classical Cepheids, they have not been well observed, and little photometric or spectroscopic data exists. For this reason, the temperatures and luminosities are generally determined from a theoretical instability strip, although a notable example of observed red and blue edges comes from Demers and

Harris (1974), who located population II variables on a colour-magnitude (C-M) diagram to determine if an instability strip could be defined. Using the tables of Bohm-Vitense (1973) they were able to transform the (M_v,B-V) values into a (M_{Bol},logT_e) plane and so plot a theoretical HR diagram (fig. 2.2). They find for their instability strip that luminosity is related to temperature by equations (2.1) and (2.2):

$$\text{Log}L/L_\odot = -10.75\ \text{Log}T_e + 43.5 \quad \text{(blue edge)} \ldots\ldots\ldots (2.1)$$

$$\text{Log}L/L_\odot = -10.75\ \text{Log}T_e + 42.4 \quad \text{(red edge)} \ldots\ldots\ldots (2.2)$$

Thus, by fixing the temperatures, we may find a range for the luminosities of BL Herculis variables.

CSV choose $5300 \leqslant T_e \leqslant 6500$ on the basis of measurements of $\langle T_e \rangle$ by Smith et al. (1978), whilst HCK construct models using $5800 \leqslant T_e \leqslant 6600$. Wallerstein and Cox (1984), on the other hand, give $4800 \leqslant T_e \leqslant 6300$ for population II globular cluster variables. However, the lower limit does take into account RR Lyrae variables and RV Tauri stars, the latter of which have a lower red edge than BL Herculis variables. In

their theoretical HR diagram (fig. 2.3; fig. 1 of above reference), the BL Herculis variables lie in the temperature range $5700\ K \leqslant T_e \leqslant 6500\ K$, with luminosities $100 \leqslant L/L_\odot \leqslant 350$. These values of luminosity are in agreement with those chosen by CSV and HCK, the latter of whom choose $75 \leqslant L/L_\odot \leqslant 350$.

It would appear on the basis of the above discussion that we may certainly take upper limits on the temperature and luminosity of $T_e = 6500\ K$ and $L/L_\odot = 350$. The lower limits, however, are slightly more difficult to establish, due largely to the problem of determining the red edge of the BL Herculis instability strip. This difficulty arises due to the fact that at lower temperatures convection in the stellar envelope becomes much more important as a mechanism for energy transport. Baker and Kippenhahn (1965) have described how stellar convection can terminate pulsation and the relation between convection and the red edge of the instability strip has been discussed by Bohm-Vitense and Nelson (1976). A little more recently, Deupree (1977) found that the convective heat flux is greatest at around maximum compression (minimum stellar radius) of the convective regions, these existing, in particular, close to the helium

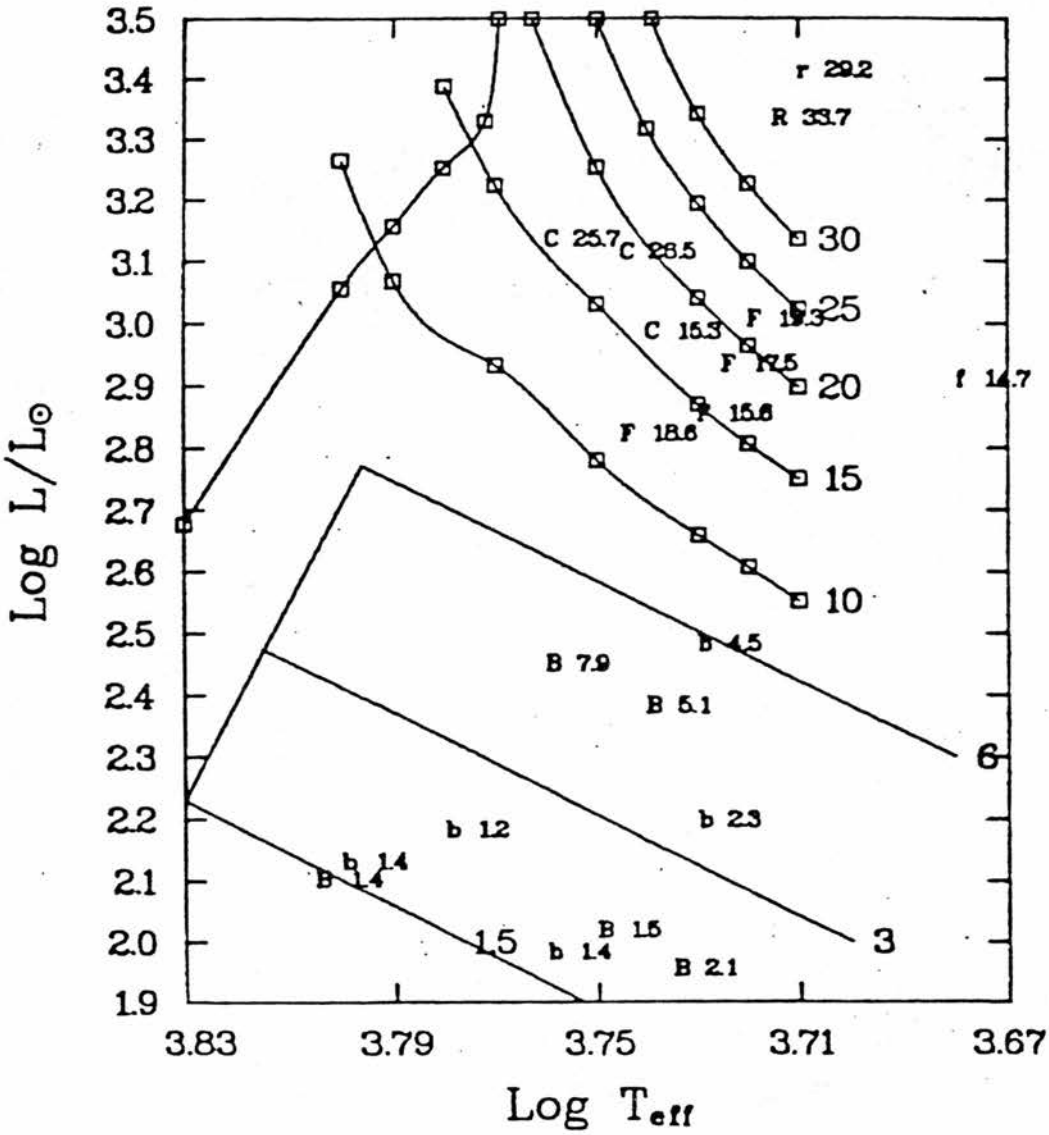

Fig. 2.3: HR diagram for globular cluster Cepheids. BL Herculis stars are denoted by b or B and the periods are shown alongside. Also, lines of equal period are shown.

(Figure 1 of Wallerstein and Cox, 1984)

and hydrogen ionisation zones. The energy which has been 'dammed up' by the operation of the γ and κ mechanisms will then be allowed to leak out due to this convective zone. According to Deupree, only a small amount of convection is required to effectively throttle pulsations on the red side of the instability strip. Unfortunately, no reasonable theories of stellar convection exist, although Stellingwerf (1982a,b; 1983a,b) seems to have produced a more or less reasonable theory for convection in RR Lyrae stars.

According to the above literature search, it would seem reasonable to take the low temperature edge of the BL Herculis instability strip to be somewhere between 5300 K and 5800 K. We will thus take an average of T =5500 K as the lowest temperature. Using these upper and lower limits of $5500\ K \leqslant T_e \leqslant 6500\ K$ for temperature, equations (2.1) and (2.2) give $150 \leqslant L/L_\odot \leqslant 324$, in good agreement with the values used by other authors, and we will therefore take $100 \leqslant L/L_\odot \leqslant 350$.

(2.2.3) Compositions.

The chemical compositions of the stars may be deduced through a variety of ways. The usual technique is to make measurements of the stellar spectra; however, because of the relatively low luminosities of BL Herculis stars, this is a fairly difficult task, and many workers in the field prefer to use theoretical means, such as plotting the evolutionary tracks for various compositions, and finding which one is likely to enter the BL Herculis region of the HR diagram. A third method involves fitting a blue-edge to the BL Herculis instability strip, again for various compositions, and comparing this to the observed blue-edge (for example, Demers and Harris, 1974).

Whichever method is used, however, it does seem to have been agreed that helium abundances must be in the range $Y = 0.2 - 0.3$. CSV infer that $0.25 \leqslant Y \leqslant 0.50$, if a comparison of the observed blue-edge in the HR diagram is made. A comparison of bump masses and pulsation masses, on the other hand, yields $Y = 0.31 \pm 0.08$ i.e. $0.23 \leqslant Y \leqslant 0.39$. This result is in good agreement with evolutionary and spectroscopic helium abundances.

Kraft (1972) suggests that only high helium content stars ($Y \sim 0.3$) can cross the instability strip. Demers and Harris (1972) and Cox and Tabor (1976) agree with this statement when they take $Y = 0.30$ and $Y = 0.29$ respectively.

In a discussion of Z (heavy element) content, CSV state that Z is unimportant as a determination of the phase of secondary bumps in theoretical light and velocity curves, since putting $Z = 0$ in the models gives similar results to those which one obtains if one chooses $Z = 0.005$. Other authors take various Z abundances, where on the whole $Z \simeq 0.005$ (for instance HCK; Carson and Stothers, 1982).

Compositions are of course important when one discusses opacities. Carson (1976), for example, has constructed tables for various abundances. Y is always equal to 0.25 and Z has the values 0.0, 0.005, 0.01 and 0.02. It is the second of these which has been chosen by the author of this thesis as a representative of the heavy element abundances in BL Herculis stars and in appendix 1, we will use an interpolated opacity table, constructed by Worrell (1984a) from a table of Carson opacities found in CSV, with chemical composition $(X,Y,Z) = (0.745, 0.25, 0.005)$.

We have so far discussed the evolutionary status and properties of the short period, population II variables (BL Herculis stars, with periods between one and three days). Later we will present a set of linear models which have been computed using these properties, but first we must discuss both qualitatively and quantitatively, the light curves of a selection of observed BL Herculis stars.

CHAPTER 3

THE LIGHT CURVES.

(3.1) Observational Data.

Much of the work of this thesis is based on the photometric observations of KD. Kwee obtained 613 UBV observations of a selection of pulsating variables between 1972 and 1973 at ESO, La Silla, Chile, the observing program containing fifteen population II variable stars with periods between one and three days. Most of the stars are rather faint, with magnitudes ranging from $11^{m}.5$ in maximum to $15^{m}.5$ in minimum.

The observations were reduced using the methods of Kwee and Braun (1967) and for four of the stars (VZ Aql, V465 Oph, V527 Sgr and V839 Sgr) the data was supplemented with the 1967 observations of Kwee and Braun. The periods for this earlier data were determined graphically by Kwee (1967), although the method used has not been given explicitly. It is assumed that a similar method is used by KD for the present data. Light curves of the data have been plotted; however, two of the stars (V477 Oph and RT Tra)

have been discarded from this study due to poor coverage of their light curves.

The stars are classified by KD according to the scheme devised by Diethelm (1983). The method depends on the shape of the light curve alone, rather than the evolutionary considerations of the previous sections. Whereas we have seen that the period domain of one to three days should be occupied by only BL Herculis variables, Diethelm suggests that one finds a variety of pulsating variables here. He states that a visual survey of 28 variable stars in our Galaxy with periods in this range leads to a distinction of four types of pulsating star (figs. 3.1-3.4).

The main points which Diethelm discusses in his scheme are as follows:

(a) The RR Lyrae variables (RRd)

(i) The light curves in V are smooth and exhibit only a small bump just before the ascending branch.

(ii) The rise to maximum light is steep.

(iii) The (B-V)-(U-B) two-colour diagrams result in a

Fig. 3.1: A selection of RRd type light curves in V magnitude.
(Figure 1 of Diethelm, 1983)

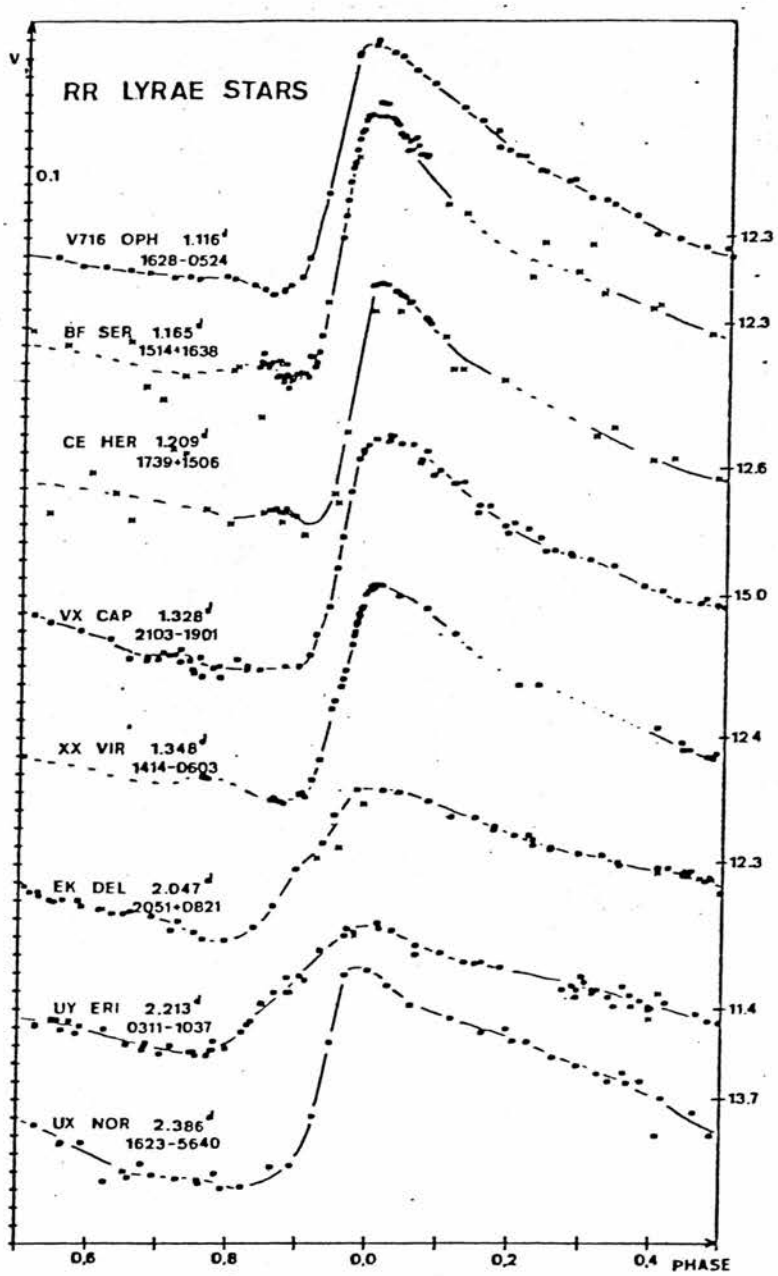

Fig. 3.2: CW type light curves in V magnitude.
(Figure 2 of Diethelm, 1983)

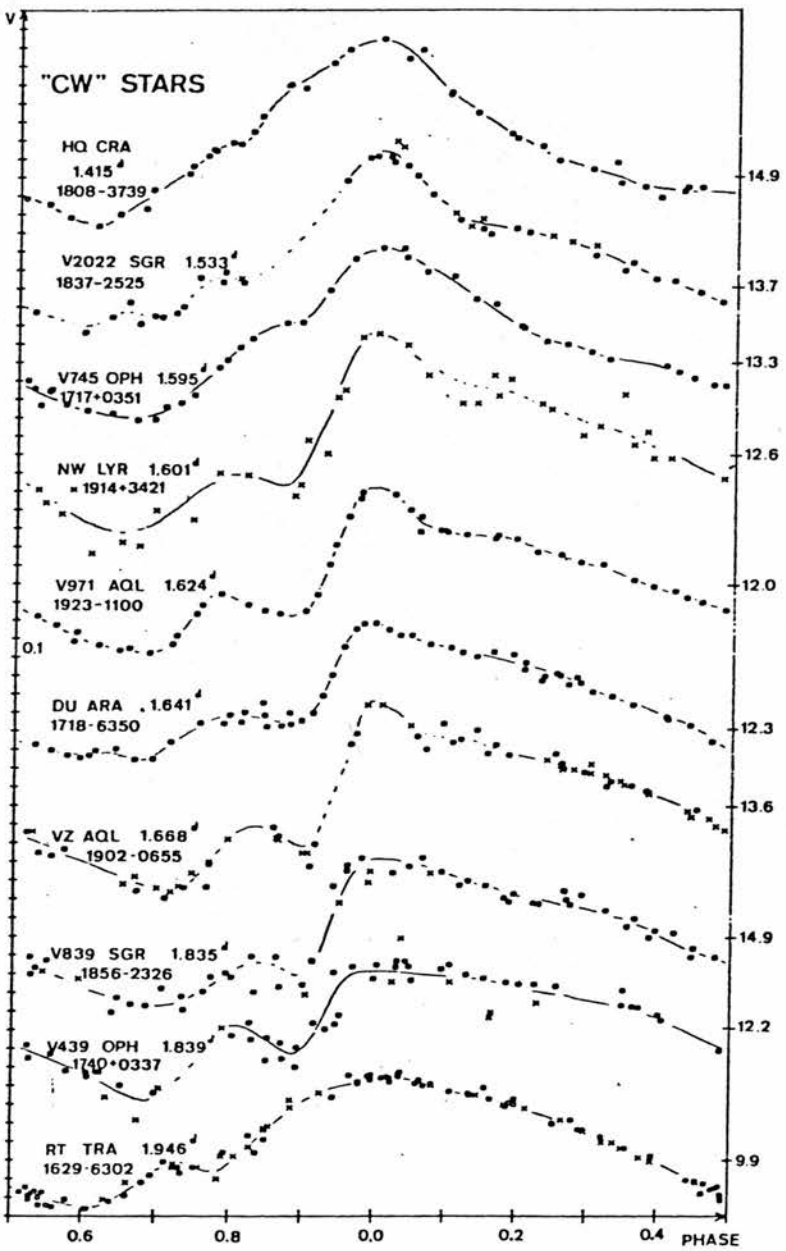

characteristic "figure-eight" loop.

This last criterion is, according to Diethelm, the most important factor in distinguishing RR Lyrae variables and it is only this type of star which exhibits this feature.

(b) W Virginis stars (CW)

(i) There is a pronounced hump on the ascending branch 0.2 periods before maximum light.

(ii) CW variables show a close correlation between V, (B-V) and (U-B) light curves, whereas RRd do not.

(iii) The pre-rise hump is broader at short wavebands.

(c) BL Herculis stars (BL).

(i) There is a hump on the descending branch 0.3 periods after maximum light. Using this as a criterion, 5 BL Herculis stars were found out of the sample of 28.

(ii) The rise times lie between $0^m.15$ to $0^m.3$, with a tendency to decrease with increasing period.

Fig. 3.3: BL type light curves.
(Figure 3 of Diethelm, 1983)

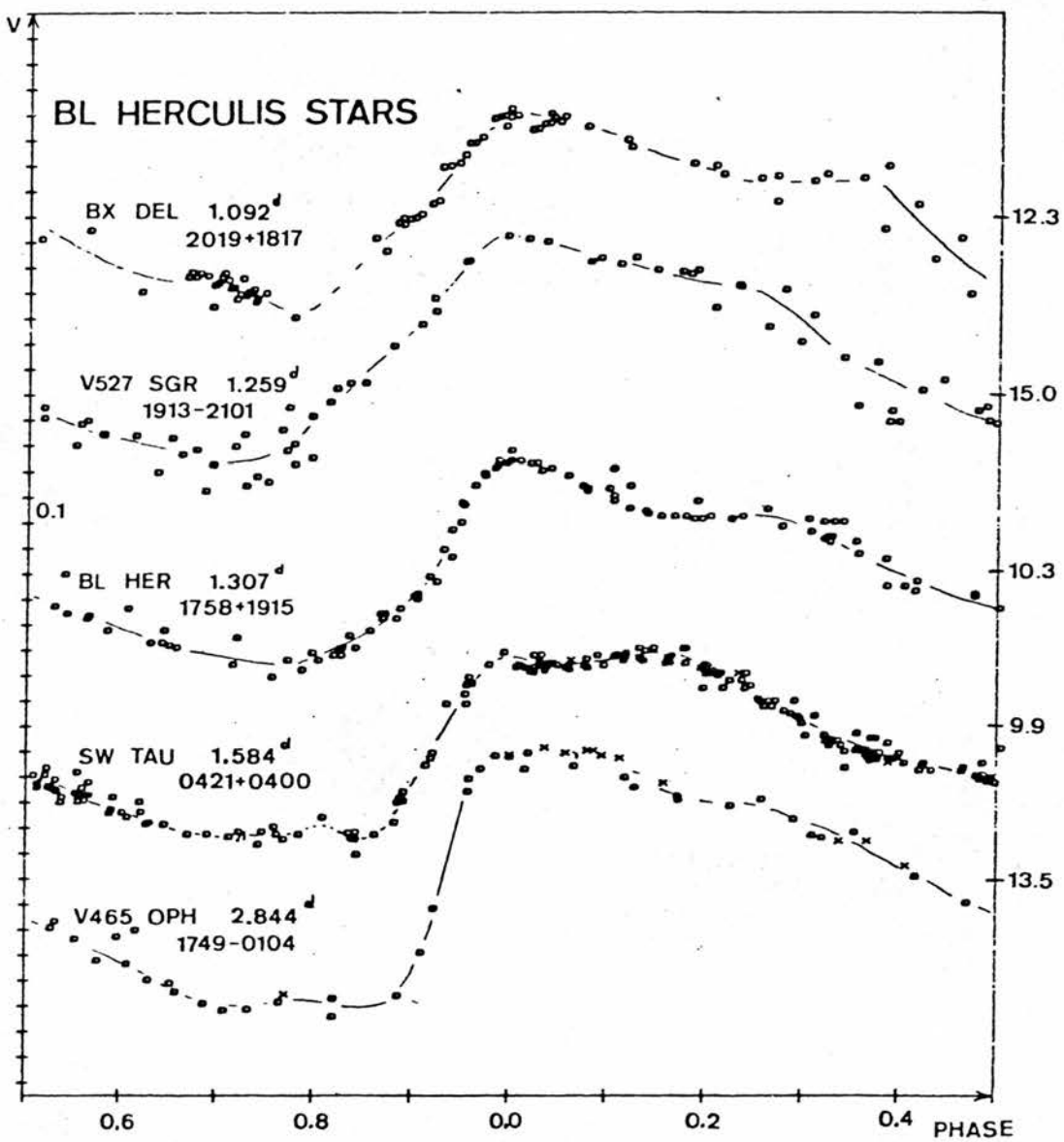

Fig. 3.4: Cδ type light curves.
(Figure 4 of Diethelm, 1983)

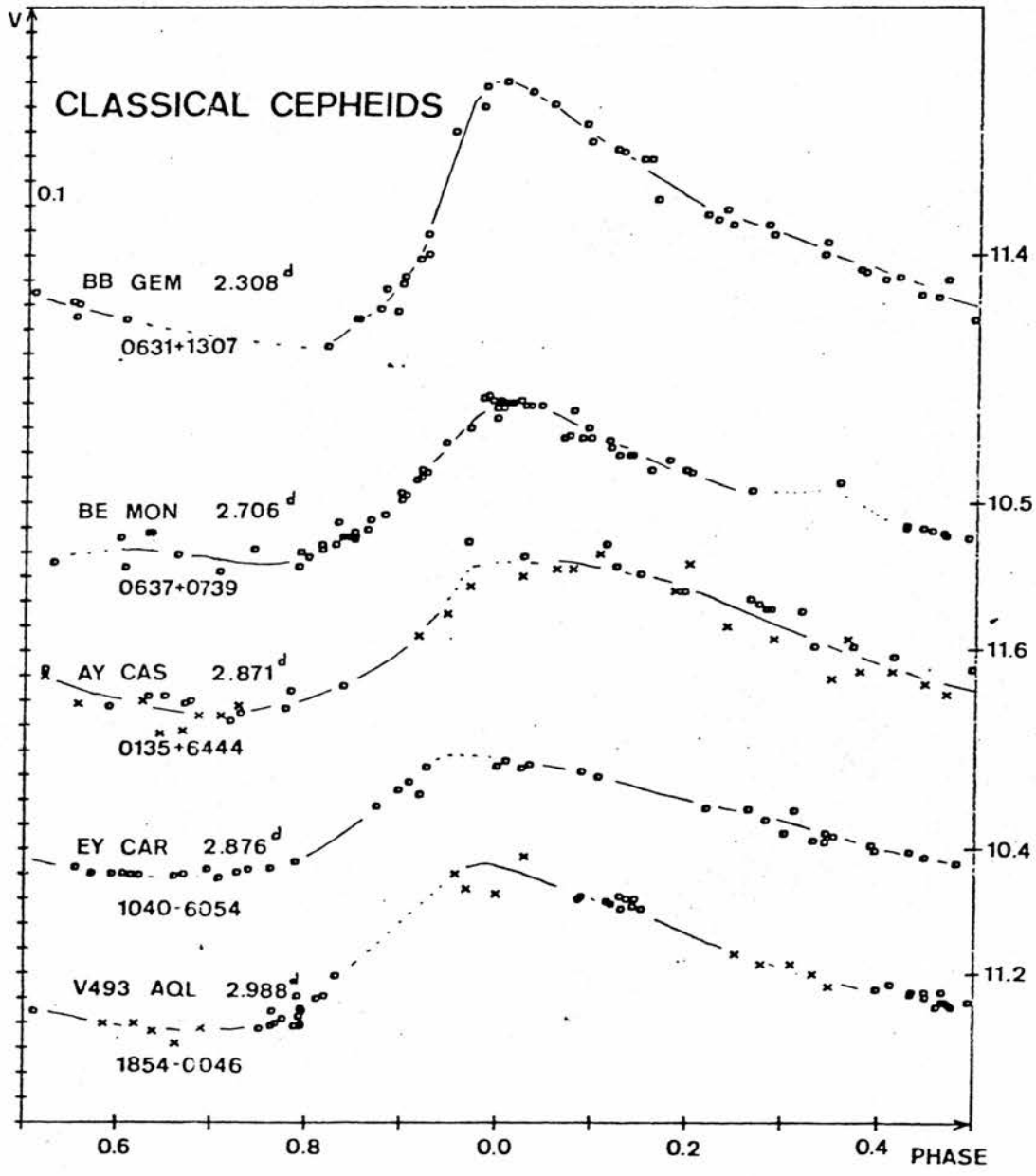

(d) Classical Cepheids ($C\delta$)

(i) These show a very smooth variation with a gradual rise to maximum light.

Diethelm also suggests that the period domain of the RRd variables ends at around 2.5 days and that there exists a clear-cut separation between population II stars and RR Lyrae variables. With regard to BL Herculis and W Virginis stars he states that:

1) Population II Cepheids (presumably incorporating both CW- and BL-type objects) with periods below three days show similar light curve differences as W Virginis variables of longer periods.

2) Both BL Herculis and W Virginis stars in the Magellanic Clouds follow the same P-L relation, namely $\langle M_v \rangle = -1.3 \log P + k$, in good agreement with that found by Demers and Harris (1974).

3) At the same period, $C\delta$ stars in the SMC are brighter by $0^m.5$ than BL Herculis and W Virginis variables.

In addition to the above remarks, we can perhaps make the following comments. Firstly with respect to RRd stars (or those stars which have RRd type light curves), it is certainly true that the peaks of the light curves are sharp and possibly a major feature of these stars, but this peak becomes very much broader at longer periods, with an increase in rise-time. For EK Del, in fact, we have a curve which is reminiscent of the CW star HQ Cra, although Diethelm does consider the extra aspect of the two-colour diagrams, and it is these which give added weight to placing some stars in the RRd class.

We may similarly compare some of the BL and CW stars in Diethelm's survey. For example, V839 Sgr has a large scatter of points before the ascending branch, making it difficult to determine whether a pre-rise bump is present or not. The descending branch also has a relatively large scatter of points with a very slow fall to minimum light. This light curve is very similar in these respects to the BL star V527 Sgr, which according to Diethelm has a hump on the descending branch, but not on the ascending branch (fig. 3.3), even though the scatter is between $0^m.2$ and $0^m.3$ in both cases.

The problem thus remains that it is very difficult to classify population II variables purely on the basis of their light curves and, in the rest of this work, all stars with periods between one and three days will be called BL Herculis stars according to the discussion in chapter 2, whatever the shape of their light curve.

In the following section, therefore, the abbreviations RRd, CW and BL will refer to the type of light curve and not to the class of star involved.

(3.2) Description of the Light Curves

KD have used their periods and data to construct light curves for each of the fifteen stars in their survey. Light curves and periods have also been computed by the writer using an independent harmonic analysis and graphics code, to be described in chapter 4. The data is least-squares fitted by a Fourier series and further information on the techniques used may also be found in chapter 4. The curves of the latter will be referred to as those of SPL and are shown in appendix 2 (figs. A2.1 - A2.13). It should be noted that, generally there is negligible difference between

the light curves of SPL and KD, this being due to the fact that the periods agree quite well, and often to the third decimal place, this probably being the limit of accuracy which can be achieved with this data. The light curves of SPL only are published here and readers are referred to KD for the light curves of these authors.

All of the light curves have been centred with maximum light at phase 0.5 and fits computed for each. The observations are denoted by crosses (+), whilst the fit is a continuous curve passing through these points. In each case, the order has been chosen by looking at several fits of different orders and choosing what is hopefully the best one. This method is purely subjective and one author may not necessarily agree with another as to which is the best fit.

The criteria chosen in this case are as follows:

1) First and foremost, the fit should look pleasing to the eye, passing through the observed points as neatly as possible. Particular emphasis is laid on the maximum light and any bumps or shoulders which may be present. In some cases, the fit will not, under any circumstances, pass

through the observed maximum, and may involve artificial bumps which are properties of the fit (see, in particular, UX Nor and VX Cap).

2) The order of fit should be as low as possible. If there is doubt between two particular fits, it is always the one of lower order which is chosen. This will then eliminate any false "wobbles" in the fit.

3) The standard deviation of fit should be small. In the stars in this survey, standard deviations range from 0.025 to 0.085 (table 6.1).

Regarding figs. A2.1 - A2.13, the period of pulsation is shown in the top left-hand corner, and opposite is the epoch, calculated from equation (3.1).

$$\text{Epoch} = (\text{Phase}_{max} - 0.5)P \qquad (3.1)$$

with P = period

Phase_{max} = phase at maximum light before centring at phase 0.5.

The light curves of each star will now be discussed, with the description referring to the diagrams of both SPL and KD. The stars appear in order of increasing period.

1) V716 Oph

This light curve has been designated as RRd by Diethelm and according to this scheme is a typical member of its class. It has a narrow peak following a quick rise to maximum and a slow fall to minimum. Just preceding minimum light is a small bump with amplitude about $0^m.1$.

2) V527 Sgr

The very large scatter of points ($\approx 0^m.3$) makes a fit to this data very difficult. A hump at a phase of about 0.65 appears on the descending branch, but it is difficult to assess whether this is due to the poor data or not. A

particularly striking feature is the bump at phase 0.95 and it is possible that this could be a bump in the Hertzsprung progression to be discussed in sections (3.3) and (3.4). This bump is not discernable in Diethelm's paper although a fit is not published here.

3) VX Cap

The fit in this curve is not well defined with several bumps appearing on the descending branch. It is likely that this is due to poor data in this region. Just before the steep rise to maximum light, there appear two bumps and again these could again be due to poor data or a property of the analysis used in producing the fit. However, because the amplitudes of these bumps are greater than those in the descending branch ($\approx 0^m.08$ as compared to $0^m.05$ on the descending branch), we can perhaps assume that they are a property of the actual star.

4) HQ Cra

Again there is a little spread of data, especially on the descending branch. When considering this light curve, there are two points to take into account: the first is that the spread of points could be a property of the light

variation in the star, and not due to poor photometry, in which case, there is a definite bump at phase ~0.8. The second point is that the fit does not account for all of the nuances of the variation of the data, in particular, the obvious bump at 0.25.

This star is a fairly typical example of those stars classified as CW by Diethelm, with a broad peak and bump on the ascending branch.

5) V2022 Sgr

Again a typical example of a CW light curve. The main features are a shoulder on the descending branch, and a shock bump on the ascending branch at phase 0.3.

6) V745 Oph

This curve is similar to that of HQ Cra, this time with the hump apparently appearing at phase 0.65 and again what is assumed to be a shock bump at phase 0.3.

7) V971 Aql

CSV suggest that a large bump on the ascending branch of their models indicates that the bump is due to the Hertzsprung progression having passed through maximum light and interacting with the stationary shock wave which is normally present at about phase 0.25 before maximum. However, this does not seem to be the case in the light curve of V971 Aql.

Although we have a very large amplitude bump on the rising light, there is still a hump on the descending branch and we see later that this feature should pass through the maximum at a period of between 1.66-1.8 days, as opposed to the 1.62 day period of this star.

8) DU Ara

Again there are problems with the fit, making it difficult to distinguish between bumps which are real, and those which are properties of the fit. There is certainly a second peak at phase 0.3, and possibly also at phase 0.6-0.7 on the descending branch.

An interesting feature in this light curve is that it bears a distinct resemblance to that of V971 Aql and the periods are comparable. There is a fairly sharp peak, falling off to form a bump on the descending branch, being at approximately the same phase in both light curves. There is then a slow decline of light and a gradual rise to the shock bump at phase 0.3. The major difference between the two curves would appear to be the fact that the descending branch of DU Ara seems to be less steep than that of V971 Aql, with the result that the second bump appears closer to the maximum.

9) VZ Aql

The bump again appears on the descending branch; however, the data is not good enough to distinguish exactly where the bump lies.

A feature of the last three light curves which should be commented on is that the maximum peak at phase 0.5 becomes very much broader with increasing period. At 1.62 days, it is sharp and well-defined, but as the period increases through to 1.66 days (VZ Aql), the peak becomes very broad, and the shoulder almost becomes part of it, as

the descending branch becomes less steep. It is proposed that this is due to a Hertzsprung progression in these stars, and is discussed further in section (3.4).

10) V839 Sgr

There is a great deal of spread again in the data, giving a series of false humps on the descending branch. It is possible that there may be no hump at all (see, for, example, the light curve of Diethelm in fig. 3.2); however, if there are, we cannot decide at what phases they should be.

11) EK Del

The hump now appears at the bottom of the descending branch and no shock bump is evident. The data is fairly good and the fit smooth.

12) UX Nor

Looking at the data only, it would seem that there should be a smooth curve from phase 0.5 to about 0.8, with a bump between 0.8 and 0.9; however, the fit is not a good one and picks up bumps at phase 0.65, 0.9, 0.2 and 0.35. The peak is not fitted as well as might be expected and

at about phase 0.6, the data is left altogether by the fit. This problem is discussed further in chapter 4 and could be related to the so-called Gibbs Phenomenon in Fourier analysis.

13) V465 Oph

The final star to be discussed has a light curve of type BL and, apparently, has a shoulder at about phase 0.7 with a shock at 0.3, although again this could be a characteristic of using too high an order of fit.

The main features to look for in the light curves then, are:

1) A post-maximum bump, which may be part of the Hertzsprung progression of phase of bumps with period.

2) A shock wave, producing a stationary bump on, or immediately preceding, the ascending branch.

Not to be confused with the bump in the true Hertzsprung progression are such features as in 2) above, and also stationary shoulders which sometimes occur at about phase 0.2 after maximum and are particularly evident in CW-

type light curves.

(3.3) Bumps in the Light Curves of Population II Cepheids.

(3.3.1) The Hertzsprung Progression.

The bump progression in classical Cepheids has been well discussed in the literature and was discovered by Hertzsprung (1926). We find that the secondary bumps in the light curves of these population I variables follow a definite trend with period. The bump first seems to appear at periods of around six days and, as the period increases, it climbs up the descending branch. At a period of about ten days, it merges with the maximum light, producing a broad, symmetric light curve. The bump then crosses over to the ascending branch and, at periods greater than about sixteen days, disappears altogether.

Stobie (1973) suggests that the only other stars to show such a progression should be the short period population II variables (BL Herculis objects with periods between 1 and 3 days) and was possibly the first to demonstrate that such a progression might exist.

Thereafter, much theoretical work has been done. CSV, for example, studied models of these stars using the Carson opacities and they pointed out the correlation between π_2/π_0 and bump phase, comparable to that found by Simon and his co-workers. A similar analysis by RCRS on field variables indicates that a progression of bumps in their models does exist and a resonance (interaction of bump with maximum light) seems to occur at around 1.6 days. This value is in close agreement with the results of HCK, who centre the progression between 1.5-1.7 days, i.e. the transition of bump from descending branch to ascending branch occurs near this period. King, Cox and Hodson (1981) suggest that observationally, for periods $\lesssim$ 1.65d, the bump ought to appear either on the descending branch or be absent altogether. As will be discussed later, this statement agrees with some of the conclusions of this thesis, in that it implies that a transition occurs at a period greater than 1.65 days.

Petersen (1984), however, disagrees with this point. By studying the light curve of the BL Herculis variable KZ Centauri and, on the basis of Fourier methods, he places the resonance at about 1.52 days. One basis for this conclusion

is that the light curve appears to be symmetric about maximum light, although the variable V2022 Sgr in the survey of KD, with a slightly different period of 1.53 days, is clearly not symmetric, whereas V745 Oph (period 1.596 days) is possibly more so.

Much work has been done in the past in an attempt to explain the origin of this secondary bump in Cepheid light curves. It is, however, the velocity curves which are generally studied, since these are dynamically more fundamental than the light curves.

Christy (1968) attempted to explain the bumps by means of a wave echoing from the central core and reaching the surface as a secondary bump. He begins by producing a series of models in order to understand the origin of these bumps. Fig. 3.5 (reproduced from fig. 15 of Christy) shows the velocity curves of each zone of a forty-two zone model during almost two periods. The velocity scale has been shifted progressively upwards in order to display the results.

Several interpretations of this diagram are possible. The one which Christy favoured was that a large acceleration begins in the helium ionisation zone (zone 32 in fig. 3.5) at about phase 0.9. A pressure wave is then sent inwards, producing the inward (negative) velocity which reaches the core (zone 2) at phase 0.45. Upon reaching the core, this wave is reflected outwards with a positive velocity at phase 0.55, with an additional pulse at phase 0.85. The former of these propagates out to the surface where it produces a secondary bump at phase 0.45. Thus, the secondary bump is an echo of a pulse produced at the helium ionisation zone 1.4 periods earlier.

The mechanism for the production of the pulse in the He^+ zone is still unclear; however, it has been found that the bumps are associated with an increase in opacity, thus causing a pressure excess in the region of pulse production. According to Whitney (1983), this could be a local phenomenon caused by rapid absorption of radiant energy or variations in the degree of ionisation, or it may be a non-local effect caused by the descent of overlying layers of gas.

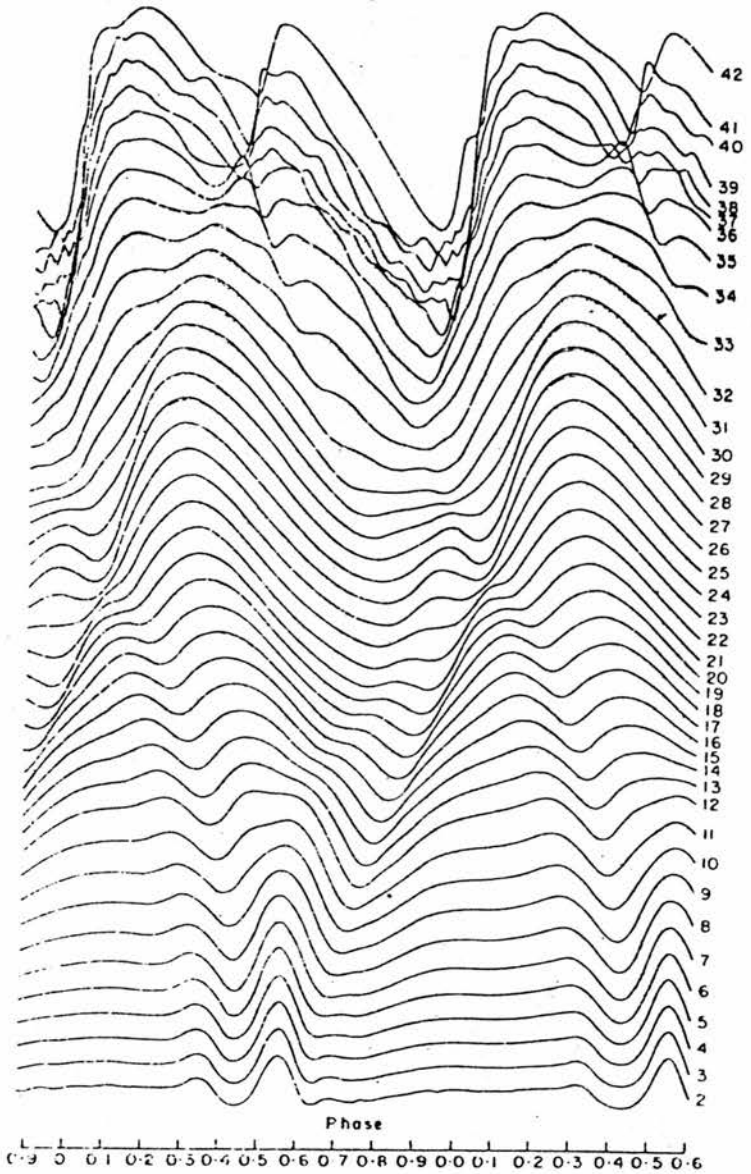

Fig. 3.5: Velocity curves for each zone of a 42 zone model, with zeros progressively shifted upwards to display the results.
(Figure 15 of Christy, 1968)

An alternative point of view to Christy's echo for the production of the secondary bump in our light and velocity curves lies in the resonance theory of Simon and Schmidt (1976) and Simon (1977). Using elementary mechanics, Simon considers the star to have a set of natural pulsation periods π_i, i=0,...,m and a set of driving frequencies P_o, $2P_o$,...,nP_o. A star with a linearly unstable mode of pulsation, with period π_o say (corresponding to the fundamental mode) will have as its driving frequencies the set $1/\pi_o(\equiv P_o)$ and its harmonics $1/2\pi_o$, $1/3\pi_o$, etc. ($\equiv 1/2P_o$, $1/3P_o$,...). If it happens that the frequency of one of the harmonics is close to that of a normal mode (i.e. a natural frequency), $1/\pi_1$ say, then the oscillation will be enhanced at the frequency of the harmonic in question. In the case of the driving force being the fundamental mode and the normal mode being the second overtone, we will have at resonance, $\pi_2/\pi_o \approx 0.5$, and as π_2/π_o decreases (increases), the bump decreases (increases) in phase from maximum light.

The literature is divided between these two views. King, Cox and Hodson (1981), for example, appeal to the overtone resonance theory of Simon and Schmidt (1976) and theoretical models do show a progression of bumps when the

ratios of the second overtone to the fundamental mode are close to this resonance of 0.5. (Stobie 1969a,b; HCK). The calculations of King, Cox and Hodson strengthen the resonance hypothesis, whereas the Christy echo is only weakly supported. On the other hand, CSV subscribe to the echo phenomenon for the origin of the bumps, having come to this conclusion by studying the velocity curves of population II globular cluster Cepheids.

There are, however, problems with each of the above two viewpoints of the presence of secondary bumps. Christy's "echo" phenomenon cannot explain why the bump is apparent in some models but not others. The theory does, however, associate a physical mechanism with the bump, which is not so in the resonance theory of Simon, who suggests that the two systems may work together to produce a bump mechanism.

Whitney (1983) has attempted to do this when he interprets fig. 3.5 in an alternative way to that described earlier. It is suggested that a pressure excess near layer 23 produces two pulse trains shortly before maximum velocity. There is an outward-travelling pulse and an inward-moving one. The outward pulse will arrive at the

surface, where it reflects with a change in sign and passes through its origin. The inward pulse will reflect off the core and meet the reflected, outgoing wave.

Suppose now that the inward and outward pulses meet when the new cycle is generating its next set of pulses (again shortly before maximum velocity). If this is to happen, the time of travel from their origin to when the two pulses meet must equal the fundamental period of pulsation of the star.

Not only must this condition in time be achieved, but we must also have a spatial condition for a resonance to occur. That is, the pulses must be produced at an appropriate depth in the star and we presume that this will be at an antinode of an overtone if interference between pulses is to be constructive. If this is so, the pulses of finite frequency width will have components which originate and meet at a point which is related to a particular overtone and only these components will remain, constructively interfering with the next set of pulses, all others being damped out.

The echo will thus be in resonance with a certain eigenmode and appear near to the maximum light or velocity in our curves. This gives the appearance of a resonance between the driving mode (fundamental) and the eigenmode with which the pulse is resonating. Hence, the appearance of Simon's resonance $\pi_1/\pi_0 \approx 0.5$. If the above "resonance" conditions are not satisfied but the pulses meet slightly away from our antinode, then the bump will occur away from the maximum light.

Whitney was able to show heuristically at least by modelling the pulses using acoustic waves that the $\pi_1/\pi_0=0.5$ resonance is selected because it permits precise repetition from one cycle to the next, rather than leading to beats. A star with such a resonance would also have an "echo pulse" period equal to the pulsation period, thus satisfying the temporal-spatial conditions defined earlier. It is the spatial condition which selects the excited overtone, whilst the temporal condition acts to choose the appropriate polytropic index, which was found to be n=2.5.

(3.3.2) Shock Bumps.

In general, the bump of the echo/resonance effect just described, is most prominent on the descending branch of the population II Cepheids. However, in several stars, an additional high amplitude feature appears on the rising light and this is particularly prominent in the light curves of V971 Aql and DU Ara (figs. A2.8 and A2.9). This feature can also be found in the models of CSV, who suggest that it could be caused by a temporary dip in light just before the rise to maximum, due to rapid ionisation and subsequent increases in opacity of the atmospheric hydrogen, caused by a shock front. CSV also suggest that this bump only occurs if the amplitude of the light variation is large and the log of the equilibrium temperature is greater than about 3.78. Bridger (1983) also states that this bump is a shock phenomenon which seems to be a reflection of the Christy echo wave which travelled inwards after being reflected off the surface at maximum velocity.

In any case, this "shock bump" probably makes no contribution to the Hertzsprung progression of bumps as discussed in this section, and except for appearing later, in table 3.1, will be largely ignored.

Having discussed the methods of production of bumps, we will go on to decide qualitatively in the next section if there is a Hertzsprung progression in the stars we have so far studied.

(3.4) Hertzsprung Progression in Observed Stars: a Qualitative View.

We have seen in section (3.2) that many of our light curves contain various secondary bumps and shoulders. We have also discovered that the bumps in the light curves of BL Herculis variables appear to follow a Hertzsprung progression in the theoretical models and possible mechanisms for production of these bumps have been commented upon. We are now ready to discuss whether a similar progression occurs in the light curves which have been constructed from the data of KD.

The phases of the bumps have been determined from a quadratic fit to the data around the bump of form $y(x_i) = ax_i + bx_i + c$ (where $y(x_i)$ represents the magnitude at phase x_i, and a, b and c are constants), and then finding

the maximum of this fit. There are of course errors in this method, the foremost of which is possibly the fact that it is difficult, if not impossible in some cases, to decide which of the many bumps in the light curves are bumps in the Hertzsprung progression; indeed, it is a controversial point whether such a bump exists at all. The representation of the bump in the light curves by a parabola is also a major source of error.

The method for determining where the true bumps are in the light curve is as follows: initially, the star of lowest period is studied, this is V716 Oph, with period 1.115 days. The light curve for this star is very smooth compared to some of the others and the fit is good. The bump is prominent at phase 0.79 after maximum. If a progression of bumps does exist in these stars, then the next bump should be visible at phase <0.79. This is indeed the case in VX Cap, where the bump appears at ≈ 0.71 after maximum. In this way, all the stars are studied to determine if a prominent bump appears at the expected place on the light curve, and only in two cases (V527 Sgr and V839 Sgr) is there a problem in detecting a bump and this may be due to poor data.

Once the bump has been located in this way, the points which make up the bump are least squares fitted by a quadratic, as described earlier, and the phase of that particular bump found. Table 3.1 gives these estimated phases. The third column denotes the phase φ_b after maximum of the "echo" or "resonance" bump, and the fourth column indicates the phase φ_s after maximum of the "shock" bump, which should pay no contribution to the Hertzsprung progression, as described in section (3.3). The final column indicates under EBUMP, where on the light curve the "echo" bump can be found. D indicates that the bump appears on the descending branch, whilst XD indicates that it appears on the descending branch, but one cycle of pulsation ahead of the bump labelled by D.

Also, in table 3.1, NB indicates that the relevant bump was either not present in the light curve, or the data was too poor to register it . The question mark in the fourth column indicates that VZ Aql is expected to show a shock bump, but that region of the light curve in which the shock ought to appear had too few data points to allow a reasonable determination of its phase.

table 3.1: Phases of Bumps in the Light Curves of SPL.

STAR	PERIOD	φ_b	φ_s	EBUMP
V716 Oph	1.1159	0.79	NB	D
V527 Sgr	1.2589	NB	NB	-
VX Cap	1.3276	0.71	NB	D
HQ Cra	1.4150	0.48	NB	D
V2022 Sgr	1.5335	0.37	NB	D
V745 Oph	1.5955	0.33	0.82	D
V971 Aql	1.6245	0.19	0.80	D
DU Ara	1.6405	0.19	0.83	D
VZ Aql	1.6653	0.14	?	D
V839 Sgr	1.8272	NB	NB	-
EK Del	2.0467	0.72	NB	XD
UX Nor	2.3858	0.60	NB	XD
V465 Oph	2.8417	0.55	NB	XD

We must now decide on the basis of the foregoing sections and the results of table 3.1 if a bump progression in the light curve does exist. Perhaps we can tentatively put forward the argument that we know that bumps appear in the light curves and, if the bump is chosen discriminately

for each star, we can see a very clear progression. However, in doing this, we are almost "willing" the progression to appear. This is not a good argument, and certainly not sound scientifically! There are so many bumps and shoulders visible in the curves that it is easy to pick out definite features, most of which are probably due to poor photometry, these stars being so faint ($V \approx 12^{m}.5$ typically) that observations accurate to better than about $0^{m}.02$ are not generally possible.

Table 3.1 does seem to indicate that a progression exists, however, and if we cautiously assume that this is true, then at what period can we expect its centre to be? The answer to this question also lies in a qualitative description of the light curves. Petersen (1984) determines this resonance centre on the basis of a symmetry about maximum light, whereas, Carson (1984) suggests that upon passing through the progression centre, the bump interacts with the stationary shock feature, producing the large "ascending branch bump" prominent in several of the stars of our sample (V971 Aql, DU Ara, VZ Aql) and this would indicate that the resonance occurs at around 1.6 days (V745 Oph) in agreement with the theoretical models of RCRS.

However, perhaps the most useful qualitative identification of the progression centre is to determine where the bump merges with the maximum light. It would appear that the bump is still climbing the descending branch at 1.66 days (VZ Aql) and we may thus assume that the resonance lies at a period greater than this, but possibly at a period less than about 1.83 days (V839 Sgr), although the data at this period is too poor to determine whether the bump has crossed over to the ascending branch or not.

On this evidence, we can possibly put the limits of $1.66 \leqslant P \leqslant 1.83$ on the period within which the progression centre lies. Further evidence for this is given by the fact that the light curve of VZ Aql appears to be fairly symmetric, as expected. However, it should be pointed out that the light curve is not wholly symmetric, indicating that the resonance centre is being approached and is at a period greater than 1.66 days, i.e. VZ Aql is not in resonance but is approaching it.

In chapter 5, further evidence is given which supports these comments. First, however, we must consider in the following chapter the Fourier methods and the computer code used to produce the light curves and periods which have been

discussed in this chapter.

CHAPTER 4

FOURIER ANALYSIS AND COMPUTATIONAL TECHNIQUES.

(4.1) Fourier Analysis.

(4.1.1) Introduction

It should be obvious from the diagrams described in the previous chapter that the light curves of the stars in KD are not sinusoidal, i.e. they cannot be reconstructed mathematically using a pure sine or cosine wave. For this reason, we must employ Fourier analysis to fit theoretically the light variations using a judiciously selected mixture of sine and cosine terms. Not only are Fourier techniques useful for this purpose, but they may also be used to derive periods of pulsation for our stars.

Consider the set of photometric data consisting of observations m_{o_i}, taken at time t_i, of a star pulsating with period P and angular velocity $w=2\pi/P$. A theoretical Nth order Fourier fit to these magnitudes will then be given by

$$f(t_i) = \langle m \rangle + \sum_{n=1}^{N} \{C_n \cos(nwt_i) + S_n \sin(nwt_i)\} \qquad (4.1)$$

where the time average magnitude $\langle m \rangle$ and coefficients C_n and S_n are constants to be found.

An obvious method for finding these unknowns is by the method of least squares, in which we minimise the error between the theoretical and observed magnitudes, thus

$$\sigma^2 = \sum_{i=1}^{ND} \{f(t_i) - m_{o_i}\}^2 / (ND - 2N - 1) \qquad (4.2)$$

must be a minimum.

with ND=number of observations,

N=order of fit in equation (4.1).

Thus, we have the 2N+1 equations of constraint (4.3) to (4.5):

$$\frac{\partial \sigma^2}{\partial \langle m \rangle} = \sum_i \{\langle m \rangle + \sum_n [C_n \cos(nwt_i) + S_n \sin(nwt_i)] - m_{o_i}\} = 0 \qquad (4.3)$$

$$\frac{\partial \sigma^2}{\partial C_j} = \sum_i \{\langle m \rangle + \sum_n [C_n \cos(nwt_i) + S_n \sin(nwt_i)] - m_{o_i}\} \cos(jwt_i) = 0 \qquad (4.4)$$

$$\frac{\partial \sigma^2}{\partial S_j} = \sum_i \{\langle m \rangle + \sum_n [C_n \cos(nwt_i) + S_n \sin(nwt_i)] - m_{o_i}\} \sin(jwt_i) = 0 \qquad (4.5)$$

We therefore have to solve 2N+1 simultaneous equations for the constants <m>, S_n and C_n.

(4.1.2) The Gibbs Phenomenon.

One observes that the Fourier fit in the light curves of the previous chapter often oscillates between gaps in the data or overshoots the maximum light. This effect could be related to the so-called Gibbs Phenomenon in Fourier analysis. First described by Wilbraham in 1848, the phenomenon demonstrates how poorly a Fourier series converges in the vicinity of a jump discontinuity in the function f(x), which the series describes, at $x=x_o$.

Gibbs discussed the sawtooth function, described by

$$f(x) = \begin{cases} x - n & n \leqslant x < n+1 \\ 0 & x = n \end{cases} \qquad n = 0, 1, 2, \ldots$$

and found that if f(x) is represented by a truncated Fourier series, then the series approximation overshoots the actual value of the function at the discontinuity by about 9 % (fig. 4.1).

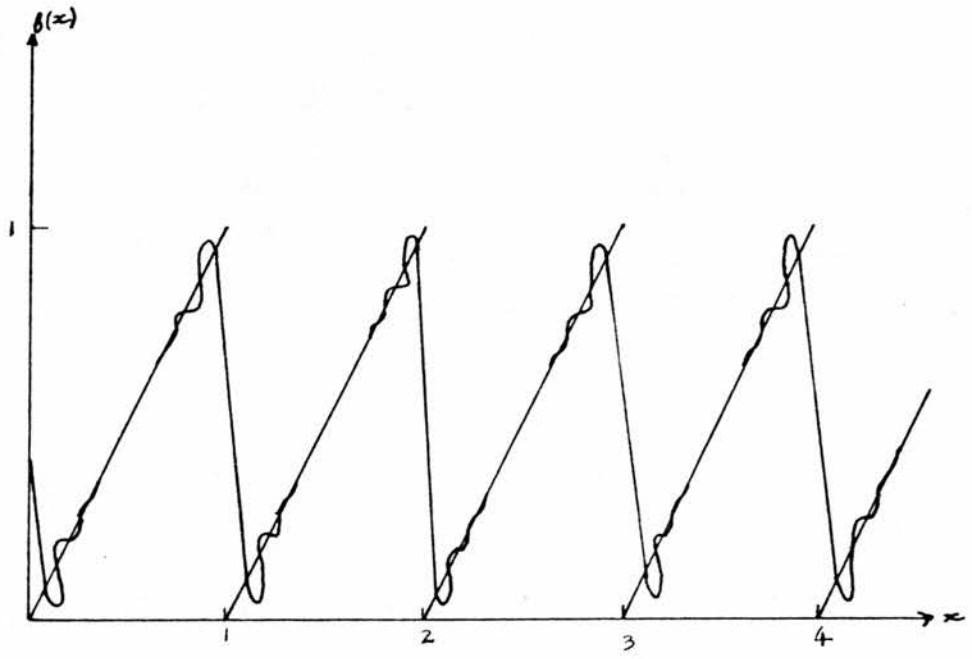

Fig. 4.1: Tenth order Fourier fit to the sawtooth function, demonstrating the Gibbs' Phenomenon.

In our analysis, we find that the Gibbs Phenomenon becomes important as the order of fit increases. As this happens, the light curves contain more "wobbles" as the fit oscillates between the gaps or "discontinuities" in the data, although these gaps may not be true, mathematical discontinuities.

Now, since the low-order amplitudes and phases change only minimally with increasing order of fit, the Gibbs phenomenon should have no effect on a quantitative description of the light curves. However, the qualitative examination of chapter 3 must suffer, and for this reason if no other, such a discussion of the light curves is extremely difficult, unless the data is very accurate and the light curves are well covered.

(4.1.3) Fourier Transforms.

Physically, we may think of a Fourier series as representing a set of harmonics $n\nu$, with $n = 1, 2, \ldots$ and if we assume that our actual oscillation or pulsation is made up of various contributions of some or all of these harmonics, then the series should give a reasonable description of that variation, whether it is the pulsation of variable stars and their associated light variations or the oscillation of a weight attached to a spring. Such an analysis will describe oscillations which are periodic, i.e. they repeat themselves faithfully after regular intervals of time.

A natural progression from this would be to study non-periodic variations in which the wave might never be repeated. An example of such a wave might be a single voltage pulse, or a flash of light. A variation of this sort can be thought of as being composed of an infinite number of harmonic contributions and is described by the temporal variable $F(\nu)$:

$$F(\nu) = \frac{1}{\pi}\left[\int_0^\infty A(\nu)\cos(2\pi\nu t)d\nu + \int_0^\infty B(\nu)\sin(2\pi\nu t)d\nu\right] \quad (4.6)$$

where $F(\nu)$ represents a continuum (spectrum) of frequencies and $A(\nu)$ and $B(\nu)$ are known as the Fourier sine and cosine transforms of $F(\nu)$ and determine the amplitudes of the sine and cosine contributions in the range ν to $\nu + d\nu$.

$A(\nu)$ and $B(\nu)$ are given by equations (4.7) and (4.8) respectively.

$$A(\nu) = \int_{-\infty}^{+\infty} f(t)\cos(2\pi\nu t)dt \quad (4.7)$$

$$B(\nu) = \int_{-\infty}^{+\infty} f(t)\sin(2\pi\nu t)dt \quad (4.8)$$

The Fourier transform of f(t) can be derived from these and is

$$F(\nu) = \int_{-\infty}^{+\infty} f(t) e^{i2\pi\nu t} dt \qquad (4.9)$$

which is equivalent to (4.6) and also represents a frequency continuum.

If we now return to a discussion of periodic pulsation (BL Herculis stars), we can see that the Fourier transform can have important implications; if the data is assumed to be continuous, then the transform in (4.9) will compute the relative importance of the frequencies in the range $-\infty < \nu < +\infty$. If the oscillation is periodic and a pure sine wave, then a frequency ν_o will be detected, since only in the vicinity of $\nu = \pm\nu_o$ will the transform be non-zero.

The above transform is approximated in the case of data which is finite by replacing the limits by T/2 and -T/2. We then compute the finite Fourier transform $F_F(\nu)$, defined as

$$F_F(\nu) = \int_{-T/2}^{+T/2} f(t) e^{i2\pi\nu t}\, dt \qquad (4.10)$$

In practice, the data can never be thought of as being infinite and rarely is it continuous. In addition, therefore, we define the discrete Fourier transform $F_D(\nu)$ as

$$F_D(\nu) = \sum_{k=1}^{ND} f(t_k) e^{i2\pi\nu t_k} \qquad (4.11)$$

and there is no restriction on the data spacing.

For multi-periodic phenomenon, the full Fourier transform $F(\nu)$ in equation (4.9) will consist of delta functions at $\pm\nu_1, \pm\nu_2, \ldots$, whereas the observed transforms $F_F(\nu)$ or $F_D(\nu)$ will differ from $F(\nu)$, and this difference can be described in terms of an interference effect between frequencies. In practice, two such effects are usually found and these are interference from:

(i) nearby frequencies

and (ii) distant frequencies.

(i) is important for data taken over a short period of time and is a product of the finite length of the data. The second effect is due to the data spacing and is called aliasing.

Aliasing occurs in its most extreme form when the data is equally spaced, whereas it is less prominent for unequally spaced data, indeed, for such data, it is not always possible to distinguish between effects (i) and (ii) above.

For determinate processes (i.e. processes for which we are able to predict what is next going to happen) the observed Fourier transform, $F_D(\nu)$ is the convolution of the true Fourier transform $F(\nu)$ with a spectral window $\delta_D(\nu)$ (Deeming,1975). Thus,

$$F_D(\nu) = F(\nu) * \delta_D(\nu) = \int_{-\infty}^{+\infty} F(\nu - \nu')\delta_D(\nu')d\nu' \qquad (4.12)$$

with

$$\delta_D(\nu) = \sum_{k=1}^{ND} e^{i 2\pi \nu t_k} \qquad (4.13)$$

The spectral window is an important indication of where the true and aliased frequencies lie, since a plot of $\delta_D(\nu)$ against ν will give a distribution which contains the times of all the observations. We may therefore define $\delta_D(\nu)$ as the Fourier transform of the distribution of the times of observation, depending only on these times. This can all be expressed in the statement by Deeming that the pathology of the data distribution is all contained in the spectral window.

Any set of astronomical observations will necessarily have a one year periodicity in its spacing, since data can only be collected when the sun is not too close in the sky. There will also be gaps at one synodic month due to lunar interference and at various other times when telescopes are not available. Such spacing in the data will represent a set of false frequencies ν_i, with the result that a set of subsidiary peaks (aliases) will appear in the spectral window at $\nu_i' = \nu_i + \nu_o$ and $\nu_i' = \nu_i - \nu_o$ due to an interference between ν_i and the true frequency ν_o. An example appears in fig. (4.2) (fig. 2 of Deeming, 1975) in which the spectral window of the quasi-stellar radio source 3C 345 is shown.

Here, we have a moderate peak at a frequency of $\sim 1\ yr^{-1}$, corresponding to the yearly spacing in the data, a smaller peak at 1 synodic month due to intervention by the moon and a much smaller peak at 1 calendar month, which is presumably when the telescope was not available.

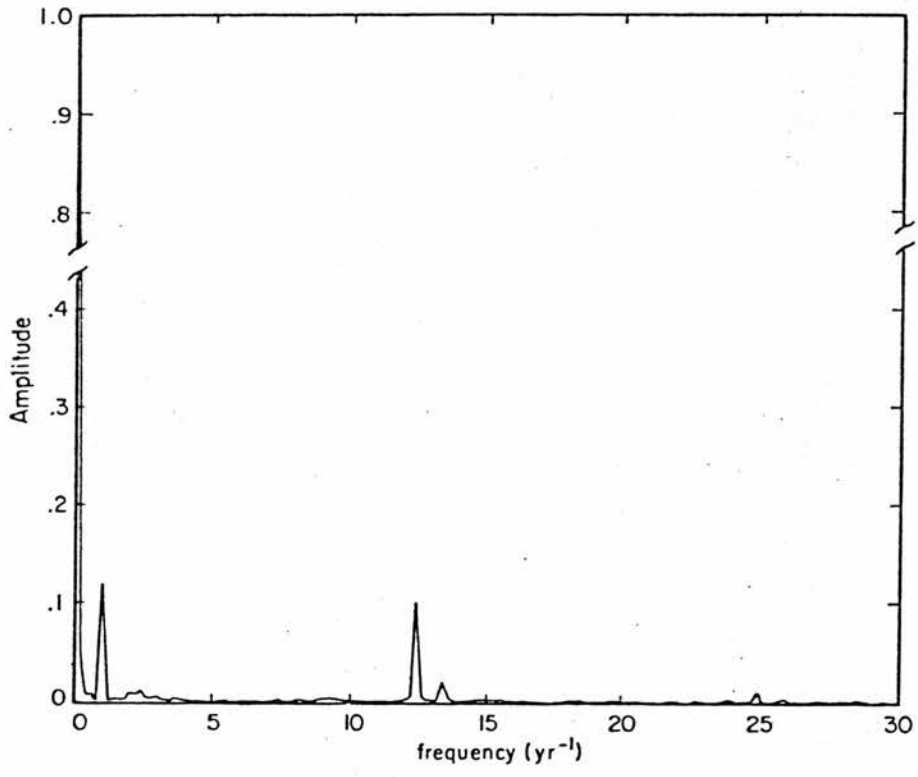

Fig. 4.2: Spectral window for observations of the quasar 3C345.
(Figure 2 of Deeming, 1975)

A major importance of calculating the spectral window lies in the fact that if $F(\nu)$ has a delta function at a frequency ν_o say (the frequency of pulsation or oscillation of a periodic function), then $F_b(\nu)$ will reproduce the shape of the normalised spectral window $\gamma_b(\nu)=\delta_b(\nu)/ND$, centred on ν_o. Thus, by comparing the shape of a peak in the transform $F_b(\nu)$ with the shape of a peak in $\gamma_b(\nu)$, we can determine whether a delta function at the frequency of this peak exists in $F(\nu)$, and hence whether a periodicity is present.

This brings us to a discussion of determining the frequency of an oscillation. Suppose we have a set of observations made at times t_i, $i=1,\ldots,ND$, with $1/(t_{ND}-t_1)\ll 1$. If a delta function in $F(\nu)$ does exist at ν_o say, then a plot of

$$P(\nu) = \frac{2}{ND}\left\{\left[\sum_{k=1}^{ND} f(t_k)\cos(2\pi\nu t_k)\right]^2 + \left[\sum_{k=1}^{ND} f(t_k)\sin(2\pi\nu t_k)\right]^2\right\}^{1/2} \quad (4.14)$$

against frequency results in a series of peaks and is called a periodogram. Such a plot will have its maximum peak close to the frequency of oscillation, the peak at ν_o being smaller, since in practice, this maximum is usually a

contribution of an alias plus the true frequency.

Physically, the quantity $P(\nu)P^{*}(\nu)$ has more relevance. It is referred to as the power of the variation, although it may not necessarily have the connotation of "energy per unit time". If the timescale of the variation is small compared with the time span of observation, then we may plot a power spectrum of $P(\nu)P^{*}(\nu)$ against ν, again the frequency of oscillation not necessarily being given by the highest peak (maximum power). The above method has been used in this study to compute approximate pulsation periods for our BL Herculis stars.

A second method which has been used and which was developed by Faulkner (1977) is to analyse the data in terms of a Fourier series rather than the Fourier transform. This process involves computing an Nth order Fourier series and calculating the standard deviation of fit σ, defined by equation (4.2) for the range of frequencies ν, 2ν,...,$m\nu$. σ is plotted against ν to provide a frequency analysis spectrum, with a minimum at ν_{o} corresponding to a periodicity in the stellar variation. Such a frequency analysis has been called a Fouriergram of order N by Faulkner and a first order Fouriergram (corresponding to a sinusoidal variation)

is equivalent to the periodogram described previously. Faulkner's technique thus has the advantage that it can be generalised to stellar variations which are not sinusoidal (i.e. those for which the order of fit $N \geqslant 2$) and can usually calculate periodicities more accurately than either the periodogram or the power spectrum. However, it is usually necessary to have a frequency increment which is comparable to the Nyquist frequency $1/\Delta T$, where ΔT is the time over which the data has been collected. Thus, if $\Delta T \sim 10^{3}$ days, then we must have an increment of at maximum 10^{-3} day^{-1} in order to have the resolution required to determine the period.

A BL Herculis star pulsating with an unknown period of between one and three days would therefore involve calculating $7X10^{2}$ Nth order Fourier series. Depending on the number of data points and the order of fit, this process may require an inordinate amount of computer time and it is therefore convenient to first calculate the power spectrum, in order to fix the frequency within reasonable limits, and then to compute a Fouriergram to calculate the frequency more accurately.

(4.2) Computational Techniques.

(4.2.1) Introduction

In this section, we consider the method of solution of our 2N+1 equations of constraint (4.3)-(4.5). Any set of linear simultaneous equations of this sort may be considered as a matrix equation (4.15):

$$AX = B \qquad (4.15)$$

Where A and B are known matrices, and X is to be found.

We may put equations (4.3) to (4.5) in this form by writing

$$\begin{pmatrix} a_{11} & a_{12} & \cdots & a_{1\,2N+1} \\ a_{21} & a_{22} & \cdots & a_{2\,2N+1} \\ \vdots & \vdots & & \vdots \\ a_{2N+1\,1} & a_{2N+1\,2} & \cdots & a_{2N+1\,2N+1} \end{pmatrix} \begin{pmatrix} x_1 \\ x_2 \\ \vdots \\ x_{2N+1} \end{pmatrix} = \begin{pmatrix} b_1 \\ b_2 \\ \vdots \\ b_{2N+1} \end{pmatrix} \qquad (4.16)$$

where

$$x_j = \begin{cases} C_{\frac{j+1}{2}} & j = 1,3,5,\ldots 2N-1 \\ S_{j/2} & j = 2,4,6,\ldots 2N \\ \langle m \rangle & j = 2N+1 \end{cases},$$

N = order of fit,

and the a_{jk} and b_k are the coefficients of the set of simultaneous equations (4.3) - (4.5).

The arrays A and B are, of course, easily determined, since t_i , m_{oi} , and w are known from the observations. If we can now find a matrix $\acute{A}$, which when multiplied by A gives the unit matrix $\tilde{1}$, then the solution to (4.15) is given by

$$\tilde{1}X = \acute{A}B \qquad (4.17)$$

The matrix which satisfies this requirement is called the inverse of A, and is denoted by A^{-1} . Perhaps the simplest method of calculating A^{-1} is by Gauss-Jordan elimination, a good account of which may be found in Bevington (1974).

To compute the Fourier fit $f(t_i)$, to the data points m_{oi} then, we must go through three steps:

1) Calculation of the coefficients a_{jk} and b_k in equation (4.16).

2) Solution of (4.16) by Gauss-Jordan elimination and

subsequent procurement of the coefficients C_n and S_n and the computed time-average magnitude <m>.

3) Calculation of $F(t_i)$ once C_n, S_n and <m> have been found.

In the following section, we describe the computer code which will perform steps one to three above. The code will also calculate periods from a set of data and appears complete with its subroutines and comment statements in appendix 4.

(4.2.2) The Computer Code.

The computer code mentioned above consists of the main program called foufit (FOUrier FITting program) and four subroutines called coeff (calculation of matrix COEFFicients), sline (solution of Simultaneous, LINear Equations), powspec (POWer SPECtrum computation) and finally fougram (calculation of FOUrierGRAMs).

Two of the subroutines (coeff and sline) are necessary for computing a Fourier fit to the data of the type described in section (4.1), whilst the second two compute periods and are not required if the period of pulsation or

oscillation is known.

After declaration of the variables in lines 51 - 60 of the program (appendix 4), the user is asked for the order of fit of the Fourier series and an integer between 1 and 24 must be input; next, the user is asked whether pre-whitened data is to be used. An answer of yes will ensure that data is pre-whitened at a later stage by removal of the contribution of the fundamental period to the Fourier series. If the answer to this question is to the negative, then the period of pulsation is required without pre-whitening taking place.

The data read by this program must consist of three parts: record 1 containing the name of the star; record 2 the epoch of observation and thereafter the data, each record consisting of 1) time of observation; 2) a number associated with the V magnitude; 3) a number associated with the colour magnitude (B-V); 4) a number associated with (U-B).

All numbers are in free format and the name of the star should consist of not more than nine characters.

Lines 101 to 108 therefore ask the user for a colour, whether V, B-V or U-B. This is stored in the character variable Ceq(1). The data is read from a file assigned to input unit 4 in lines 118 to 151. The magnitudes m_{oi} (either in V, B-V or U-B) are placed in the double precision variable F(I) and times in T(I). The variable VF(I) is single precision and is used in the graphics routines to be described in the next section.

In lines 157 to 165, the subroutines coeff and sline are called. The former sets up the matrices A and B in equation (4.16) and appears in lines 400 to 449, whilst the latter solves (4.16) by inversion of A and multiplication of B by A^{-1}. Coeff calculates sine and cosine terms from w and T(I) and places them in the arrays Q(J,I2) and P(J,I2). If I2 is odd in line 422, then Q and P are multiplied by cos mwt, with m=1,..., N. The results are placed in the array A in lines 424 to 425 and the previous value of A added from the preceding progression through the loop in line 157.

This is equivalent to producing a_{jk}, (j=2m-1, all k and m=1,...,N) in (4.15) and summing over i for times t . Lines 429 to 430 produce the similar result of a_{jk} for j=2m (all k). After all elements of A and B have been calculated,

sline uses the results to compute C_n, S_n and <m> by Gauss-Jordan elimination.

The subroutine foucalc is next called to calculate the Fourier series from C_n, S_n and <m>. The result is contained in the array FC (computed magnitude, as opposed to observed magnitude F). The standard deviation of fit is calculated from the sum of the residuals squared, these being contained in error in line 513.

After the results have been either printed at the terminal or sent to output unit 7, the amplitudes and phases of the series are computed, as in (4.18) below:

$$F(t_i) = \sum_n A_n \cos(nwt_i - \varphi_n) + \langle m \rangle \qquad (4.18)$$

according to

$$\left.\begin{aligned} A_n &= (S_n^2 + C_n^2)^{1/2} \\ \varphi_n &= \mathrm{Tan}^{-1}(-S_n / C_n) \end{aligned}\right\} \qquad (4.19)$$

(4.18) is merely an alternate way of writing (4.1), but has the disadvantage that $\partial\sigma/\partial\langle m\rangle$, $\partial\sigma/\partial A_n$ and $\partial\sigma/\partial\varphi_n$ represent a set of <u>non-linear</u> simultaneous equations, and so are less convenient to solve.

At this stage, we also compute the quantities

$$\left.\begin{aligned} R_{21} &= A_2/A_1 \\ R_{31} &= A_3/A_1 \\ \varphi_{21} &= \varphi_2 - 2\varphi_1 \\ \varphi_{31} &= \varphi_3 - 3\varphi_1 \end{aligned}\right\} \qquad (4.20)$$

The importance of the set of equations (4.20) is discussed in chapter 5.

Lines 215 to 264 ask the user if a power spectra and Fouriergram are to be computed. If a power spectrum is required, then powspec in line 587 is called. After the frequency increment has been asked for in line 600 and the frequency range in line 603, the routine goes on to compute the transform for the data as in equation (4.11). The power will then simply be this transform multiplied by its complex conjugate. Thus,

$$\text{Power} = F_D(\nu)F^*(\nu) = \sum_k F(t_k)e^{i2\pi\nu t_k} \sum_k F(t_k)e^{-i2\pi\nu t_k} \qquad (4.21)$$

which is similar to $P(\nu)P^*(\nu)$ with a normalising factor. $P(\nu)$ is simply the periodogram variable as seen in equation (4.14).

The argument of (4.21) is $2\pi\nu t$ and is calculated in line 617. The real and imaginary parts of the transform are stored in FTR and FTI respectively.

The power in array PS will then be

$$PS = \frac{1}{ND^2}(FTR^2 + FTI^2) \qquad (4.22)$$

ND is the number of observations and 1/ND normalises the power PS.

It should be noted that the average magnitude AVF is calculated in line 609. This is then removed from the value F(I) to avoid bias from non-physical zeros in the data. It does, however, force the power at zero frequency to be zero. If the power data is not required (and it usually is not), it is stored in a file assigned to unit 8 and the power

spectra plotted if required.

A Fouriergram may now be computed using fougram. This is a simple subroutine which calls coeff, sline and foucalc for a range of frequencies ν to $\nu + md\nu$, where m, ν and $d\nu$ are input by the user. The standard deviation is calculated for each frequency and stored in the array Error, which is printed on the screen with period and frequency and plotted if required.

If pre-whitened data is to be used, then this is computed in lines 232 to 235 or 259 to 262. If only the fundamental frequency is present, a power spectrum or Fouriergram will merely result in noise if pre-whitening of the data does take place.

(4.2.3) Graphics Routines

It may have been noticed that several lines of program in foufit, powspec and fougram have not been discussed. These share a special section since they form part of the routines used for graphics purposes. These routines have been taken from the Ghost graphics library implemented by W.A.J.Prior of the Culham Laboratory for use on the digital

VAX 11/780 computer system at St. Andrews.

The method of plotting curves using Ghost is essentially the same in all cases and can be summarised as follows:

(i) Setting limits on X- and Y-axes.

The y-axis limits are set in lines 169 to 285 of foufit; 644 to 649 of powspec and 737 to 747 in fougram.

Lines 280 to 294 in foufit are necessary to place the maximum of the light curve at phase 0.5 on the completed graph. Note that the x-axis variables are always known and so can be placed immediately into the graphics routines without previously computing them.

(ii) Select a piece of graph paper.

Paper is selected by the "call paper (I)" command, with I=1 always.

(iii) Select physical space.

The physical space is set by a call to pspace (XP_1, XP_2, YP_1, YP_2) where XP_1, YP_1, XP_2 and YP_2 are chosen according to the size of the window to be mapped and the graphics device being used (always Tektronix T4010 in this case).

(iv) Choose the mathematical space.

The mathematical space is chosen by call map (XM_1, XM_2, YM_1, YM_2). It is this space onto which the axes are mapped, and so XM_1, XM_2, YM_1 and YM_2 represent the limits on the x- and y-axes.

(v) Plot axis labels and titles.

(a) Once the axes have been plotted, the mathematical and physical spaces are altered to be larger than the set of axes so that the axis labels and graph titles can be plotted.

(b) The cursor is positioned by call positn (x,y), with x and y being variables in the physical space.

(c) The labels are plotted, beginning at the point (x,y) in the call to positn. The labels are rotated and magnified if necessary.

(d) The arguments of pspace and map are returned to their original values in steps (iii) and (iv), so that a curve may be plotted.

(vi) Plotting characters.

Call plotnc (x(I), y(I), 232) will plot a character from the current St. Andrews Computing Laboratory character font, with font number 232, at point (x(I), y(I)) in pspace co-ordinates.

All points in foufit are plotted in this way in lines 345 to 347, with font number 232 being a cross (+).

(vii) Plotting a continuous line.

A continuous line may be plotted by the "call join (x(I), y(I))" command, with points x(I) and y(I) being joined to points (x(I-1), y(I-1)) by a continuous line. It should be noted that no character is plotted in this case.

(viii) End of graphics routines.

Call grend should be the final call to the graphics library. This ensures that all graphical output is printed and communications with Ghost are broken.

It should finally be noted that the Ghost graphics library uses single precision variables only, i.e. those beginning with the letter V in foufit and its subroutines.

(4.2.4) Error Analysis

An important aspect of any physical calculation is the estimation of errors. foufit is able to compute errors in the Fourier amplitudes and phases which we have discussed so far.

Suppose we have the function F=F(x,y), then the error in F is given by

$$\delta F = \{ [\frac{\partial F}{\partial x} \delta x]^2 + [\frac{\partial F}{\partial y} \delta y]^2 \}^{1/2} \qquad (4.23)$$

where δx and δy are the errors in x and y.

Equation (4.23) is the usual formula for propagating the errors in x and y through the function F(x,y). The analysis can be extended to describe the errors in a Fourier fit, where we have discovered that the coefficients of the series may be found by using Gauss-Jordan elimination.

In this case, the errors in the coefficients C_n, S_n and <m> will be given by equation (4.24):

$$\delta x_j = \sqrt{a^{-1}_{jj}}\ \sigma \qquad (4.24)$$

where $C_n = x_{2n-1}$

$S = x_{2n}$

and $\langle m \rangle = x_{2n+1}$ $\quad (n=1,2,\ldots,N)$

The least-squares fit yields a standard deviation of σ between the fit and the observations and the a^{-1}_{jj} are the diagonal elements of the inverted matrix A^{-1} (equation (4.17)).

Now, since the amplitudes A_n and phases φ_n are related to the C_n and S_n by the set of equations (4.20), the errors δA_n and $\delta \varphi_n$ in the former quantities follow easily from equation (4.23).

They are:

$$\left.\begin{aligned} \delta A_n &= \left\{ \frac{S^2 \delta S^2}{(C^2+S^2)} + \frac{C^2 \delta C^2}{(C^2+S^2)} \right\}^{1/2} \\ \delta \varphi_n &= \left\{ \frac{S^2 \delta C^2}{(C^2+S^2)^2} + \frac{C^2 \delta S^2}{(C^2+S^2)^2} \right\}^{1/2} \end{aligned}\right\} \qquad (4.25)$$

We finally note in this chapter that foufit has been tested completely by comparison with an independent periodic signals analysis package written by Skillen (1984).

CHAPTER 5.

QUANTITATIVE DESCRIPTION OF THE LIGHT CURVES.

(5.1) Basic Analysis as Applied to Classical Cepheids.

We have seen in chapter 3 that there is a Hertzsprung progression in classical Cepheids and we have discussed the possibility of there being a similar progression in the population II variables. Simon and Schmidt (1976) showed that such a progression of bumps is related to the resonance $P_1/P_0 \approx 0.5$. If $0.46 \lesssim P_1/P_0 \lesssim 0.5$, then the bump appears during rising light, whereas $0.5 \lesssim P_1/P_0 \lesssim 0.53$ show bumps on the descending branch. At periods approaching 10 days, P_1/P_0 is equal to 0.5. It now seems to have been acknowledged through the work of Cox (1980), King, Cox and Hodson (1981) and others that the movement of secondary bumps in the theoretical light curves of both population types is always related to this resonance.

A qualitative study is not always possible, however, since the models have always exhibited non-physical artifacts of the computation in the form of numerical noise; whereas, the observations do not often have the accurate

photometry necessary to fully describe the light curves. We have certainly encountered this problem in chapter 3, where we discovered the difficulty of describing the progression in terms of the movement of bumps in the light curves, with the stars being so faint that secure detection of definite physical features is not normally possible, even among population I objects. Early authors (for example, Fricke, Stobie and Strittmatter, 1972) in fact often read these quantities from ill-defined light curves, drawn by hand through the observed points. Even more recently, Diethelm (1983) followed this procedure when he classified his twenty-eight population II light curves.

There had thus been few reasonable attempts at quantifying the light curves and the initial approach to the problem began with Simon (1977), who iteratively described theoretical light curves in terms of a Fourier series and predicted that the resonance $P_2/P_0 \approx 0.5$ should be described by the quantity $\varphi_{21} = \varphi_2 - 2\varphi_1$, with φ_2 and φ_1 having the same definitions as in section (4.2.2).

Simon and Lee (1981, hereafter SL) continued with the analysis and computed φ_{21} for fifty-seven classical Cepheids, along with the quantities R_{21}, R_{31} and φ_{31}, defined below:

$$\left.\begin{aligned} R_{21} &= A_2/A_1 \\ R_{31} &= A_3/A_1 \\ \varphi_{21} &= \varphi_2 - 2\varphi_1 \\ \varphi_{31} &= \varphi_3 - 3\varphi_1 \end{aligned}\right\} \qquad (5.1)$$

The first two quantities in equation (5.1) measure the relative importance of the second and third Fourier amplitudes in equation (4.18), as compared to the amplitude A_1, of the fundamental mode and φ_{21} and φ_{31} are the phase differences between the second and third terms and the phase φ_1.

Fig. 5.1 (fig. 1 of SL) shows φ_{21} plotted against period and shows a rise in short periods to a maximum at about ten days. There is then a sharp drop at this period and thereafter a scatter in points as the period increases.

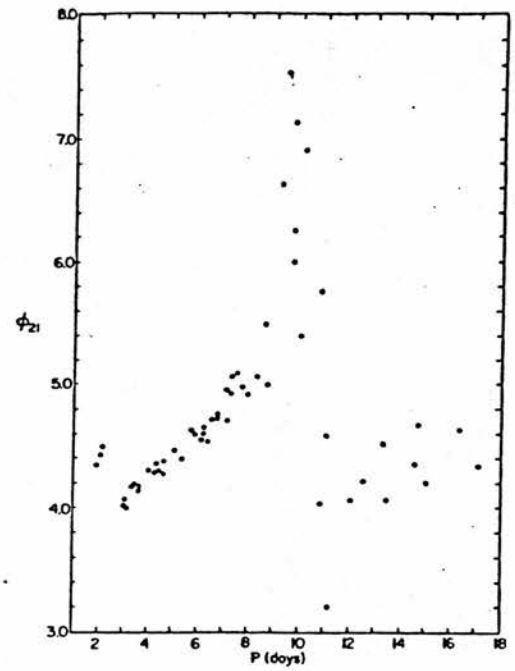

Fig. 5.1: The phase difference ϕ_{21} versus period for a set of observed classical Cepheids. (Figure 1 of SL)

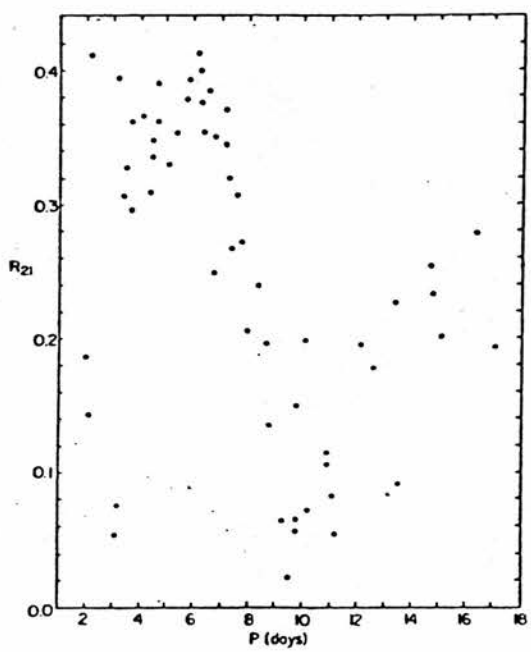

Fig. 5.2: The amplitude ratio R_{21} versus period. (Figure 2 of SL)

At this point, φ_{21} appears to be almost independent of period. SL suggest that the discontinuity in fig. 5.1 at about ten days is the result of the π_2/π_0 resonance, and is possibly the most dramatic evidence of this interaction so far published.

We see that the resonance is also apparent in fig. 5.2 (R_{21} versus period). Here, R_{21} takes on large values at the shorter periods, and drops almost asymptotically at periods between nine and ten days. As the period increases, we note a recovery of R_{21} as this parameter attains a more constant value.

SL similarly plot φ_{31} against period, noting that there is again a rapid jump at around ten days (fig. 5.3). Fig. 5.4 shows R_{31} against period, and here a discontinuity is again apparent at the period of resonance, even though R_{31} shows a large amount of scatter over the full period range.

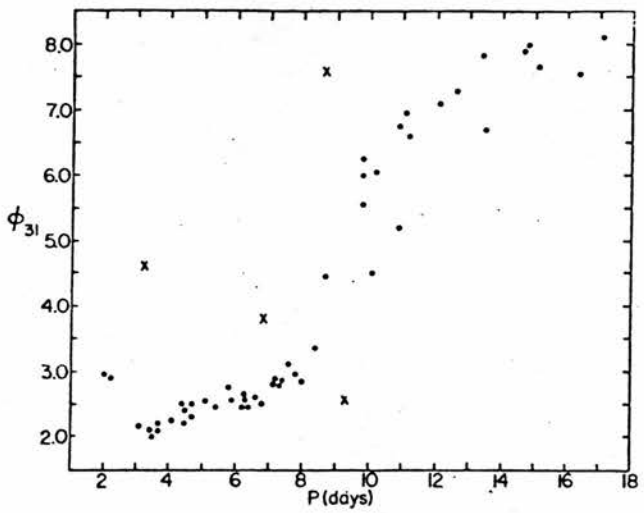

Fig. 5.3: The phase difference φ_{31} versus period.
(Figure 4 of SL)

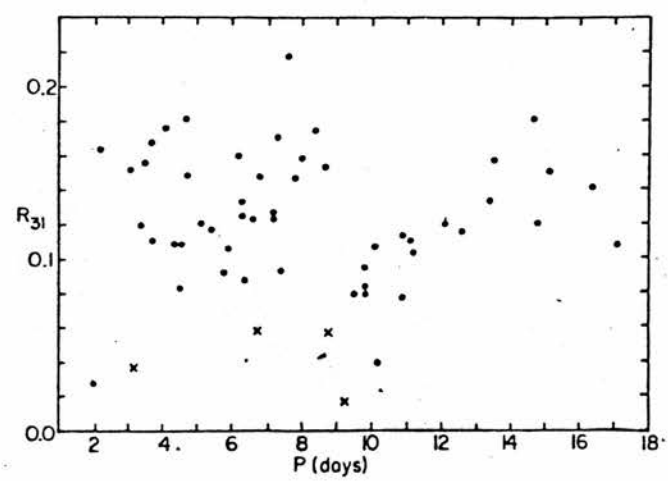

Fig. 5.4: The amplitude ratio R_{31} versus period.
(Figure 5 of SL)

(5.2) Population II Cepheids: a Similar Approach.

(5.2.1) Description of the "Resonance" Diagrams.

We have seen how the above analysis describes the bump progression in observed classical Cepheids. An obvious step from here would be to apply these techniques to short-period population II Cepheids, since besides population I variables, it is only these stars which should have the necessary relation between period and bump phase to exhibit the Hertzsprung progression, as discussed in chapter 3 (Stobie, 1973).

Many theoretical models indicate that the bump progression in the BL Herculis stars does exist and is centred at a period of about 1.6-1.7 days. However, to date, the procedure of SL has not been adopted for observed stars of this type. The data of KD therefore provides a very convenient basis for doing this. In this section then, we will discuss the diagrams of SL as applied to the stars of KD, all of which, as we have seen, are short-period, population II Cepheids; i.e. they are BL Herculis stars with periods between one and three days.

We have seen in chapter 3 that a qualitative description of the bump progression indicates that the centre of the progression (i.e. a resonance interaction) ought to occur somewhere between 1.66 and 1.83 days, and we present below further evidence for this view by consideration of plots of φ_{21} , φ_{31} , R_{21} and R_{31} against period. Such plots will often be termed "resonance" diagrams hereafter.

Table 5.1 shows results for each star, with column 2 giving the name of the star and columns 3, 4, 5 and 6 the values of φ_{21} , R_{21} , φ_{31} and R_{31} , calculated from the amplitudes and phases presented in table 6.1. We show the error below each quantity, estimated from the general formula for propagation of errors presented in equation (4.23).

At this juncture, we should perhaps point out that the values of the relative amplitudes and phase differences in equations (5.1) and (5.2) vary only slightly with increasing orders of fit, and so for a given period and data set, we can assume these quantities to be constant.

Table 5.1: Phase Differences and Amplitude Ratios for Pop. II Cepheids.

	STAR	φ_{21} (ERROR)	R_{21} (ERROR)	φ_{31} (ERROR)	R_{31} (ERROR)
1	V716 Oph	4.002	0.478	1.903	0.314
		(0.033)	(0.013)	(0.050)	(0.012)
2	V527 Sgr	-1.959	0.241	-2.927	0.118
		(0.134)	(0.030)	(0.264)	(0.030)
3	VX Cap	-8.154	0.500	-10.240	0.291
		(0.050)	(0.022)	(0.083)	(0.019)
4	HQ Cra	-2.459	0.265	-6.409	0.064
		(0.087)	(0.022)	(0.318)	(0.021)
5	V2022 Sgr	-1.962	0.278	-5.028	0.192
		(0.209)	(0.042)	(0.256)	(0.034)
6	V745 Oph	-8.345	0.344	-12.595	0.047
		(0.061)	(0.018)	(0.358)	(0.017)
7	V971 Aql	-1.541	0.221	-4.758	0.173
		(0.073)	(0.015)	(0.094)	(0.015)
8	DU Ara	4.538	0.140	1.378	0.162
		(0.146)	(0.020)	(0.136)	(0.020)

Table 5.1 (contd.)

	STAR	φ_{21} (ERROR)	R_{21} (ERROR)	φ_{31} (ERROR)	R_{31} (ERROR)
9	VZ Aql	-1.005	0.225	-4.508	0.176
		(0.310)	(0.066)	(0.421)	(0.062)
10	V839 Sgr	-1.218	0.229	-4.040	0.219
		(0.174)	(0.039)	(0.200)	(0.039)
11	EX Del	4.674	0.464	2.762	0.219
		(0.044)	(0.016)	(0.080)	(0.015)
12	UX Nor	-1.600	0.374	-3.480	0.230
		(0.088)	(0.028)	(0.142)	(0.025)
13	V465 Oph	-1.383	0.316	-9.385	0.232
		(0.074)	(0.019)	(0.101)	(0.019)

From the data in table 5.1, we plot the φ_{21} resonance diagram shown in fig. 5.5, noting that if $\varphi_{21} < 0$, then we add $2n\pi$ to φ_{21}, n being an integer sufficiently large to make φ_{21} positive. Similarly, if $\varphi_{21} > 2\pi$, then we subtract $2n\pi$ from φ_{21}. We also note that the numbers following each point refer to the numbers in column 1 of

table 5.1, for easy identification of the points.

The first feature in fig. 5.5 which one observes is the striking discontinuity at around 1.66 days, with a rapid rise from about 1.58 days and a more moderate fall-off from about 1.8 days. The second point to comment upon is that at periods greater than about two days, the curve is noticeably flat, with stars 11, 12, and 13 having almost identical values of φ_{21}.

We now note the resemblance between fig. 5.5 and the corresponding diagram of SL (fig. 5.1). We therefore paraphrase the remarks of SL by suggesting that the discontinuity at about 1.66 days is the result of the π_1/π_0 resonance of Simon and Schmidt (1976).

Following the discussion in sections (3.3) and (3.4), we see that this resonance is related to the movement of the secondary bumps in the light curves. For periods less than about 1.66 days, this bump should appear on the descending branch; whereas, stars with periods greater than about 1.9 days ought to show bumps on the rising light.

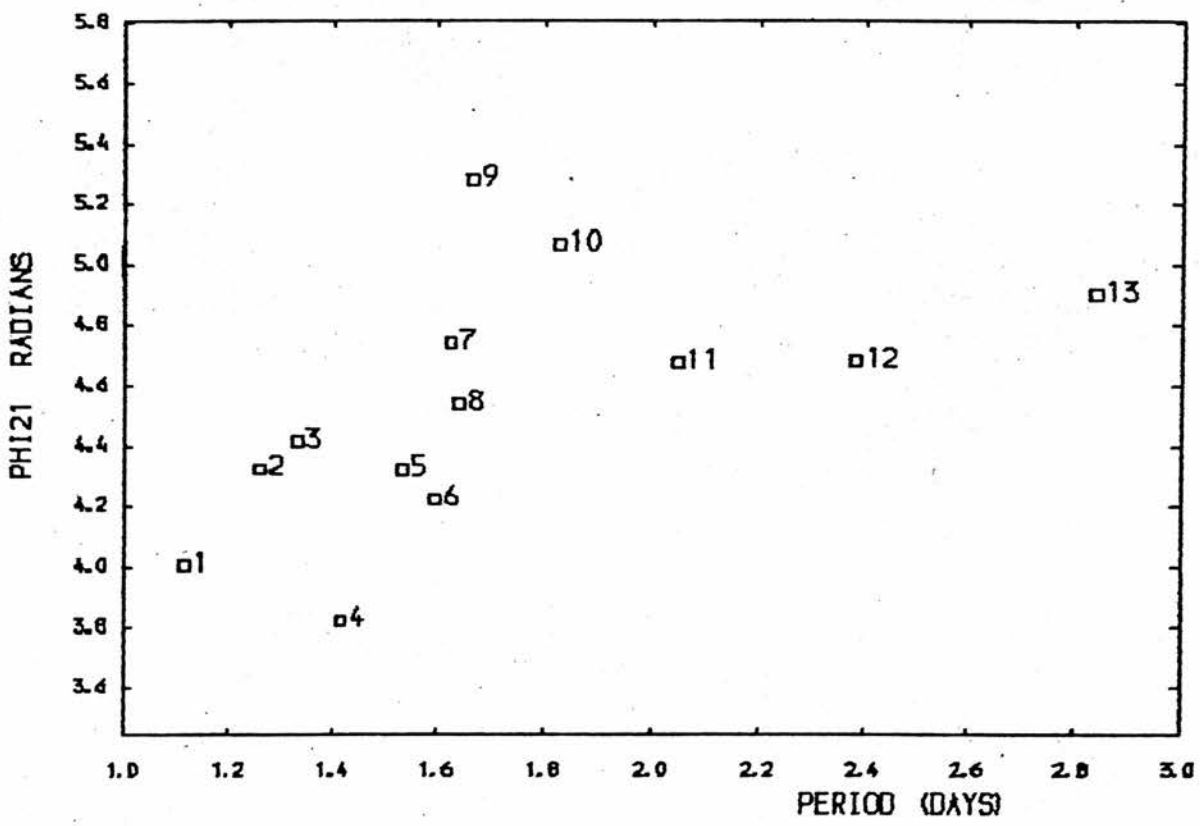

Fig. 5.5: φ_{21} versus period for the observed stars of KD. The numbers following each point refer to the numbers in column 1 of table 5.1, for easy identification of which star is associated with each point.

Now, by extrapolating from points 8, 7, and 9, and 10 and 11 in fig. 5.5, we argue that the curve will reach its maximum at about 1.7 days, i.e. observationally, the centre of the bump progression in population II Cepheids lies at approximately this period. This is in very good agreement with the qualitative description of the light curves in section (3.4), where we suggested that the star with the 1.66 day period, VZ Aql, was not in resonance, but was approaching it.

An obvious difficulty in the interpretation of fig. 5.5 lies in the position of the points 2, 3 and 4, corresponding to V527 Sgr, VX Cap and HQ Cra respectively, these stars departing from the expected curve. We should perhaps expect the curve to continue to points 5 and 6 from point 1 directly between these two sets of points, without passing near either. To solve this problem, we turn to the data and note that the faintest stars of KD's survey are VX Cap ($\langle m \rangle \sim 15^m.0$), V839 Sgr ($\langle m \rangle \sim 15^m.0$), V527 Sgr ($\langle m \rangle \sim 14^m.9$) and HQ Cra ($\langle m \rangle \sim 14^m.7$), the magnitudes of these being higher than any of the other stars (table 6.2).

This statement would seem to imply that there is a correlation between the scatter of these stars in fig. 5.5 and their relatively high magnitudes. Thus, the indication is that a Fourier fit to the data of these stars might be difficult, with the possibility of a poor determination of φ_{21}. It is also interesting to note that the faintest star with perhaps the poorest data, V839 Sgr (point no. 10), would produce a smoother curve if it had $\varphi_{21} \sim 4.8$ or $\varphi_{21} \sim 5.3$, thus emphasizing the point that the brightness of the star does play a role in determining φ_{21} and its subsequent position in the φ_{21} resonance diagram.

Fig. 5.6 shows a plot of the relative amplitude R_{21} against period. Here it is difficult to discern any hint of a progression, with several points to the left of centre, two points (1 and 3) above these and several to the right of the diagram. However, if we again neglect the fainter stars, denoted by numbers 2 and 4 in the plot, the diagram seems to be rather clearer, with the points between periods 1.0 to 1.3 days forming a more or less horizontal line (points 1 and 3, with $0.45 \lesssim R_{21} \lesssim 0.5$) and then an abrupt drop to $R_{21} \sim 0.35$ (point 6). The curve continues its descent to a minimum at about 1.6 days and then ascends

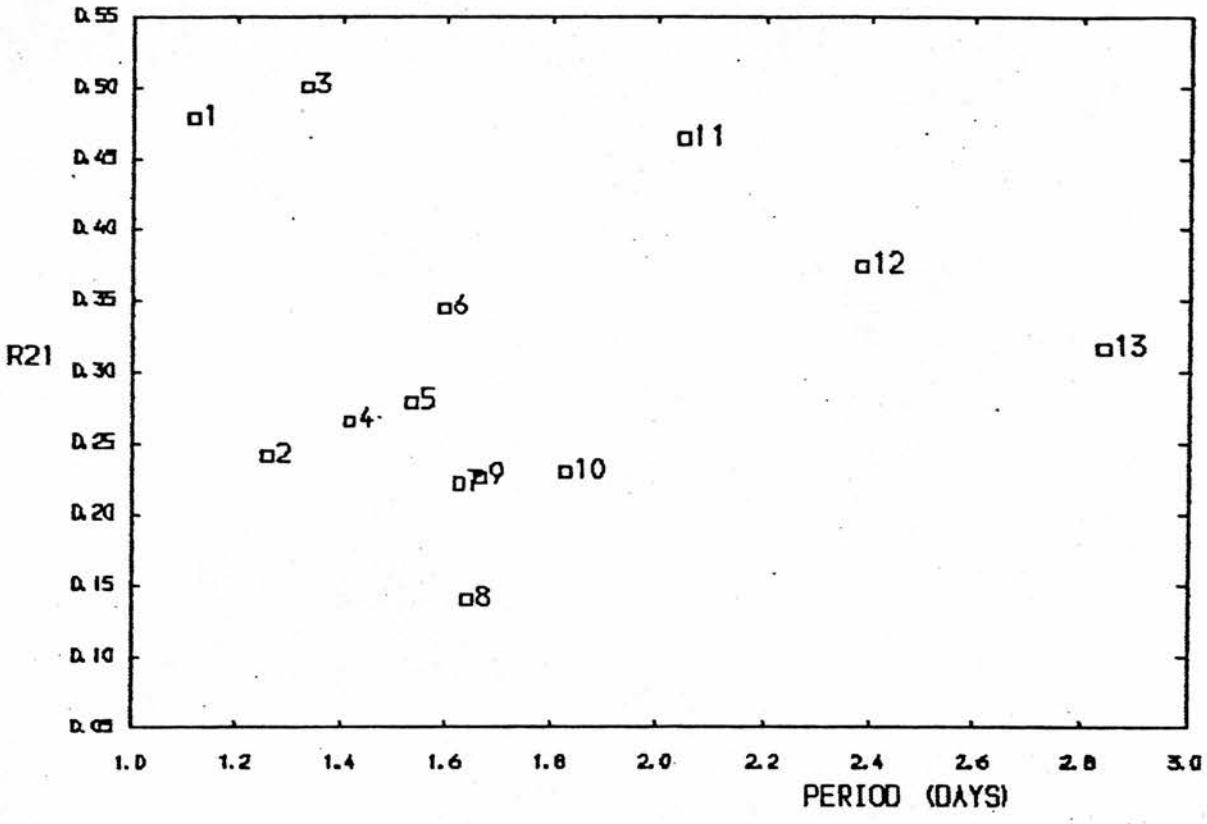

Fig. 5.6: R_{21} versus period for the observed stars.

again to point 11 in the diagram, with a period of 2.04 days.

We note the similarity between figs. 5.6 and 5.5, with a discontinuity again occurring at a period of between 1.64 to 1.7 days.

In fig 5.7, we plot φ_{31} against period and see that with the exception of points 2, 4 and 6, the curve is very much flatter than the previous two plots. We can make several comments concerning fig. 5.7: firstly, we see again that it is points 2 and 4 (V527 Sgr and HQ Cra) which receive the most scatter in this diagram. Excepting these points, we find a relatively horizontal curve from points 1 through to 5, with a sharp rise through points 8,7 and 9. Thereafter, we note the horizontal portion of the curve, consisting of points 10, 11, 12 and 13. Thus, we again assume that points 2 and 4 (and to some extent 3) do not contribute to this progression, and so can be excepted from this analysis (see also the following section).

We now note the position of point 6 in our diagram. With regard to this star, there are two possibilities; either it forms the apex of the discontinuity at 1.6 days,

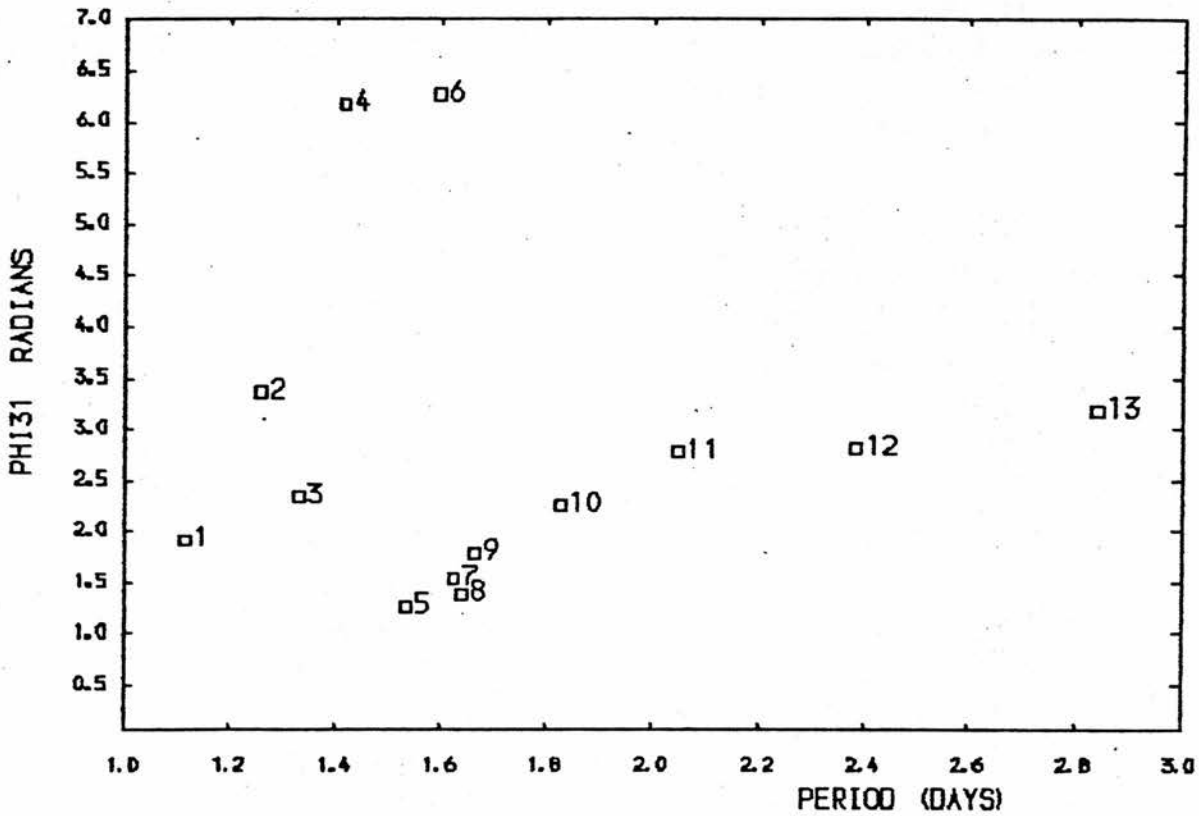

Fig. 5.7: φ_{31} versus period for the observed stars.

or it is another migratory point, and so should be disregarded.

Examination of the preceding diagrams indicates that this star is well-behaved and does not appear to diverge considerably from the expected curves and this would of course imply that this star is in its correct position in the φ_{31}-period diagram. The period of resonance in fig. 5.7 thus appears to be lower than is indicated by the φ_{21} resonance diagram. In fact, we should perhaps expect the two to differ, since φ_{31} and φ_{21} refer to different physical quantities, and so might not necessarily yield similar results when we consider our resonance diagrams.

However, inspection of the corresponding point in the R_{31} diagram shows that the value of R_{31} for this star is small compared with other stars, and so indicates that there is only a minor contribution from the third Fourier term A_3 (amplitude of second harmonic). This suggests a difficulty in determining the phase φ_3 corresponding to A_3. Thus, the position of star 6 in fig. 5.7 may be due to a poor determination of φ_3. If this is the case, then stars 2, 4 and 6 do not contribute to our progression of bumps in the φ_{31} diagram and we may be able to neglect point 6 as well as

points 2 and 4.

To find the true status of these stars, and particularly that of star 6, it will be necessary to analyse more stars with periods around 1.2 - 1.7 days, in order to cover this region well enough to see the trend in φ_{31} at these periods. We will suggest for the time being, however, that the resonance <u>has</u> shifted to a slightly lower period as compared to the φ_{21} chart, and that point 6 (V745 Oph) is at the centre of this resonance.

We finally discuss in this subsection the R_{31}-period diagram for our population II stars (fig. 5.8). Again there are the anomalous points 2 and 4 lying well away from a curve drawn through the remaining points. In conjunction with these, we again have star 6. As discussed earlier, this star has a particularly low value of R_{31}, indicating that there is barely any contribution from the third Fourier term.

We again note a discontinuity beginning at around 1.5 days, reaching a minimum at about 1.6 days and climbing to a value of $R_{31} = 0.22$. The curve flattens off from about 2.0 days with constant values of R_{31}.

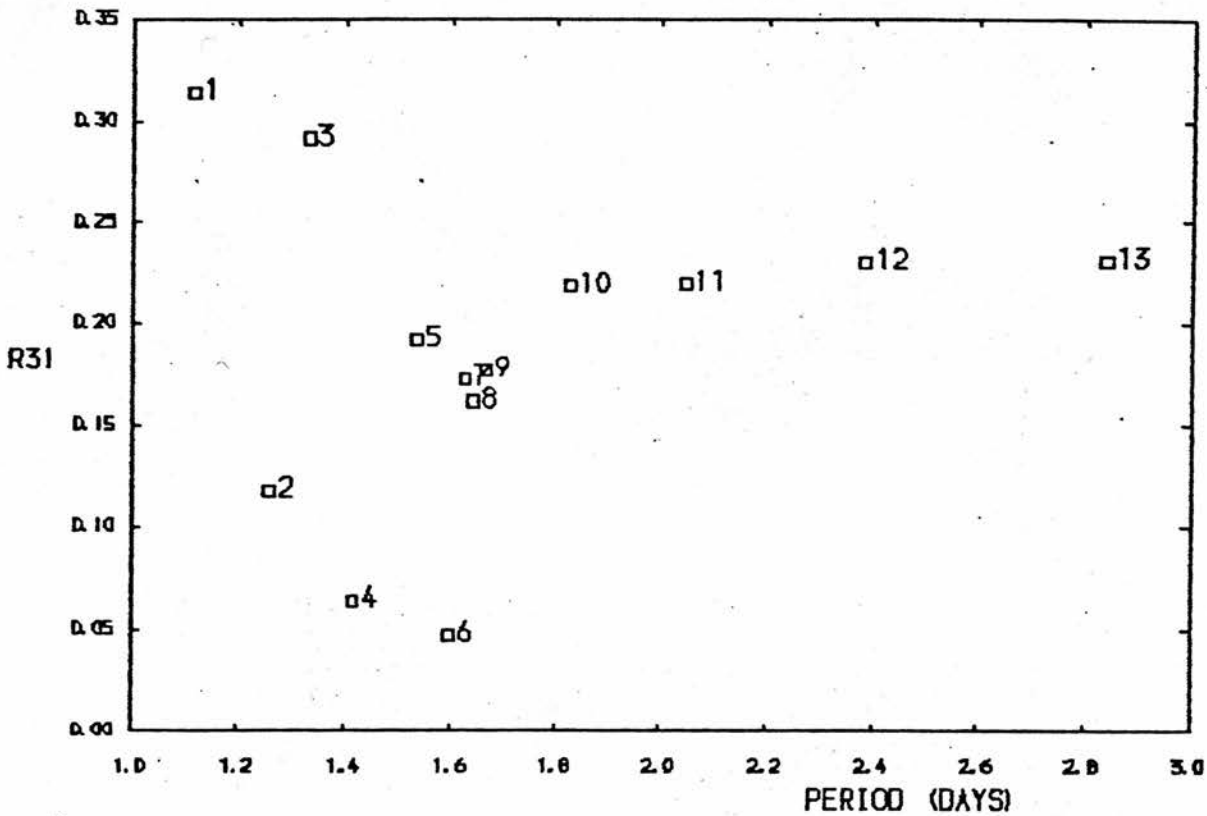

Fig. 5.8: R_{31} versus period for the observed stars.

Because of the poor coverage of some of our light curves, accurate determination of the higher Fourier terms (A_i and φ_i, for $i \geqslant 3$) is not normally possible. For this reason, one should perhaps be careful when discussing the φ_{31} - and R_{31}-resonance diagrams (figs. 5.7 and 5.8). To illustrate the point, we note that percentage errors in R_{31} range from about 3.9% for V716 Oph to over 35% for V745 Oph, whilst we calculate errors in R_{21} for these stars to be 2.7% and 5.2%, respectively.

From this and previous discussions, we may deduce that:

(a) The resonance in the R_{21} and φ_{21} charts appears at a period in the range $1.64 \leqslant P \leqslant 1.70$ days.

(b) The resonance appears at a period of $P \approx 1.60$ days if one studies the R_{31} and φ_{31} charts and one assumes that the resonance has shifted to a lower period as compared to the R_{21} and φ_{21} diagrams.

It therefore appears that all four of our resonance diagrams show a discontinuity at around 1.6-1.7 days, and we assume this to be associated with the echo bump of Christy (1968) and the π_1/π_0 resonance of Simon and Schmidt (1976).

We may deduce from these charts and the qualitative discussion in chapter 3 that for periods $P \lesssim 1.60$ days, the bump appears on the descending branch of the light curves, whilst if $P \gtrsim 1.70$ days, the bump should either appear on rising light, or be absent altogether. At periods between 1.60 to 1.70 days, the bump merges with, and is indistinguishable from, maximum light, thus forming a broad, symmetric light curve.

(5.2.2) Discussion of V527 Sgr and HQ Cra in Relation to the Resonance Diagrams.

We note that there are two stars in the survey of KD which cause a certain amount of difficulty in all of our resonance diagrams. These are of course the points which are numbered 2 and 4, corresponding to the stars V527 Sgr and HQ Cra, respectively. Both of these stars depart quite drastically from the expected curves and there are three apparent reasons why this may be so. Either,

1) The stars are pulsating in an overtone rather than the fundamental mode.

2) They are pulsating in two modes simultaneously; i.e. they are double-mode or "beat" cepheids.

or 3) They have poorly-covered light curves, which results in an inaccurate determination of the amplitudes and phases.

The second of the three alternatives above is easily checked by pre-whitening the data (i.e. removal of the contribution of the strongest pulsation mode) and testing the result for periodicities by the usual power spectrum-Fouriergram method. We have gone through this process as a matter of course for all thirteen of the stars in this study and no second periods have been detected.

We now note that V527 Sgr is not only a very faint star, with average magnitude $15^{m}.0$, but its light curve shows a great deal of scatter, varying between about $0^{m}.3$ on the ascending branch to $0^{m}.2$ on the descending branch (fig. A2.2) making a Fourier fit to this data very difficult indeed. This would indicate with a fair degree of certainty that it is 3) above which is affecting the position of V527 Sgr in figs. 5.5 - 5.8.

The same argument may also be applied to HQ Cra, since although there is only a little scatter in the light curve of this star, there are several gaps in the data, particularly at maximum light. Such gaps may result in an

exaggerated maximum or minimum if they occur near a turning point, or the light curves will result in a loss of certain features if the gaps are present at a maximum gradient; for example, on rising light in most asymmetric light curves, where a shock bump may or may not be present in the fit.

Overtone pulsation is also a possibility for HQ Cra showing dispersion in the resonance diagrams. However, if variable stars in the population II class follow the classical Cepheids as far as overtone pulsations are concerned, then according to suggestions by Gieren (1982) and Antonelli and Mantegazza (1984), φ_{21} for such stars should be larger than normal. This is clearly not the case for HQ Cra, and it is assumed that poor observations account for its peculiar locations in figs. 5.5 - 5.8.

(5.3) Comparison with Classical Cepheids

We have just discussed the resonance diagrams of classical Cepheids (taken from SL) and the short-period population II objects of KD. We now briefly attempt to compare the two, noting that there are differences, but that

the general shapes of the diagrams of SL are very similar to the corresponding plots in figs. 5.5 - 5.8.

We begin with a discussion of the φ_{21} diagrams in figs. 5.1 (classical Cepheids) and 5.5 (BL Herculis stars). In the latter case, the curve begins with a slowly increasing value of φ_{21} and then takes on a sharp rise, culminating in a peak at what we consider to be the period of resonance. In these last two respects, the curve is identical to that of SL. After maximum, both curves show almost constant values of φ_{21}.

The diagrams of R_{21} are also similar in a very general sense. If we disregard the controversial points 2 and 4 in fig. 5.6, we see that both this diagram and fig. 5.2 begin with large values of R_{21} :- 0.48 for the BL Herculis stars and 0.3 for the classical Cepheids. The curves then rise to a maximum and then drop precipitously to a minimum. In the case of fig. 5.6 , we note a second rise to a similar maximum and then a drop to lower values. In the diagram of SL, however, we cannot be sure exactly what happens to R_{21} after its fall to minimum. However, like fig. 5.6, R_{21} does increase again to a value of around 0.25.

Figs. 5.3 and 5.7 show φ_{31} for the two classes of variable. In the diagram of SL (fig. 5.3), we note a slow, almost zero increase in φ_{31} for periods between three and eight days. At about nine days, φ_{31} increases rapidly to a value of about 7.5. Thereafter, we have a new, constant value of φ_{31}. At first glance, this may not seem at all similar to the corresponding plot for type II Cepheids. However, if we are able to overlook points 2 and 4 in figure 5.7, as discussed earlier, and we suppose that the maximum of φ_{31} in figure 5.3 does not occur at $\varphi_{31} \approx 7.5$, but at a higher value, then this diagram does compare with fig. 5.3, with a much smaller amplitude. We now note that the large scatter of points in fig 5.4 precludes any comparison of the R_{31} diagrams.

It would seem reasonable to suggest from the above discussion that the resonance diagrams of BL Herculis stars compare very well <u>in general shape</u> to those of the classical Cepheids, even though the two are in a very different population group. This result is perhaps not surprising, since the same physical mechanism drives the pulsations in each case and so a Fourier decomposition of the type discussed in this chapter might be expected to provide

similar, but not necessarily identical results.

(5.4) A Comparison With Theoretical Resonance Diagrams.

RCRS have computed a set of models for 11 BL Herculis field variables. The author of this thesis does not intend to discuss these models or their light curves, which he has produced using Foufit and data provided by Carson and Stothers (1984a). However, the light curves have been published and appear in appendix 3.

The data is in the form of times (in seconds), luminosities and radial velocities. The first two of these have been reduced to times in days and magnitudes using the formula $M_v = -2.5 \text{ Log } L_*$, where L_* refers to the luminosity of the star. Since no reasonable velocity data exists for the observed stars, only the luminosity data of the models of RCRS will be analysed here.

The periods of the models have been computed by Foufit and all agree with those of RCRS to two decimal places, except for YZC, which has a period of 2.47 days, and not 2.67 as published by RCRS. The latter period is therefore assumed to be a typing error.

Figs. 5.9 to 5.12 thus show the resonance diagrams for the models and will be referred to as "theoretical resonance diagrams" in what follows. Here we show two plots in each figure. The first is a plot of φ_{i1} or R_{i1} for the models (i = 2 or 3), denoted by a square and a number, and the second shows an envelope which indicates the domain of the observed stars in these theoretical resonance diagrams. This envelope has been sketched in to enable us to make a direct comparison of the observations with the models.

Fig 5.9 then, shows the quantity φ_{21} plotted against period. The main features are the drop in φ_{21} at low periods ($P \lesssim 1.3$ days) and the sharp rise in φ_{21} at about 1.6 days. At periods greater than about 2.0 days, points 10 and 11 show some scatter.

One notices that at periods less than two days, the majority of points lie within the observational envelope, and in fact, only one lies outside to a marked extent (point 5). The important point to comment upon here is the resemblance of fig. 5.9 to the observed chart, <u>with a resonance occurring in the models at about 1.6 days</u>, in excellent agreement with the discussion in section (5.2).

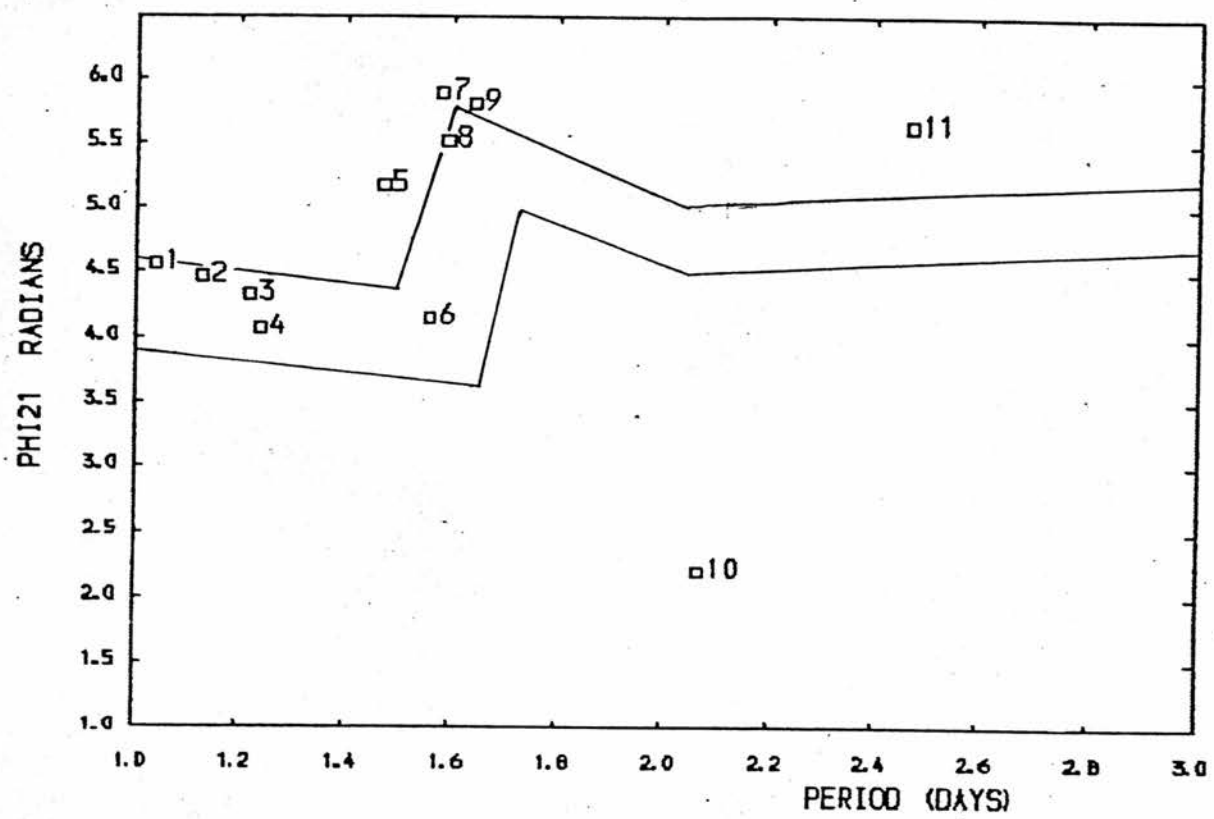

Fig. 5.9: φ_{21} versus period for the models of RCRS. Here, the squares refer to the models, and the envelope has been sketched in for comparison of the observed stars with the models.

Now, points 10 and 11 seem to cause a problem, since neither of them lies near the envelope of the observed stars. Examination of RCRS reveals that both of the models corresponding to these points were given rather high luminosities and low effective temperatures for stars of their periods. The object here was to make the light curves of these stars represent the prominent bumps which are sometimes present on the rising branch of stars with periods between 1.8 - 2.2 days.

The opinion of the author of this thesis, however, is that the amplitude of the pre-maximum bump of model 11 is much too large for a star in this period range, whilst model 10 has a rather peculiar light curve which could account for its position in fig. 5.9. The light curves thus contain exaggerated features which are not found in other models at the same period.

The large pre-maximum bump in model 11 might explain the position of point 11 in the φ_{21} diagram and is in fact verified by the position of the corresponding point in fig. 5.11 (the R_{21} resonance diagram for the models). If the pre-maximum bump in this model is too large and the bump on the ascending branch is related to the amplitude of the

first harmonic A_1, then we ought to expect the quantity A_2/A_1 to be larger than normal. This is in fact what happens, since in fig. 5.11, point 11 does lie well above the envelope of the observed stars.

We now move on to discuss the φ_{31} resonance diagram in fig. 5.10. Here, we find that this plot is very similar to that displayed in fig. 5.9 . Once more, there is a decrease in φ_{31} at low periods and a rapid rise at a period of about 1.6 days. After about two days, the curve flattens off, with points 10 and 11 having similar values of φ_{31} .

Again we note the resemblance between this diagram and the φ_{31} diagram of the observed stars, once more denoted by the envelope in fig 5.10. Particular attention should be paid to the region of the resonance, at periods of about 1.6 days, where all points lie within the envelope. However, several points lie outside the envelope on both sides of the resonance. At periods greater than about two days, points 10 and 11 lie well above the observed stars and this can possibly be explained by the previous argument that the models represented by these points behave unexpectedly.

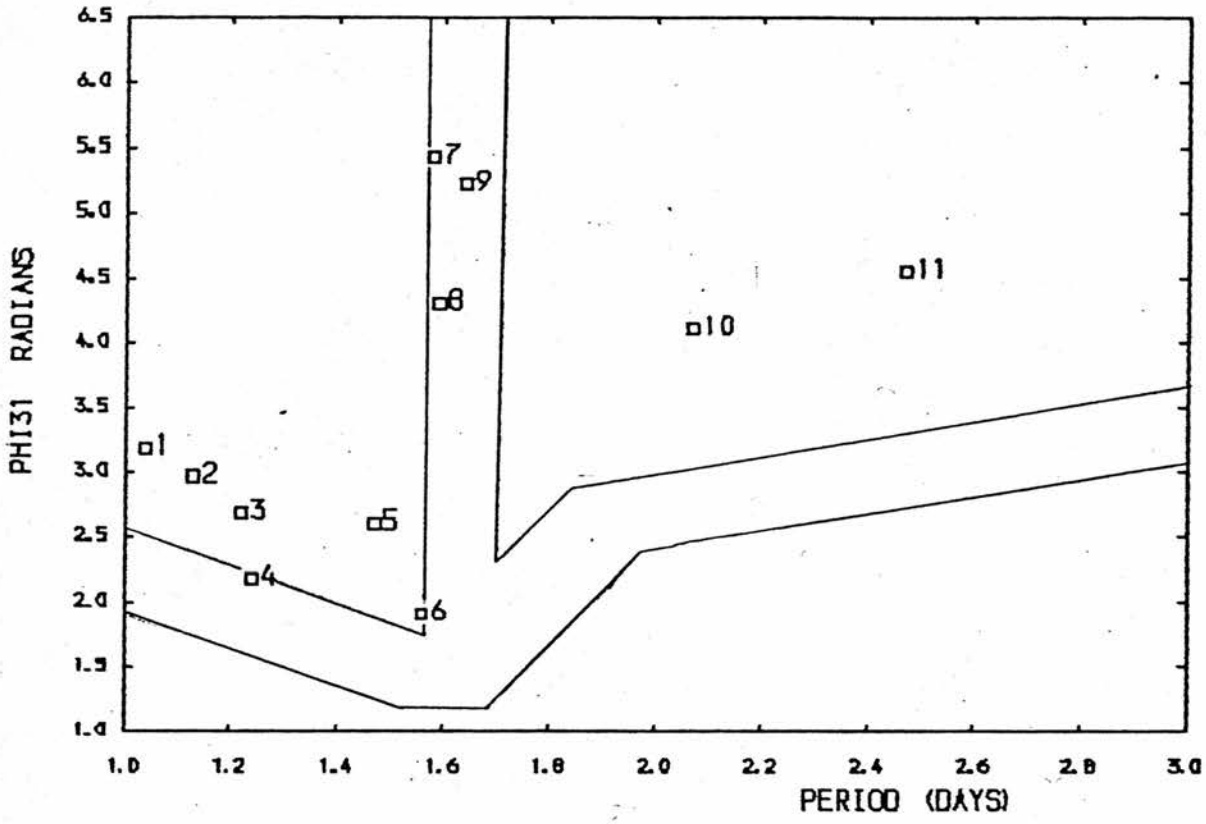

Fig. 5.10: φ_{31} versus period for the models. Notation is the same as in figure 5.9.

To the left of the diagram, we find that models 1, 2 and 3 also lie outside the observational envelope. Unfortunately, there do not appear to be any satisfactory reasons for this discrepancy between the theoretical and observed φ_{31} resonance diagrams. One possible explanation might be that the parameters of mass, temperature and luminosity have not been optimally chosen for these models, although it is difficult to see why the values of φ_{21} are not affected in a similar manner.

We continue now with a discussion of the R_{i1} resonance diagrams (i = 2 or 3) in figs. 5.11 and 5.12. The first of these shows R_{21} plotted against period, whilst the latter shows R_{31} against period. Both diagrams show the same basic structure for periods P less than 2.0 days, with a rapidly decreasing value of R_{i1} for $P \lesssim 1.3$ days, and for periods $\gtrsim$ 1.4 days, R_{i1} increases. This decrease/increase of these quantities is reminiscent of the corresponding resonance diagrams of the observed stars at longer periods. In fact a comparison of the theoretical diagrams in figs. 5.11 and 5.12 with their respective observational envelope reveals that these former curves would fit very nicely if one pushed them slightly to the right.

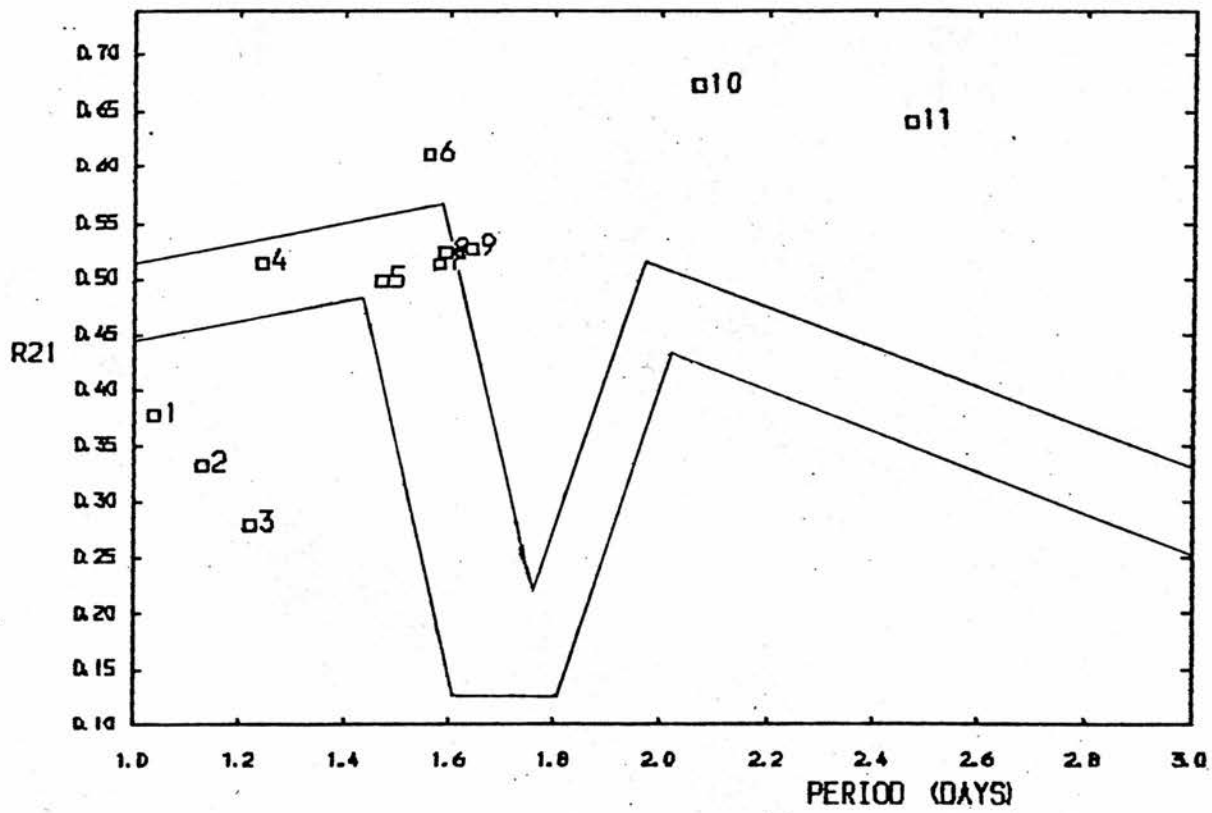

Fig. 5.11: R_{21} versus period for the models.

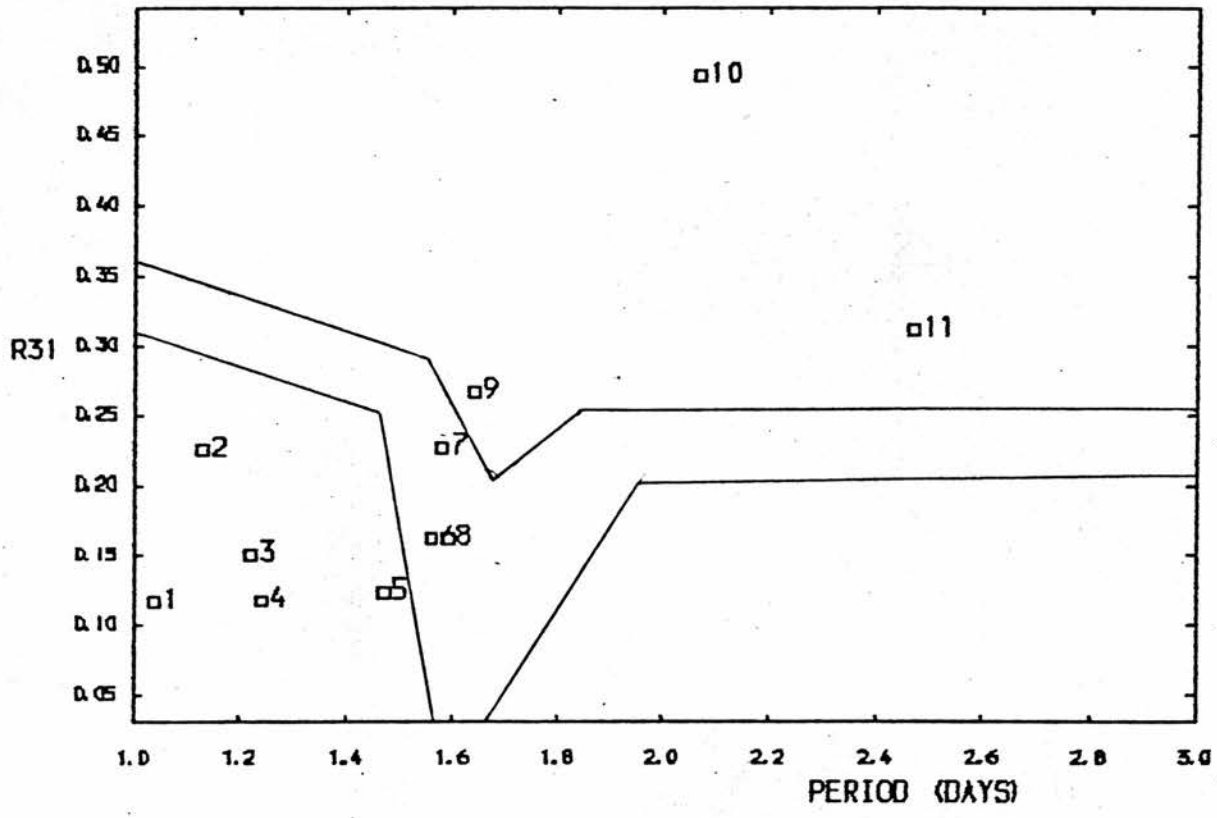

Fig. 5.12: R_{31} versus period for the models.

Thus, the resonance in the models seems to occur at a period of between 1.3 - 1.4 days when one considers the theoretical R_{21} and R_{31} resonance diagrams, this being about 0.3 periods earlier than in the observed stars.

We suggested earlier that the φ_{31} diagram for the models differed from that of the observed stars because of a non-optimal choice of mass, temperature or luminosity. The problem with the R_{i1} diagrams tends to confirm this view. The situation is analogous to similar problems encountered in the resonance diagrams of the classical Cepheids (Simon and Davis, 1983), where the diagrams of the models were compared with those of the observed stars.

Two sets of models were examined in this case, the first used the Carson (1976) opacities and were computed by Vermury and Stothers (1978) and the second set were computed by Adams, Castor and Davis (1980) using the Los Alamos opacities. In the latter case, the models follow the observed stars in the resonance diagrams at shorter periods, but tend to fall away as the period increases. The Vermury-Stothers models, on the other hand, never really follow the observed stars at all, particularly in the φ_{21} diagram for the velocity data, and the R_{21} diagram for

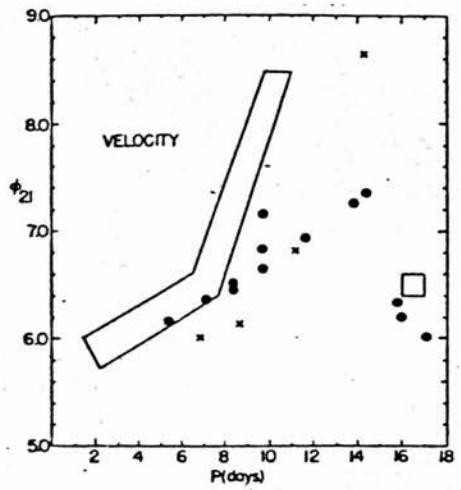

Fig. 5.13: φ_{21} versus period for models of classical Cepheids. This diagram uses velocity data of the Vermury-Stothers models (crosses) and the Los Alamos models (circles). The envelope indicates the domain of the observed classical Cepheids.

(Figure 2 of Simon and Davis, 1983)

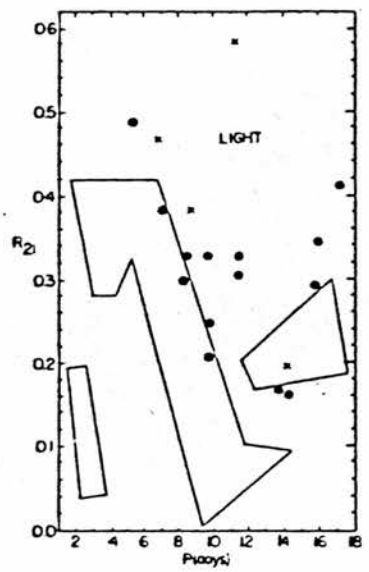

Fig. 5.14: R_{21} versus period for light, with similar notation to the above diagram.

(Figure 5 of Simon and Davis, 1983)

light (fig. 5.13 and 5.14). However, the shapes of the theoretical resonance diagrams for the Vermury-Stothers models are very similar to those of the observations. All that was required, therefore, was to "push" the resonance in the models over to the left by about four days. This was done by Carson and Stothers (1984b) by judiciously selecting the physical parameters and computing models which included convection. The theoretical resonance diagrams now resemble those of the observed classical Cepheids to a very reasonable extent.

Unfortunately, however, the BL Herculis models are not as straightforward as those of the classical Cepheids, since they are very difficult to compute. However, it is possible to compute some BL Herculis models which are comparable to the observed stars and the techniques for making these comparisons are there in the form of the Simon and Lee resonance diagrams.

We end this chapter by suggesting that just as in the Vermury-Stothers models, the Carson and Stothers BL Herculis models do appear to have a Hertzsprung progression, and a transition of bumps occurs at about 1.6 if one considers the φ_{21} and φ_{31} resonance diagrams. However, as suggested

previously, comparisons of the theoretical R_{21} and R_{31} resonance diagrams indicate that the resonance occurs at a lower period. The models must thus be altered in some way so that the resonance complies with that of the observed stars for all four quantities φ_{i1} and R_{i1} (i = 2 or 3).

CHAPTER 6. SUMMARY AND CONCLUSIONS.

(6.1) Introduction.

In this chapter, we summarise the methods, results and conclusions of previous chapters and give some suggestions for further work in the area. Section (6.3) contains a summary of chapter 3, in which we discussed, among other things, the Hertzsprung progression in population II variables. In section (6.4), the work of chapter 5 is briefly discussed and finally, in section (6.6), we consider the main conclusions of this thesis and include a discussion on how our results could be improved.

We begin, however, with a summary of the properties of short-period population II Cepheids.

(6.2) Properties of Population II Cepheids

In chapter 2, we discovered that the population II variables which have periods in the range of one to three days should be occupied by only one type of star, the BL Herculis variables, named after the prototype of their

class.

Evolutionary considerations reveal that the masses of these stars must lie in the range $0.5 \leqslant M/M_{\odot} \leqslant 0.8$, with temperatures $5500\ K \leqslant T_e \leqslant 6500\ K$, where the lower limit on the temperature, corresponding to the red-edge of the BL Herculis instability strip, is rather more difficult to establish than the upper one.

We also discovered that luminosities lie in the range $100 \leqslant L/L_{\odot} \leqslant 350$, these limits being imposed on both evolutionary and observational grounds.

We also found in chapter 2 that the helium content of these stars lies in the range $0.2 \leqslant Y \leqslant 0.35$ and we have decided on $Y = 0.25$.

Compositions then have been taken to be $(X,Y,Z) = (0.745, 0.25, 0.005)$.

(6.3) Hertzsprung Progression in Population II Cepheids.

We have discovered that many pulsating stars show secondary bumps in their light curves and this may be due to two physical effects.

The first is that a pressure wave produced in either the helium or hydrogen ionisation zones reflects off the interior core and reaches the surface as a secondary maximum in the light or velocity curve. This is known as the Christy (1968) echo phenomenon.

The second effect, which is possibly related to the first, is based on elementary mechanics. Discussed initially by Simon and Schmidt (1976), it assumes the star to be undergoing pulsation in several normal modes, with natural frequencies ν_i $(i = 0,\ldots,n)$, one of which, the fundamental mode ν_0 say, is a driving frequency. If one of the harmonics of ν_0 is close to that of a normal mode, then the normal mode will be in resonance with this harmonic. Simon and Schmidt suggested that it is the first harmonic with frequency $2\nu_0$ which is driving the second overtone of frequency ν_2. Here, we have, at resonance, the period ratio $\pi_2/\pi_0 = 0.5$ and the secondary bump in the light

curves will be indistinguishable from maximum light.

We thus have a Hertzsprung progression, in which stars with $0.5 \lesssim \pi_1/\pi_0 \lesssim 0.53$ show bumps on the descending branch and stars with $0.46 \lesssim \pi_1/\pi_0 \lesssim 0.50$ show bumps on rising light.

In this work, we have discussed a set of population II variable stars, data for which has been published by Kwee and Diethelm (1984). All of the stars in KD are assumed to be BL Herculis stars, that is, population II variables which have periods between one and three days, according to the definition in chapter 2.

We discussed the light curves of these stars in chapter 3 and attempted to discover if a Hertzsprung progression was present. One conclusion to be drawn from this chapter was that a study of the light curves, or a Fourier fit to the light curves, is extremely difficult, due to the poor data and coverage of the light curves of such faint objects. However, we did find that a subjective view on the part of the author revealed that a Hertzsprung progression does seem to exist in BL Herculis stars, with a transition of bump from descending to ascending branch occurring at a period of

greater than about 1.66 days.

As has been often stated in this thesis, a qualitative discussion of light curves of population II variables is unsatisfactory and the results of chapter 3 perhaps should not be treated as definitive without further corroboration. However, the conclusions so far presented do agree very well with those of chapter 5 and which we give below.

(6.4) Further evidence for a Hertzsprung Progression

The methods of Simon and Lee (1981) were applied to our stars in order to establish with greater certainty if there is a Hertzsprung progression in BL Herculis stars.

Plots of the quantities φ_{i1} and R_{i1} (i = 2 or 3) against period reveal that a Hertzsprung progression exists in observed stars. The techniques for describing the progression are now quantitative as opposed to the qualitative arguments of chapter 3. Much of the subjective criticism is thus removed and we can conclude with more conviction that a transition of bumps occurs at a period of around 1.60 - 70 days, in good agreement with the results presented in the previous section.

We also discussed in chapter 5 an analysis of the models of Carson and Stothers (1982). Here, the object was to compare the models with observed stars, using the techniques of Simon and Lee. The following conclusions were drawn:

1) The models show a Hertzsprung progression of bumps when one considers the φ_{21} , φ_{31} , R_{21} and R_{31} resonance diagrams.

2) The φ_{i1} diagrams show a resonance in the expected range. Here, the important conclusions to make are that both the general shape of the curves and the fact that the resonance occurs at about 1.6 days agrees well with the observed stars.

3) A comparison of the theoretical and observational R_{i1} diagrams reveals that the curves are very similar in general shape, but that the resonance in the models occurs about 0.3 periods earlier than in the observed stars.

It was suggested that better agreement might result if the parameters of mass, luminosity and temperature were varied in the models. We also pointed out that no convection was included in the models.

(6.5) Results of Fourier Analysis.

In this section, we review the results of the Fourier analysis of the data of Kwee and Diethelm (1984). In table (6.1), we present, in the first three columns, the name of the star, its period and the number of observations. Column four shows the order of fit and thereafter we give the time-average computed magnitude <m> and the amplitudes A_i and phases φ_i (i=1 - 4). Below each of these is a number in brackets corresponding to the error in that quantity. The final column denotes the standard deviation of fit multiplied by 100.

One notices that the first amplitude A_1, corresponding to the amplitude of the fundamental mode, is the principal component in all our stars, as expected in population II Cepheids in this period range.

Table 6.2 shows a second set of results of our analysis. Here, we show the name of the star followed by the quantities maximum and minimum magnitude, denoted by f_{min} and f_{max}, and the amplitude $f_{max} - f_{min}$, all of which are computed from the fit. In column 5, we give the asymmetry $\mathfrak{S}$. This quantity can be of importance in

Table 6.1: Fourier Amplitudes and Phases for the Stars in the Survey of KD.

STAR	PERIOD	ND	N	<m>	A_1	A_2	A_3	A_4	φ_1	φ_2	φ_3	φ_4	$SD_{N=100}$
V716 Oph	1.1159	49	8	12.111	0.505	0.241	0.159	0.100	-0.375	3.252	0.777	4.607	2.676
				0.004	0.006	0.006	0.006	0.006	0.011	0.024	0.037	0.061	
V527 Ser	1.2589	68	8	14.893	0.422	0.102	0.050	0.028	1.451	0.944	1.427	-0.678	6.756
				0.009	0.012	0.012	0.012	0.012	0.029	0.121	0.250	0.448	
VX Cap	1.3276	74	7	14.986	0.486	0.243	0.142	0.104	3.397	-1.361	-0.050	1.471	4.597
				0.006	0.009	0.010	0.009	0.008	0.019	0.033	0.061	0.085	
HQ Cra	1.4150	40	6	14.746	0.408	0.108	0.026	0.032	2.596	2.732	1.378	1.335	3.511
				0.006	0.008	0.009	0.009	0.008	0.021	0.077	0.312	0.269	
V2022 Ser	1.5335	34	5	13.547	0.332	0.092	0.064	0.061	1.578	1.194	-0.295	-1.261	3.908
				0.010	0.015	0.013	0.011	0.013	0.046	0.188	0.216	0.195	
V745 Oph	1.5955	40	6	13.219	0.364	0.125	0.017	0.024	3.977	-0.390	-0.663	1.237	2.480
				0.004	0.006	0.006	0.006	0.006	0.017	0.050	0.355	0.242	
V971 Aql	1.6245	45	7	11.994	0.321	0.071	0.056	0.082	1.401	1.262	-0.554	-0.926	2.117
				0.003	0.004	0.005	0.005	0.005	0.015	0.066	0.082	0.057	
DU Ara	1.6405	54	8	12.130	0.299	0.042	0.048	0.049	-0.214	4.110	0.735	-1.212	2.795
				0.004	0.006	0.006	0.006	0.006	0.020	0.140	0.122	0.117	
VZ Aql	1.6653	33	4	13.642	0.370	0.083	0.065	0.064	1.922	2.839	1.259	1.963	8.744
				0.017	0.024	0.024	0.023	0.023	0.065	0.281	0.373	0.366	
V839 Ser	1.8272	51	6	14.917	0.349	0.080	0.076	0.064	1.585	1.951	0.715	0.374	6.092
				0.009	0.014	0.013	0.013	0.012	0.035	0.159	0.169	0.212	
EX Del	2.0467	50	6	12.339	0.315	0.146	0.069	0.037	-0.255	4.165	1.998	0.501	2.127
				0.003	0.004	0.004	0.005	0.005	0.015	0.032	0.067	0.128	
UX Nor	2.3858	41	7	13.678	0.470	0.176	0.108	0.087	2.215	2.830	3.166	3.547	5.234
				0.009	0.012	0.012	0.012	0.012	0.026	0.070	0.117	0.143	
V465 Oph	2.8417	40	8	13.480	0.487	0.154	0.113	0.067	2.892	4.402	-0.708	0.374	3.740
				0.007	0.009	0.009	0.009	0.009	0.020	0.062	0.082	0.136	

Table 6.2: Light Curve Parameters for the Observed Stars of KD.

STAR	f_{max}	f_{min}	$f_{max}-f_{min}$	σ	m_{max}	m_{min}	$\langle m_{oi} \rangle$	φ_b
V716 Oph	12.61	11.18	1.42	0.16	12.61	11.21	12.09	0.79
V527 Sgr	15.32	14.40	0.92	0.40	15.43	14.40	14.97	-
VX Cap	15.52	14.14	1.39	0.17	15.51	14.17	14.90	0.71
HQ Cra	15.18	14.19	0.99	0.68	15.19	14.18	14.75	0.48
V2022 Sgr	13.89	13.00	0.90	0.55	13.94	13.01	13.53	0.37
V745 Oph	13.62	12.70	0.92	0.51	13.63	12.71	13.25	0.33
V971 Aql	12.38	11.49	0.89	0.51	12.38	11.52	11.98	0.19
DU Ara	12.46	11.71	0.75	0.52	12.46	11.73	12.12	0.19
VZ Aql	14.11	13.20	0.91	0.69	14.11	13.18	13.58	0.14
V839 Sgr	15.29	14.44	0.85	0.48	15.33	14.50	14.91	-
EK Del	12.73	11.90	0.83	0.30	12.74	11.91	12.36	0.72
UX Nor	14.15	12.94	1.22	0.32	14.18	12.98	13.73	0.60
V465 Oph	14.06	12.95	1.11	0.15	14.00	12.90	13.45	0.55

distinguishing the centre of the Hertzsprung progression, since at the transition period, the light curve should be symmetric, as discussed in chapter 3. Asymmetry in this case has been computed from the fit, thus:

$$\hat{\delta} = \frac{\varphi_{max} - \varphi_{min}}{1 - \varphi_{max} + \varphi_{min}}$$

Where, φ_{max} is the phase at maximum of the fit,

φ_{min} " " " " minimum " " "

In columns 6 and 7, we show the maximum magnitude m_{max}, minimum magnitude m_{min} and average magnitude $\langle m_{o_i} \rangle$, given by

$$\langle m_{o_i} \rangle = \frac{\sum_{i=1}^{ND} m_{o_i}}{ND}$$

Here, m_{o_i} is the magnitude of the star at time t_i,

ND is the number of observations.

Finally, in table 6.2, we show the phase of bumps in the observed stars, denoted by φ_b.

In table 6.3, we give the phase differences φ_{21} and φ_{31} and the amplitude ratios R_{21} and R_{31} for the models. The error is shown in brackets below each quantity.

Table 6.3: Phase Differences and Amplitude Ratios for the Models of RCRS.

	STAR	φ_{21} (ERROR)	φ_{31} (ERROR)	R_{21} (ERROR)	R_{31} (ERROR)
1	BXD	4.562	3.188	0.377	0.177
		(0.069)	(0.214)	(0.024)	(0.022)
2	BFS	-1.822	2.962	0.333	0.225
		(0.095)	(0.141)	(0.030)	(0.028)
3	XXZ	-1.964	2.678	0.275	0.151
		(0.102)	(0.187)	(0.026)	(0.025)
4	CEH	-2.221	-4.101	0.514	0.117
		(0.056)	(0.181)	(0.023)	(0.020)
5	SWT	-1.114	2.601	0.498	0.124
		(0.050)	(0.152)	(0.019)	(0.017)
6	839	-2.131	1.917	0.610	0.162
		(0.037)	(0.097)	(0.017)	(0.015)

Table 6.3 (contd.)

	STAR	φ_{21} (ERROR)	φ_{31} (ERROR)	R_{21} (ERROR)	R_{31} (ERROR)
7	745	-0.398	-0.870	0.513	0.226
		(0.050)	(0.096)	(0.020)	(0.018)
8	NWL	-0.769	-1.982	0.524	0.162
		(0.079)	(0.198)	(0.032)	(0.029)
9	VZA	-0.479	-1.073	0.527	0.266
		(0.056)	(0.098)	(0.023)	(0.021)
10	UYE	-4.083	-8.462	0.672	0.492
		(0.226)	(0.323)	(0.111	(0.104)
11	YZC	-6.938	-8.019	0.639	0.311
		(0.088)	(0.150)	(0.040)	(0.036)

(6.6) General Conclusions.

We finally conclude this thesis by summarising the results of chapters 3 and 5 and making suggestions for further work in this field.

We have seen that a Hertzsprung progression exists both in the observed BL Herculis stars and in the models. We have also suggested that the period of resonance lies in the range $1.6 \lesssim P \lesssim 1.7$ days in the observed stars with a reasonable degree of certainty, this conclusion being formulated on the basis of two independent methods. The first involved a subjective analysis of the light curves by the author and the second, more objective description, used the quantitative methods of Simon and Lee (1981). Both approaches give comparable results.

The results in both cases may improved upon in two major ways. Firstly, more accurate photometry of the stars in Kwee and Diethelm is required. At the present time, this may not be viable, but when it is, the qualitative description of the light curves will certainly be ameliorated. Further, since the second method of describing the Hertzsprung progression relies on the data, although to a lesser extent than the previous method, this also ought to improve with a reduction in noise in the data, and so should enable a more accurate estimation of the R_{i1} and φ_{i1}. Because of the poor photometry, the calculation of higher amplitude ratios and phase differences ($i \gtrsim 4$) is not

feasible, since, unpublished results show a great deal of scatter in the resonance diagrams corresponding to these quantities.

The second way in which we can refine our results is by analysing the data of a greater number of stars, particularly those with periods of around 1.6 days. In this way, we can be certain of positioning the transition period more accurately.

Further theoretical work may also be undertaken. For example, the problem of why the bump should occur in classical Cepheids and BL Herculis stars and not, for instance, in W Virginis stars, has not yet been solved. We must also produce a reasonable theory of the bump mechanism. Whitney (1983) appears to be working in approximately the correct area, although many problems are yet to be solved. For example, Whitney's modelling of pulses by acoustic wave cannot explain why it is the P_2/P_0 resonance which is selected, nor can it explain the actual mechanism which produces the Christy pulse. The model is also rather basic in that it does not take into account physical effects, for example, convection or non-adiabaticity in the star.

We finally suggest that the techniques of Simon and Lee (1981) should encourage more accurate modelling of the BL Herculis stars and, just as with classical Cepheids, many of the barriers between the theory and observation of these stars may be removed.

REFERENCES

Adams, T.F., Castor, J.L., and Davis, C.G.: 1980, in Current Problems in Stellar Instabilities., ed. D.Fischel, J.R.Lesh, and W.M.Sparks (N.A.S.A. TM 80625), p. 175.

Antonelli, E., and Mantegazza, R.: Astron. Astrophys., 133, 52.

Baade, W.: 1952, Trans. I.A.U., 8, 397.

Baker, N., and Kippenhahn, R.: 1965, Ap.J., 142, 868

Bevington, P.R.: 1974, Data Reduction and Error Analysis for the Physical Sciences., (McGraw-Hill).

Bohm-Vitense, E.: 1973, Astron. Astrophys., 24, 447.

Bohm-Vitense, E., and Nelson, G.D.: 1976, Ap.J., 210, 741.

Bridger, A.: 1983, Thesis, University of St. Andrews, Scotland.

Carson, T.R.: 1976, Ann. Rev. Astron. Astrophys., 14, 95.

Carson, T.R.: 1984, private communication.

Carson, T.R., and Stothers, R. (RCRS): 1982, Ap.J., 259, 740.

---------- : 1984a, private communication.

---------- : 1984b, Proc. 25th Liege International Astrophys. Colloq., p.29.

Carson, T.R., Stothers, R., and Vermury, S.K. (CSV): 1981, Ap.J., 244, 230.

Christy, R.F.: 1968, Quart. J.R.A.S., 9, 13.

Cox, A.N.: 1980, Ann. Rev. Astron. Astrophys., 18, 15.

Cox, A.N., and Tabor, J.E.: 1976, Ap.J. Suppl. Ser., 31, 271.

Deeming, T.J.: 1975, Astrophys. and Sp. Sci., 36, 137.

Demers, S., and Harris, W.E.: 1974, A.J., 79, 627.

Deupree, R.G.: 1977, Ap.J., 211, 509.

Diethelm, R.: 1983, Astron. Astrophys., 124, 108.

Faulkner, D.J.: 1977, Ap.J., 216, 49.

Fricke, K., Stobie, R.S., and Strittmatter, P.A.: 1972, Ap.J., 171,593.

Gieren, W.: 1982, Pub. A.S.P.,94, 960.

Gingold, R.A.: 1976, Ap.J., 204, 116.

Hertzsprung, E.: 1926, B.A.N., 3, 115.

Hodson, S.W., Cox, A.N., and King, D.S. (HCK): 1982, Ap.J., 253, 260.

Iben Jr., I.: 1972, in The Evolution of Population II Stars., ed. A.G.D. Philip (Albany, NY: Dudley Observatory), p.1.

King, D.S., Cox, A.N., and Hodson, S.W.: 1981, Ap.J., 244, 242.

Kraft, R.P.: 1972, in The Evolution of Population II Stars., ed. A.G.D. Philip (Albany, NY: Dudley Obsevatory), p.69.

Kwee, K.K.: 1967, B.A.N. Suppl. Ser., 2, 97.

Kwee, K.K., and Braun, L.D.: 1967, B.A.N. Suppl. Ser., 2, 77.

Kwee, K.K., and Diethelm, R. (KD): 1984, Astron. Astrophys. Suppl. Ser., 55, 77

Petersen, J.O.: 1981, Astron. Astrophys., 96, 146.

Petersen, J.O.: 1984, preprint.

Schwarzschild, M., and Harm, R.: 1965, Ap.J., 142, 855.

Schwarzschild, M., and Harm, R.: 1970, Ap.J., 160, 341.

Simon, N.R.: 1977, Ap.J., 217, 160.

Simon, N.R., and Davis, C.G.: 1983, Ap.J., 266, 787.

Simon, N.R., and Lee, A.S. (SL): 1981, Ap.J., 248, 291.

Simon, N.R., and Schmidt, E.G.: 1976, Ap.J., 205, 162.

Skillen, I.: 1984, private communication.

Smith, H.A., Jacques, J., Lugger, P.M., Deming, D., and Butler, D.: 1978, Pub. A.S.P., 90, 422.

Stellingwerf, R.F.: 1982a, Ap.J., 262, 330.

---------- : 1982b, Ap.J., 262, 339.

---------- : 1983a, preprint.

---------- : 1983b, preprint.

Stobie, R.S.: 1969a, M.N.R.A.S., 144, 461.

-------- : 1969b, M.N.R.A.S., 144, 485.

-------- : 1973, Observatory, 93, 111.

Struve, O., and Zebergs, V.: 1962, in Astronomy of the 20th Century., (Macmillan, New York), p.398.

Sweigart, A.V., and Gross, P.G.: 1976, Ap.J. Suppl. Ser., 32, 367.

Vermury, S.K., and Stothers, R.: 1978, Ap.J., 225, 939.

Wallerstein, G., and Cox, A.N.: 1984, preprint.

Weigert, A.: 1966, Zs.f.Ap., 64, 395. Whitney, C.S.: 1983, Ap.J., 274, 830.

Worrell, J.K.: 1984a, private communication.

Worrell, J.K.: 1984b, private communication.

APPENDIX 1.

BL HERCULIS MODELS.

(A1.1) Introduction.

In this appendix, we briefly discuss some of the models which have been computed to represent the stars in the survey of KD.

Using these models, a bump phase-radius law is derived and the bump masses of the observed stars are estimated using the methods of CSV and Petersen (1984).

To begin with, however, we discuss the linear pulsation code which has been used to compute the models.

(A1.2) Linear Pulsation Code.

Models of the stars in KD have been computed using the linear pulsation code of Worrell (1984b). The code is able to compute up to five non-adiabatic and twenty adiabatic eigenvalues for a set of parameters of mass, temperature, luminosity and chemical composition, using the opacity tables of Christy, Stellingwerf or a cubic spline

interpolation of the Carson opacity tables (Carson, Stothers and Vermury, 1981). The code can compute models with a varying number of zones, from 100 - 300, depending on what is required by the user.

(A1.3) The Models.

According to the discussion in chapter 2, a grid of models has been made, with the following parameters:

$$0.5 \leqslant M/M_{\odot} \leqslant 0.8$$

$$5500\,K \leqslant T_e \leqslant 6500\,K$$

$$100 \leqslant L/L_{\odot} \leqslant 350$$

The grid thus consists of 264 models, with periods between about one and eight days.

We now wish to compute a set of BL Herculis models from this grid, and this can be done by formulating a period - (mass, luminosity, temperature) (PMLT) law, by least-squares fitting the data to the following equation and calculating the exponents α, β and γ, and the constant term κ:

$$P = k(M/M_{\odot})^{\alpha} (L/L_{\odot})^{\beta} T_e^{\gamma} \qquad (A1.1)$$

Here, we find that

$$\alpha = -0.74$$

$$\beta = 0.88$$

$$\gamma = -3.52$$

$$\ln k = 28.43$$

Thus,

$$P = k(M/M_{\odot})^{-0.74} (L/L_{\odot})^{0.88} T_e^{-3.52} \qquad (A1.2)$$

These results are in good agreement with CSV, who choose $\alpha = -0.75$, $\beta = 0.87$ and $\gamma = -3.5$.

Once the PMLT law has been derived, periods of the stars in KD are input into equation (A1.2) and for each combination of two parameters (mass and temperature, luminosity and mass, temperature and luminosity) the third is calculated.

In this way, a grid of models is acquired for each star with parameters of mass, luminosity and temperature within the range selected earlier. All models have been computed with the chemical composition (Y,Z) = (0.25, 0.005) and an interpolated opacity table of the Carson opacities, found in CSV. Each model is also computed with three eigenvalues, corresponding to the fundamental mode and first and second overtones.

The models are listed in table A1.1, where the first column denotes the name of the star, the second column the period and the third and fourth columns the period ratios Π_1/Π_0 and Π_2/Π_0, respectively. Thereafter, we show the mass, temperature and luminosity in columns 5, 6 and 7.

By computing this large set of models, the author hopes that the data provided will be of use to other authors, for example, in solving the problem of the comparison of non-linear models with observation, as discussed in chapter 5 (section 5.5).

Table A1.1: Linear Models of BL Herculis Stars.

STAR	PERIOD	π_1/π_0	π_2/π_0	$M/M_\odot$	T_e/K	$L/L_\odot$
V716 Oph	1.123	0.71	0.54	0.70	6500.0	105.2
	1.122	0.71	0.54	0.70	6423.1	100.0
	1.124	0.72	0.54	0.80	6300.0	103.2
	1.125	0.72	0.55	0.80	6400.0	110.3
	1.126	0.72	0.55	0.80	6500.0	117.8
	1.123	0.72	0.54	0.80	6253.9	100.0
	1.123	0.72	0.54	0.77	6300.0	100.0
	1.122	0.71	0.54	0.71	6400.0	100.0
	1.121	0.71	0.53	0.66	6500.0	100.0
V527 Sgr	1.260	0.70	0.52	0.60	6500.0	105.9
	1.260	0.70	0.52	0.60	6412.9	100.0
	1.263	0.71	0.53	0.70	6300.0	105.7
	1.263	0.71	0.53	0.70	6400.0	113.0
	1.264	0.71	0.53	0.70	6500.0	120.7
	1.261	0.71	0.53	0.70	6218.3	100.0
	1.261	0.71	0.53	0.80	6100.0	103.2
	1.264	0.71	0.53	0.80	6200.0	110.6
	1.266	0.71	0.54	0.80	6300.0	118.4
	1.267	0.71	0.54	0.80	6400.0	126.6
	1.268	0.71	0.54	0.80	6500.0	135.2
	1.260	0.71	0.53	0.80	6054.5	100.0
	1.260	0.71	0.53	0.77	6100.0	100.0
	1.262	0.71	0.53	0.71	6200.0	100.0
	1.261	0.71	0.52	0.66	6300.0	100.0
	1.261	0.70	0.52	0.61	6400.0	100.0
	1.259	0.70	0.52	0.56	6500.0	100.0
VX Cap	1.328	0.70	0.52	0.60	6400.0	105.3
	1.328	0.70	0.52	0.60	6500.0	112.5
	1.328	0.70	0.51	0.60	6322.1	100.0
	1.329	0.71	0.52	0.70	6200.0	104.9
	1.331	0.71	0.52	0.70	6300.0	112.3
	1.332	0.71	0.52	0.70	6400.0	120.1
	1.332	0.71	0.53	0.70	6500.0	128.2
	1.328	0.70	0.52	0.70	6130.2	100.0
	1.327	0.71	0.53	0.80	6000.0	102.2
	1.330	0.71	0.53	0.80	6100.0	109.7
	1.332	0.71	0.53	0.80	6200.0	117.5

VX Cap	1.334	0.71	0.53	0.80	6300.0	125.8
	1.335	0.71	0.53	0.80	6400.0	134.5
	1.336	0.71	0.54	0.80	6500.0	143.6
	1.326	0.71	0.53	0.80	5968.7	100.0
	1.327	0.71	0.53	0.78	6000.0	100.0
	1.329	0.71	0.52	0.72	6100.0	100.0
	1.329	0.70	0.52	0.66	6200.0	100.0
	1.328	0.70	0.51	0.61	6300.0	100.0
	1.328	0.70	0.51	0.56	6400.0	100.0
	1.326	0.70	0.51	0.52	6500.0	100.0
HQ Cra	1.410	0.69	0.50	0.50	6500.0	103.6
	1.412	0.69	0.50	0.50	6445.3	100.0
	1.416	0.70	0.51	0.60	6300.0	106.0
	1.415	0.70	0.51	0.60	6400.0	113.3
	1.415	0.70	0.51	0.60	6500.0	121.0
	1.415	0.69	0.51	0.60	6214.6	100.0
	1.415	0.70	0.52	0.70	6100.0	105.3
	1.416	0.70	0.52	0.70	6200.0	112.8
	1.418	0.70	0.52	0.70	6300.0	120.8
	1.418	0.70	0.52	0.70	6400.0	129.1
	1.418	0.70	0.52	0.70	6500.0	137.9
	1.414	0.70	0.51	0.70	6026.0	100.0
	1.411	0.71	0.52	0.80	5900.0	102.4
	1.415	0.71	0.52	0.80	6000.0	110.0
	1.417	0.71	0.53	0.80	6100.0	118.0
	1.419	0.71	0.53	0.80	6200.0	126.4
	1.421	0.71	0.53	0.80	6300.0	135.3
	1.421	0.71	0.53	0.80	6400.0	144.6
	1.422	0.71	0.53	0.80	6500.0	154.4
	1.410	0.71	0.52	0.80	5867.2	100.0
	1.422	0.71	0.53	0.80	6455.6	150.0
	1.411	0.71	0.52	0.78	5900.0	100.0
	1.414	0.70	0.52	0.71	6000.0	100.0
	1.414	0.70	0.51	0.66	6100.0	100.0
	1.415	0.70	0.51	0.61	6200.0	100.0
	1.415	0.69	0.50	0.56	6300.0	100.0
	1.413	0.69	0.50	0.52	6400.0	100.0
	1.421	0.71	0.53	0.77	6500.0	150.0
V2022 Sgr	1.530	0.68	0.50	0.50	6400.0	106.4
	1.528	0.69	0.50	0.50	6500.0	113.6
	1.532	0.68	0.49	0.50	6307.5	100.0
	1.533	0.69	0.50	0.60	6100.0	101.3
	1.533	0.69	0.50	0.60	6200.0	108.5

V2022 Sgr	1.533	0.69	0.50	0.60	6300.0	116.1
	1.533	0.69	0.51	0.60	6400.0	124.2
	1.532	0.69	0.51	0.60	6500.0	132.6
	1.533	0.69	0.50	0.60	6081.7	100.0
	1.529	0.70	0.51	0.70	5900.0	100.2
	1.532	0.70	0.51	0.70	6000.0	107.6
	1.533	0.70	0.51	0.70	6100.0	115.4
	1.535	0.70	0.51	0.70	6200.0	123.7
	1.536	0.70	0.51	0.70	6300.0	132.4
	1.536	0.70	0.52	0.70	6400.0	141.5
	1.535	0.70	0.52	0.70	6500.0	151.1
	1.529	0.70	0.51	0.70	5897.2	100.0
	1.536	0.70	0.52	0.70	6488.5	150.0
	1.526	0.70	0.52	0.80	5800.0	104.4
	1.529	0.70	0.52	0.80	5900.0	112.2
	1.532	0.70	0.52	0.80	6000.0	120.5
	1.535	0.70	0.52	0.80	6100.0	129.3
	1.537	0.70	0.52	0.80	6200.0	138.5
	1.538	0.70	0.52	0.80	6300.0	148.2
	1.539	0.71	0.52	0.80	6400.0	158.5
	1.540	0.71	0.53	0.80	6500.0	169.3
	1.523	0.70	0.52	0.80	5741.8	100.0
	1.538	0.70	0.52	0.80	6317.6	150.0
	1.525	0.70	0.51	0.76	5800.0	100.0
	1.532	0.69	0.50	0.64	6000.0	100.0
	1.533	0.69	0.50	0.59	6100.0	100.0
	1.533	0.69	0.49	0.55	6200.0	100.0
	1.532	0.68	0.49	0.50	6300.0	100.0
	1.537	0.70	0.52	0.75	6400.0	150.0
	1.535	0.70	0.52	0.69	6500.0	150.0
V745 Oph	1.594	0.68	0.49	0.50	6300.0	104.1
	1.592	0.68	0.49	0.50	6400.0	111.3
	1.590	0.68	0.50	0.50	6500.0	118.9
	1.595	0.68	0.49	0.50	6240.6	100.0
	1.596	0.69	0.50	0.60	6100.0	106.0
	1.595	0.69	0.50	0.60	6200.0	113.5
	1.595	0.69	0.50	0.60	6300.0	121.5
	1.594	0.69	0.50	0.60	6400.0	129.9
	1.593	0.69	0.51	0.60	6500.0	138.7
	1.594	0.69	0.49	0.60	6017.2	100.0
	1.591	0.69	0.50	0.70	5900.0	104.8
	1.594	0.69	0.51	0.70	6000.0	112.6
	1.596	0.70	0.51	0.70	6100.0	120.8
	1.597	0.70	0.51	0.70	6200.0	129.4

V745 Oph	1.597	0.70	0.51	0.70	6300.0	138.5
	1.598	0.70	0.51	0.70	6400.0	148.1
	1.597	0.70	0.52	0.70	6500.0	158.1
	1.589	0.69	0.50	0.70	5834.6	100.0
	1.597	0.70	0.51	0.70	6419.7	150.0
	1.583	0.70	0.51	0.80	5700.0	101.4
	1.588	0.70	0.51	0.80	5800.0	109.2
	1.591	0.70	0.51	0.80	5900.0	117.4
	1.595	0.70	0.52	0.80	6000.0	126.1
	1.597	0.70	0.52	0.80	6100.0	135.3
	1.599	0.70	0.52	0.80	6200.0	144.9
	1.600	0.70	0.52	0.80	6300.0	155.1
	1.600	0.70	0.52	0.80	6400.0	165.8
	1.601	0.70	0.52	0.80	6500.0	177.1
	1.582	0.70	0.51	0.80	5680.9	100.0
	1.599	0.70	0.52	0.80	6250.6	150.0
	1.592	0.69	0.50	0.66	5900.0	100.0
	1.593	0.69	0.50	0.61	6000.0	100.0
	1.596	0.68	0.49	0.56	6100.0	100.0
	1.594	0.68	0.49	0.52	6200.0	100.0
	1.599	0.70	0.52	0.77	6300.0	150.0
	1.597	0.70	0.51	0.71	6400.0	150.0
	1.595	0.70	0.51	0.66	6500.0	150.0
V971 Aql	1.625	0.68	0.49	0.50	6200.0	100.0
	1.623	0.68	0.49	0.50	6300.0	106.3
	1.620	0.68	0.49	0.50	6400.0	113.6
	1.618	0.68	0.50	0.50	6500.0	121.3
	1.624	0.68	0.49	0.50	6210.6	100.0
	1.623	0.68	0.49	0.60	6000.0	100.8
	1.625	0.69	0.50	0.60	6100.0	108.2
	1.625	0.69	0.50	0.60	6200.0	115.9
	1.624	0.69	0.50	0.60	6300.0	124.0
	1.623	0.69	0.50	0.60	6400.0	132.6
	1.622	0.69	0.51	0.60	6500.0	141.6
	1.623	0.68	0.49	0.60	5988.3	100.0
	1.620	0.69	0.50	0.70	5900.0	107.0
	1.623	0.69	0.50	0.70	6000.0	114.9
	1.625	0.69	0.51	0.70	6100.0	123.3
	1.626	0.70	0.51	0.70	6200.0	132.1
	1.627	0.70	0.51	0.70	6300.0	141.4
	1.626	0.70	0.51	0.70	6400.0	151.1
	1.626	0.70	0.52	0.70	6500.0	161.4
	1.617	0.69	0.50	0.70	5806.5	100.0
	1.626	0.70	0.51	0.70	6388.8	150.0

V971 Aql	1.611	0.70	0.51	0.80	5700.0	103.5
	1.617	0.70	0.51	0.80	5800.0	111.5
	1.620	0.70	0.51	0.80	5900.0	119.8
	1.624	0.70	0.51	0.80	6000.0	128.7
	1.626	0.70	0.52	0.80	6100.0	138.1
	1.627	0.70	0.52	0.80	6200.0	147.9
	1.629	0.70	0.52	0.80	6300.0	158.3
	1.629	0.70	0.52	0.80	6400.0	169.2
	1.630	0.70	0.52	0.80	6500.0	180.8
	1.610	0.70	0.51	0.80	5653.5	100.0
	1.628	0.70	0.52	0.80	6220.5	150.0
	1.628	0.69	0.51	0.76	5700.0	100.0
	1.617	0.69	0.50	0.70	5800.0	100.0
	1.621	0.69	0.50	0.65	5900.0	100.0
	1.624	0.68	0.49	0.59	6000.0	100.0
	1.625	0.68	0.49	0.55	6100.0	100.0
	1.627	0.70	0.51	0.75	6300.0	150.0
	1.626	0.70	0.51	0.69	6400.0	150.0
	1.624	0.69	0.51	0.64	6500.0	150.0
DU Ara	1.640	0.68	0.48	0.50	6200.0	100.4
	1.638	0.68	0.49	0.50	6300.0	107.4
	1.637	0.68	0.49	0.50	6400.0	114.9
	1.634	0.68	0.50	0.50	6500.0	122.7
	1.640	0.68	0.48	0.50	6194.2	100.0
	1.640	0.68	0.49	0.60	6000.0	102.0
	1.641	0.69	0.49	0.60	6100.0	109.4
	1.641	0.69	0.50	0.60	6200.0	117.2
	1.640	0.69	0.50	0.60	6300.0	125.4
	1.639	0.69	0.50	0.60	6400.0	134.1
	1.638	0.69	0.51	0.60	6500.0	143.2
	1.639	0.68	0.49	0.60	5972.5	100.0
	1.632	0.69	0.50	0.70	5800.0	100.6
	1.636	0.69	0.50	0.70	5900.0	108.2
	1.639	0.69	0.50	0.70	6000.0	116.2
	1.641	0.69	0.51	0.70	6100.0	124.7
	1.642	0.69	0.51	0.70	6200.0	133.6
	1.642	0.70	0.51	0.70	6300.0	142.9
	1.642	0.70	0.51	0.70	6400.0	152.8
	1.642	0.70	0.51	0.70	6500.0	163.2
	1.633	0.69	0.50	0.70	5791.2	100.0
	1.642	0.70	0.51	0.70	6371.9	150.0
	1.628	0.70	0.51	0.80	5700.0	104.7
	1.632	0.70	0.51	0.80	5800.0	112.7
	1.637	0.70	0.51	0.80	5900.0	121.2

DU Ara	1.640	0.70	0.51	0.80	6000.0	130.2
	1.642	0.70	0.51	0.80	6100.0	139.6
	1.644	0.70	0.52	0.80	6200.0	149.6
	1.645	0.70	0.52	0.80	6300.0	160.1
	1.646	0.70	0.52	0.80	6400.0	171.2
	1.646	0.70	0.52	0.80	6500.0	182.8
	1.625	0.70	0.51	0.80	5638.6	100.0
	1.644	0.70	0.52	0.80	6204.1	150.0
	1.632	0.69	0.50	0.69	5800.0	100.0
	1.637	0.69	0.50	0.64	5900.0	100.0
	1.640	0.68	0.49	0.59	6000.0	100.0
	1.640	0.68	0.49	0.54	6100.0	100.0
	1.643	0.70	0.51	0.74	6300.0	150.0
	1.641	0.70	0.51	0.69	6400.0	150.0
	1.638	0.69	0.51	0.63	6500.0	150.0
VZ Aql	1.665	0.68	0.48	0.50	6200.0	102.1
	1.663	0.68	0.49	0.50	6300.0	109.3
	1.661	0.68	0.49	0.50	6400.0	116.9
	1.658	0.68	0.50	0.50	6500.0	124.8
	1.666	0.67	0.48	0.50	6169.3	100.0
	1.664	0.68	0.49	0.60	6000.0	103.7
	1.666	0.68	0.49	0.60	6100.0	111.3
	1.665	0.69	0.50	0.60	6200.0	119.2
	1.665	0.69	0.50	0.60	6300.0	127.6
	1.664	0.69	0.50	0.60	6400.0	136.4
	1.662	0.69	0.51	0.60	6500.0	145.7
	1.664	0.68	0.49	0.60	5948.5	100.0
	1.658	0.69	0.50	0.70	5800.0	102.4
	1.662	0.69	0.50	0.70	5900.0	110.1
	1.664	0.69	0.50	0.70	6000.0	118.2
	1.665	0.69	0.50	0.70	6100.0	126.8
	1.667	0.69	0.51	0.70	6200.0	135.9
	1.667	0.69	0.51	0.70	6300.0	145.4
	1.667	0.70	0.51	0.70	6400.0	155.5
	1.666	0.70	0.51	0.70	6500.0	166.0
	1.657	0.69	0.50	0.70	5767.9	100.0
	1.667	0.70	0.51	0.70	6346.3	150.0
	1.653	0.70	0.51	0.80	5700.0	106.5
	1.658	0.70	0.51	0.80	5800.0	114.7
	1.662	0.70	0.51	0.80	5900.0	123.3
	1.664	0.70	0.51	0.80	6000.0	132.4
	1.667	0.70	0.51	0.80	6100.0	142.0
	1.669	0.70	0.51	0.80	6200.0	152.2
	1.670	0.70	0.52	0.80	6300.0	162.9

VZ Aql	1.670	0.70	0.52	0.80	6400.0	174.1
	1.670	0.70	0.52	0.80	6500.0	185.9
	1.648	0.70	0.51	0.80	5616.0	100.0
	1.668	0.70	0.51	0.80	6179.1	150.0
	1.653	0.69	0.50	0.74	5700.0	100.0
	1.658	0.69	0.50	0.68	5800.0	100.0
	1.662	0.68	0.49	0.63	5900.0	100.0
	1.664	0.68	0.49	0.57	6000.0	100.0
	1.666	0.68	0.48	0.53	6100.0	100.0
	1.667	0.70	0.51	0.79	6200.0	150.0
	1.668	0.70	0.51	0.73	6300.0	150.0
	1.666	0.69	0.51	0.67	6400.0	150.0
	1.663	0.69	0.51	0.62	6500.0	150.0
V839 Sgr	1.830	0.67	0.47	0.50	6100.0	106.0
	1.827	0.67	0.48	0.50	6200.0	113.5
	1.825	0.67	0.48	0.50	6300.0	121.5
	1.822	0.67	0.49	0.50	6400.0	129.9
	1.818	0.68	0.49	0.50	6500.0	138.7
	1.831	0.67	0.47	0.50	6017.4	100.0
	1.827	0.68	0.48	0.60	5900.0	107.4
	1.828	0.68	0.48	0.60	6000.0	115.3
	1.829	0.68	0.49	0.60	6100.0	123.7
	1.828	0.68	0.49	0.60	6200.0	132.5
	1.826	0.68	0.49	0.60	6300.0	141.8
	1.824	0.68	0.50	0.60	6400.0	151.6
	1.822	0.69	0.50	0.60	6500.0	161.9
	1.824	0.67	0.48	0.60	5802.0	100.0
	1.825	0.68	0.50	0.60	6383.8	150.0
	1.817	0.68	0.49	0.70	5700.0	105.7
	1.821	0.68	0.49	0.70	5800.0	113.8
	1.825	0.69	0.49	0.70	5900.0	122.4
	1.827	0.69	0.50	0.70	6000.0	131.4
	1.829	0.69	0.50	0.70	6100.0	141.0
	1.828	0.69	0.50	0.70	6200.0	151.0
	1.828	0.69	0.50	0.70	6300.0	161.6
	1.828	0.69	0.51	0.70	6400.0	172.8
	1.827	0.69	0.51	0.70	6500.0	184.6
	1.813	0.68	0.49	0.70	5625.9	100.0
	1.829	0.69	0.50	0.70	6190.0	150.0
	1.803	0.69	0.50	0.80	5500.0	101.7
	1.809	0.69	0.50	0.80	5600.0	109.8
	1.815	0.69	0.50	0.80	5700.0	118.4
	1.820	0.69	0.50	0.80	5800.0	127.5
	1.823	0.69	0.50	0.80	5900.0	137.0

V839 Sgr	1.827	0.69	0.51	0.80	6000.0	147.2
	1.829	0.69	0.51	0.80	6100.0	157.9
	1.830	0.70	0.51	0.80	6200.0	169.1
	1.831	0.70	0.51	0.80	6300.0	181.0
	1.831	0.70	0.51	0.80	6400.0	193.5
	1.831	0.70	0.52	0.80	6500.0	206.7
	1.827	0.69	0.51	0.80	6027.0	150.0
	1.831	0.70	0.51	0.80	6449.8	200.0
	1.803	0.69	0.50	0.78	5500.0	100.0
	1.812	0.68	0.49	0.72	5600.0	100.0
	1.817	0.68	0.49	0.66	5700.0	100.0
	1.827	0.67	0.48	0.55	5900.0	100.0
	1.829	0.69	0.50	0.75	6100.0	150.0
	1.829	0.69	0.50	0.69	6200.0	150.0
	1.827	0.69	0.50	0.64	6300.0	150.0
	1.831	0.67	0.47	0.51	6000.0	100.0
	1.825	0.68	0.50	0.59	6400.0	150.0
	1.821	0.68	0.50	0.55	6500.0	150.0
	1.829	0.70	0.51	0.77	6500.0	200.0
EK Del	2.055	0.65	0.46	0.50	5900.0	104.7
	2.054	0.66	0.46	0.50	6000.0	112.4
	2.052	0.66	0.47	0.50	6100.0	120.6
	2.049	0.66	0.47	0.50	6200.0	129.2
	2.045	0.66	0.48	0.50	6300.0	138.3
	2.040	0.67	0.48	0.50	6400.0	147.8
	2.036	0.67	0.49	0.50	6500.0	157.9
	2.054	0.65	0.46	0.50	5836.7	100.0
	2.039	0.67	0.48	0.50	6422.0	150.0
	2.045	0.67	0.47	0.60	5700.0	105.6
	2.047	0.67	0.47	0.60	5800.0	113.6
	2.050	0.67	0.47	0.60	5900.0	122.2
	2.050	0.67	0.48	0.60	6000.0	131.2
	2.050	0.67	0.48	0.60	6100.0	140.8
	2.048	0.67	0.48	0.60	6200.0	150.8
	2.046	0.68	0.49	0.60	6300.0	161.4
	2.044	0.68	0.49	0.60	6400.0	172.6
	2.041	0.68	0.50	0.60	6500.0	184.3
	2.041	0.66	0.47	0.60	5627.7	100.0
	2.049	0.67	0.48	0.60	6192.1	150.0
	2.028	0.67	0.48	0.70	5500.0	103.4
	2.034	0.68	0.48	0.70	5600.0	111.6
	2.039	0.68	0.48	0.70	5700.0	120.3
	2.043	0.68	0.48	0.70	5800.0	129.5
	2.047	0.68	0.49	0.70	5900.0	139.3

EK Del	2.049	0.68	0.49	0.70	6000.0	149.6
	2.049	0.68	0.49	0.70	6100.0	160.4
	2.049	0.68	0.49	0.70	6200.0	171.9
	2.048	0.68	0.50	0.70	6300.0	184.0
	2.047	0.69	0.50	0.70	6400.0	196.7
	2.045	0.69	0.50	0.70	6500.0	210.0
	2.049	0.68	0.49	0.70	6004.1	150.0
	2.046	0.69	0.50	0.70	6425.3	200.0
	2.024	0.68	0.49	0.80	5500.0	115.8
	2.031	0.68	0.49	0.80	5600.0	125.0
	2.036	0.68	0.49	0.80	5700.0	134.7
	2.042	0.69	0.49	0.80	5800.0	145.1
	2.046	0.69	0.50	0.80	5900.0	156.0
	2.048	0.69	0.50	0.80	6000.0	167.5
	2.050	0.69	0.50	0.80	6100.0	179.7
	2.050	0.69	0.50	0.80	6200.0	192.5
	2.050	0.69	0.50	0.80	6300.0	206.0
	2.050	0.69	0.51	0.80	6400.0	220.3
	2.049	0.69	0.51	0.80	6500.0	235.2
	2.043	0.69	0.49	0.80	5845.9	150.0
	2.050	0.69	0.50	0.80	6256.1	200.0
	2.029	0.67	0.48	0.67	5500.0	100.0
	2.038	0.67	0.47	0.62	5600.0	100.0
	2.046	0.66	0.47	0.56	5700.0	100.0
	2.052	0.66	0.46	0.52	5800.0	100.0
	2.046	0.68	0.49	0.76	5900.0	150.0
	2.049	0.68	0.49	0.70	6000.0	150.0
	2.049	0.68	0.48	0.65	6100.0	150.0
	2.049	0.67	0.48	0.60	6200.0	150.0
	2.046	0.67	0.48	0.55	6300.0	150.0
	2.051	0.69	0.50	0.77	6300.0	200.0
	2.039	0.67	0.48	0.51	6400.0	150.0
	2.047	0.69	0.50	0.71	6400.0	200.0
	2.043	0.68	0.50	0.66	6500.0	200.0
UX Nor	2.401	0.64	0.45	0.50	5700.0	107.7
	2.403	0.64	0.45	0.50	5800.0	116.0
	2.402	0.64	0.45	0.50	5900.0	124.7
	2.400	0.65	0.45	0.50	6000.0	133.9
	2.395	0.65	0.46	0.50	6100.0	143.6
	2.390	0.65	0.46	0.50	6200.0	153.9
	2.384	0.65	0.47	0.50	6300.0	164.7
	2.378	0.66	0.48	0.50	6400.0	176.1
	2.372	0.66	0.48	0.50	6500.0	188.0
	2.399	0.64	0.44	0.50	5601.1	100.0

UX Nor	2.392	0.65	0.46	0.50	6162.8	150.0
	2.381	0.65	0.46	0.60	5500.0	108.0
	2.387	0.65	0.46	0.60	5600.0	116.6
	2.392	0.65	0.46	0.60	5700.0	125.7
	2.395	0.65	0.46	0.60	5800.0	135.4
	2.395	0.66	0.46	0.60	5900.0	145.5
	2.395	0.66	0.47	0.60	6000.0	156.3
	2.393	0.66	0.47	0.60	6100.0	167.6
	2.390	0.66	0.47	0.60	6200.0	179.6
	2.386	0.67	0.48	0.60	6300.0	192.2
	2.382	0.67	0.48	0.60	6400.0	205.5
	2.378	0.67	0.49	0.60	6500.0	219.5
	2.396	0.66	0.46	0.60	5942.2	150.0
	2.384	0.67	0.48	0.60	6359.0	200.0
	2.373	0.66	0.47	0.70	5500.0	123.1
	2.380	0.66	0.47	0.70	5600.0	132.9
	2.386	0.67	0.47	0.70	5700.0	143.3
	2.390	0.67	0.47	0.70	5800.0	154.3
	2.392	0.67	0.47	0.70	5900.0	165.9
	2.392	0.67	0.48	0.70	6000.0	178.1
	2.392	0.67	0.48	0.70	6100.0	191.1
	2.390	0.67	0.48	0.70	6200.0	204.7
	2.388	0.67	0.49	0.70	6300.0	219.1
	2.385	0.68	0.49	0.70	6400.0	234.2
	2.383	0.68	0.50	0.70	6500.0	250.2
	2.388	0.67	0.47	0.70	5761.8	150.0
	2.391	0.67	0.48	0.70	6166.0	200.0
	2.383	0.68	0.50	0.70	6499.0	250.0
	2.367	0.67	0.48	0.80	5500.0	137.9
	2.375	0.67	0.48	0.80	5600.0	148.9
	2.381	0.67	0.48	0.80	5700.0	160.5
	2.386	0.68	0.48	0.80	5800.0	172.8
	2.390	0.68	0.48	0.80	5900.0	185.8
	2.391	0.68	0.49	0.80	6000.0	199.5
	2.392	0.68	0.49	0.80	6100.0	214.0
	2.392	0.68	0.49	0.80	6200.0	229.3
	2.391	0.68	0.49	0.80	6300.0	245.4
	2.389	0.68	0.50	0.80	6400.0	262.3
	2.388	0.69	0.50	0.80	6500.0	280.2
	2.376	0.67	0.48	0.80	5610.0	150.0
	2.391	0.68	0.49	0.80	6003.6	200.0
	2.390	0.68	0.50	0.80	6327.8	250.0
	2.387	0.64	0.45	0.55	5500.0	100.0
	2.400	0.64	0.44	0.50	5600.0	100.0
	2.383	0.67	0.48	0.74	5700.0	150.0

UX Nor	2.391	0.66	0.47	0.68	5800.0	150.0
	2.394	0.66	0.47	0.62	5900.0	150.0
	2.395	0.66	0.46	0.57	6000.0	150.0
	2.396	0.65	0.46	0.53	6100.0	150.0
	2.391	0.67	0.48	0.74	6100.0	200.0
	2.390	0.67	0.48	0.68	6200.0	200.0
	2.386	0.67	0.48	0.63	6300.0	200.0
	2.381	0.67	0.48	0.58	6400.0	200.0
	2.387	0.68	0.50	0.76	6400.0	250.0
	2.373	0.67	0.49	0.54	6500.0	200.0
	2.384	0.68	0.50	0.70	6500.0	250.0
V465 Oph	2.871	0.62	0.43	0.50	5500.0	113.0
	2.874	0.62	0.43	0.50	5600.0	122.0
	2.875	0.62	0.43	0.50	5700.0	131.5
	2.873	0.63	0.44	0.50	5800.0	141.5
	2.871	0.63	0.44	0.50	5900.0	152.2
	2.865	0.63	0.44	0.50	6000.0	163.4
	2.858	0.63	0.45	0.50	6100.0	175.3
	2.849	0.64	0.46	0.50	6200.0	187.8
	2.841	0.64	0.46	0.50	6300.0	201.0
	2.832	0.65	0.47	0.50	6400.0	214.9
	2.824	0.65	0.48	0.50	6500.0	229.5
	2.871	0.63	0.44	0.50	5879.9	150.0
	2.842	0.64	0.46	0.50	6292.4	200.0
	2.855	0.64	0.44	0.60	5500.0	131.9
	2.860	0.64	0.45	0.60	5600.0	142.4
	2.864	0.64	0.45	0.60	5700.0	153.5
	2.864	0.64	0.45	0.60	5800.0	165.2
	2.863	0.64	0.45	0.60	5900.0	177.6
	2.861	0.65	0.46	0.60	6000.0	190.8
	2.856	0.65	0.46	0.60	6100.0	204.6
	2.851	0.65	0.47	0.60	6200.0	219.3
	2.845	0.65	0.47	0.60	6300.0	234.7
	2.838	0.66	0.48	0.60	6400.0	250.9
	2.832	0.66	0.49	0.60	6500.0	267.9
	2.862	0.64	0.45	0.60	5669.4	150.0
	2.858	0.65	0.46	0.60	6067.1	200.0
	2.838	0.66	0.48	0.60	6394.7	250.0
	2.843	0.65	0.46	0.70	5500.0	150.3
	2.850	0.65	0.46	0.70	5600.0	162.3
	2.854	0.65	0.46	0.70	5700.0	174.9
	2.857	0.65	0.46	0.70	5800.0	188.3
	2.859	0.65	0.46	0.70	5900.0	202.5
	2.857	0.66	0.47	0.70	6000.0	217.4

V465 Oph	2.855	0.66	0.47	0.70	6100.0	233.2
	2.851	0.66	0.47	0.70	6200.0	249.9
	2.847	0.66	0.48	0.70	6300.0	267.4
	2.842	0.67	0.49	0.70	6400.0	285.9
	2.839	0.67	0.49	0.70	6500.0	305.4
	2.858	0.65	0.46	0.70	5883.0	200.0
	2.851	0.66	0.47	0.70	6200.7	250.0
	2.839	0.67	0.49	0.70	6472.9	300.0
	2.834	0.66	0.47	0.80	5500.0	168.3
	2.842	0.66	0.47	0.80	5600.0	181.7
	2.848	0.66	0.47	0.80	5700.0	195.9
	2.852	0.66	0.47	0.80	5800.0	210.9
	2.855	0.66	0.47	0.80	5900.0	226.8
	2.855	0.67	0.47	0.80	6000.0	243.5
	2.854	0.67	0.48	0.80	6100.0	261.2
	2.853	0.67	0.48	0.80	6200.0	279.9
	2.849	0.67	0.49	0.80	6300.0	299.5
	2.846	0.67	0.49	0.80	6400.0	320.2
	2.844	0.68	0.50	0.80	6500.0	342.0
	2.849	0.66	0.47	0.80	5728.0	200.0
	2.855	0.67	0.48	0.80	6037.3	250.0
	2.849	0.67	0.49	0.80	6302.4	300.0
	2.844	0.65	0.46	0.70	5500.0	150.0
	2.856	0.64	0.45	0.64	5600.0	150.0
	2.865	0.64	0.45	0.58	5700.0	150.0
	2.872	0.63	0.44	0.54	5800.0	150.0
	2.853	0.66	0.47	0.75	5800.0	200.0
	2.859	0.65	0.46	0.69	5900.0	200.0
	2.861	0.65	0.46	0.63	6000.0	200.0
	2.857	0.65	0.46	0.58	6100.0	200.0
	2.854	0.66	0.47	0.76	6100.0	250.0
	2.852	0.64	0.46	0.54	6200.0	200.0
	2.852	0.66	0.47	0.70	6200.0	250.0
	2.844	0.66	0.48	0.65	6300.0	250.0
	2.836	0.66	0.48	0.60	6400.0	250.0
	2.844	0.67	0.49	0.74	6400.0	300.0
	2.829	0.66	0.48	0.55	6500.0	250.0
	2.836	0.67	0.49	0.69	6500.0	300.0

(A1.4) Estimated Masses for the Observed Stars.

In this section, we derive a bump phase-period-radius law from the non-linear models of RCRS, and use this law to derive masses for the observed stars of KD, using the data provided in table 3.1 and the PMLT law of the previous section.

According to physical considerations, the radius of a star should be proportional to the quantity $\varphi_l P$, where φ_l is the phase from maximum light of the bump plus unity and P is the period. To obtain a bump phase-radius law then, we fit equation (A1.3) to the data in RCRS using the phases of bumps estimated from the light curves in Appendix 3.

$$\varphi_l P = C(R/R_\odot) \qquad (A1.3)$$

Here, we find that C = 0.24 with an estimated error of no more than about 0.05, in agreement with CSV, who find that $P\varphi_v \approx 0.21\ (R/R_\odot)$ days, where φ_v is the phase of bump on the velocity curve, and $\varphi_v - \varphi_l = 0.00 \pm 0.04$ (see, for example, CSV).

We now substitute equation (A1.3), with the estimated value of C, into equation (A1.2) - the PMLT law, given that $L = 4\pi R^2 \sigma T_e^4$.

We find that

$$M/M_\odot = 0.46 \varphi_l P^{-0.35} \qquad (A1.4)$$

Application of the above equation to the observed stars which have been discussed in this work, and using the bump phases listed in table 3.1, yields the results of table A1.2, where the first column denotes the name of the star and the second column the phase φ_l from maximum light of the second bump plus unity. The third column denotes the period of the star and the final column the mass estimated from equation (A1.4).

Table A1.2: Bump Masses of Short-Period Population II Cepheids.

STAR	φ_L	PERIOD	$M/M_\odot$
V716 Oph	1.79	1.1159	0.79 ± 0.09
V527 Sgr	-	1.2589	- -
VX Cap	1.71	1.3276	0.71 ± 0.08
HQ Cra	1.48	1.4150	0.60 ± 0.07
V2022 Sgr	1.37	1.5335	0.54 ± 0.06
V745 Oph	1.33	1.5955	0.52 ± 0.06
V971 Aql	1.19	1.6245	0.46 ± 0.05
DU Ara	1.19	1.6405	0.46 ± 0.05
VZ Aql	1.14	1.6653	0.44 ± 0.05
V839 Sgr	-	1.8272	- -
EK Del	1.72	2.0467	0.62 ± 0.07
UX Nor	1.70	2.3858	0.58 ± 0.06
V465 Oph	1.55	2.8417	0.49 ± 0.06

(A1.5) Summary.

A grid of models for each star has been computed using a PMLT law to compute the parameters for each model. From the PMLT law, we are able to compute a period-mass-radius law, from which we formed an equation relating the mass of a BL Herculis star to the phase of bump in its light curve.

This equation was then used to compute masses for the BL Herculis stars in the survey of KD.

APPENDIX 2.

LIGHT CURVES OF OBSERVED STARS.

This appendix contains thirteen light curves which have been computed using the data of KD and which have been mentioned throughout the text. The light curves have been described in detail in chapter 3 and the methods used to produce them in chapter 4. The diagrams appear in order of increasing period.

Fig. A2.1: Light Curve for V716 Oph.

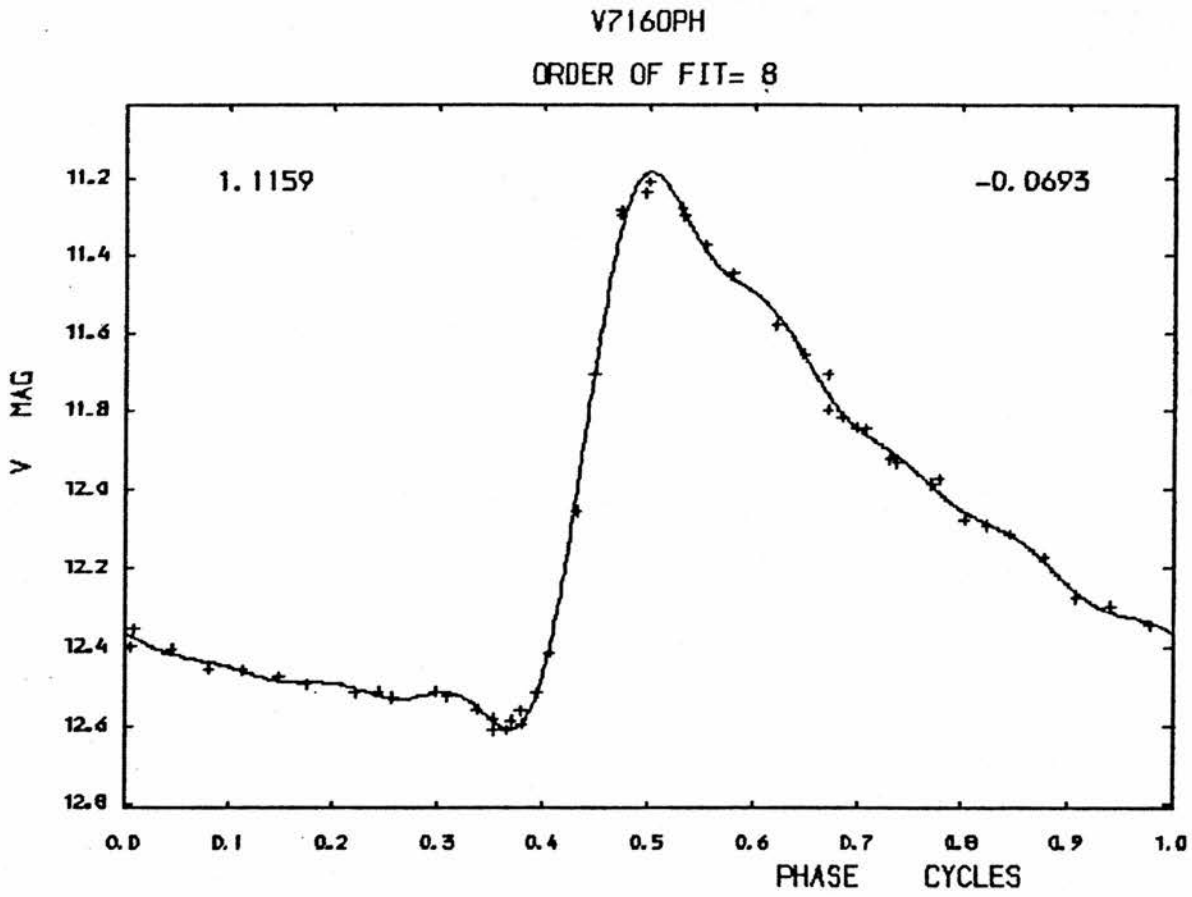

Fig. A2.2: Light Curve for V527 Sgr.

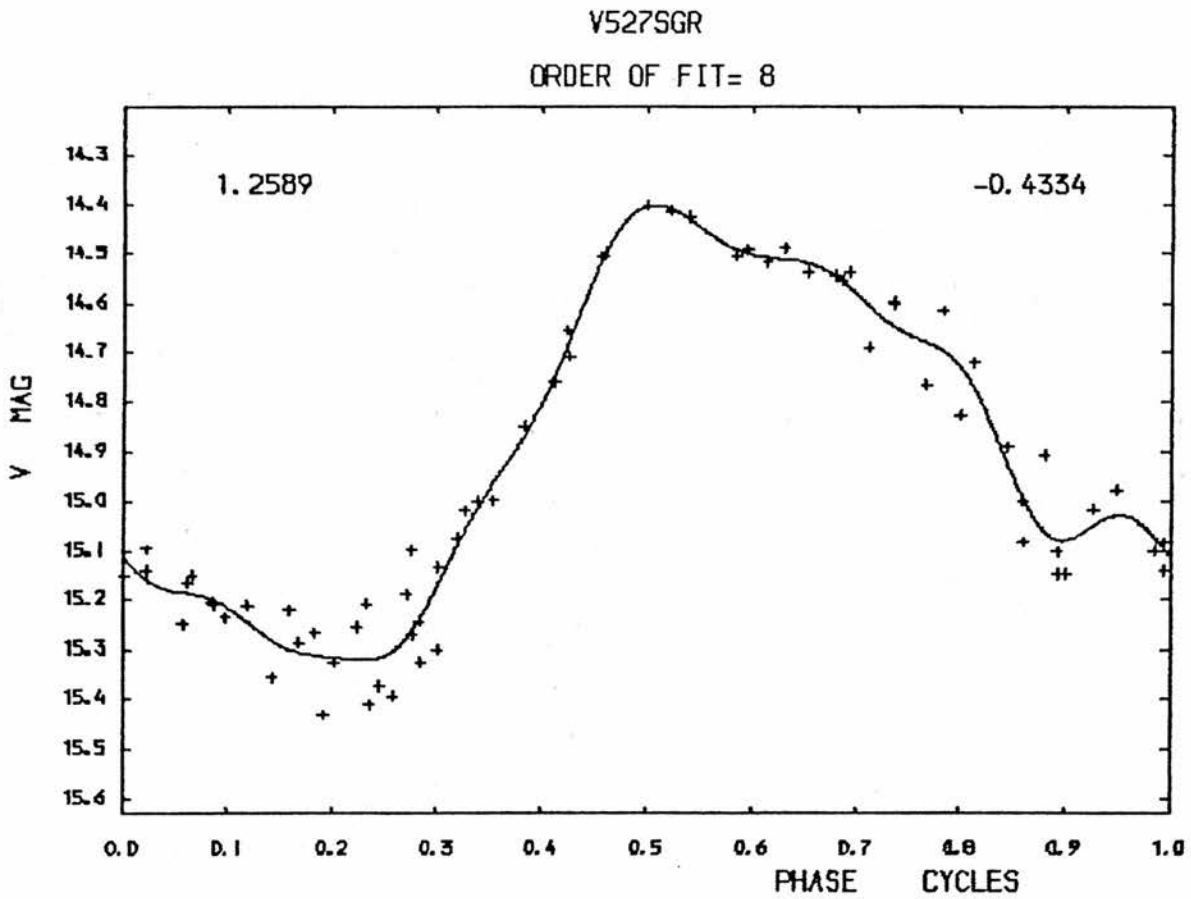

Fig. A2.3: Light Curve for VX Cap.

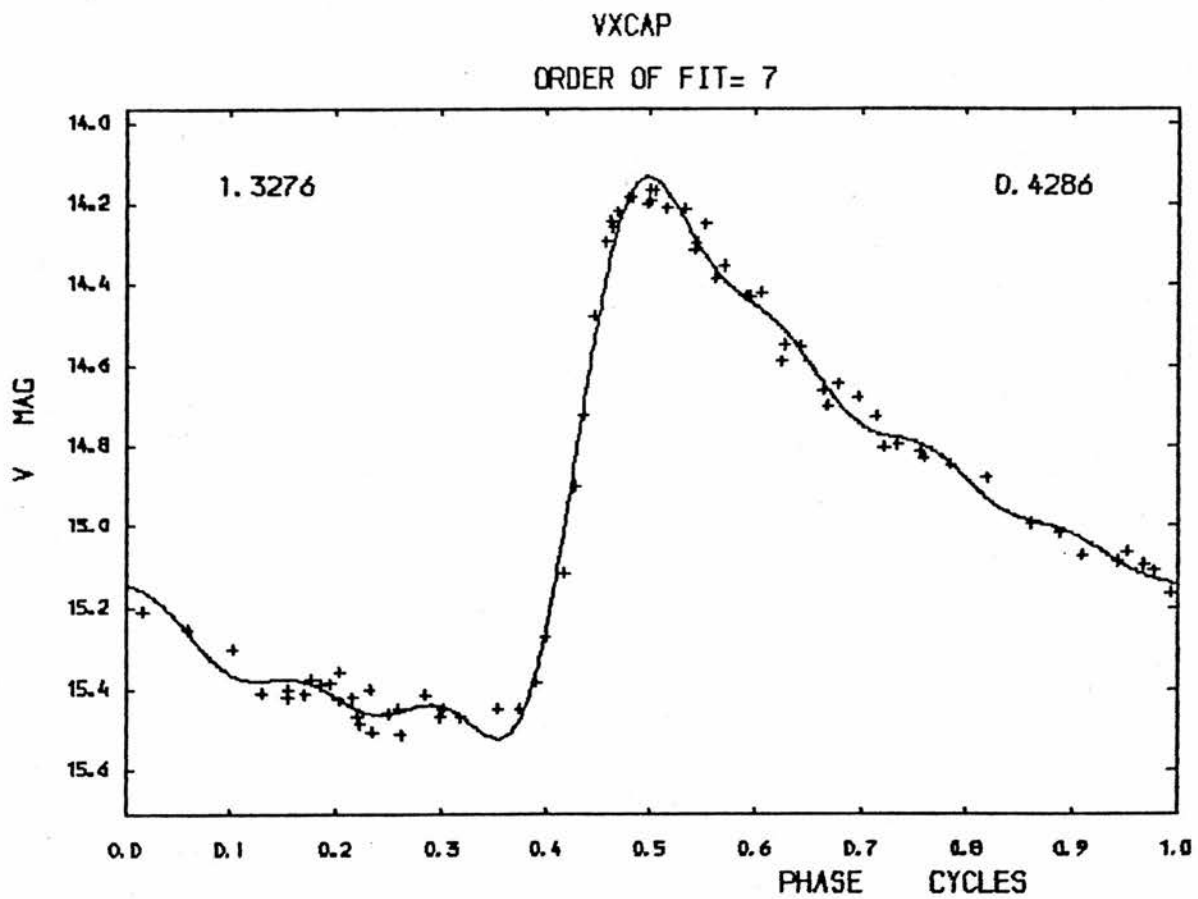

Fig. A2.4: Light Curve for HQ Cra.

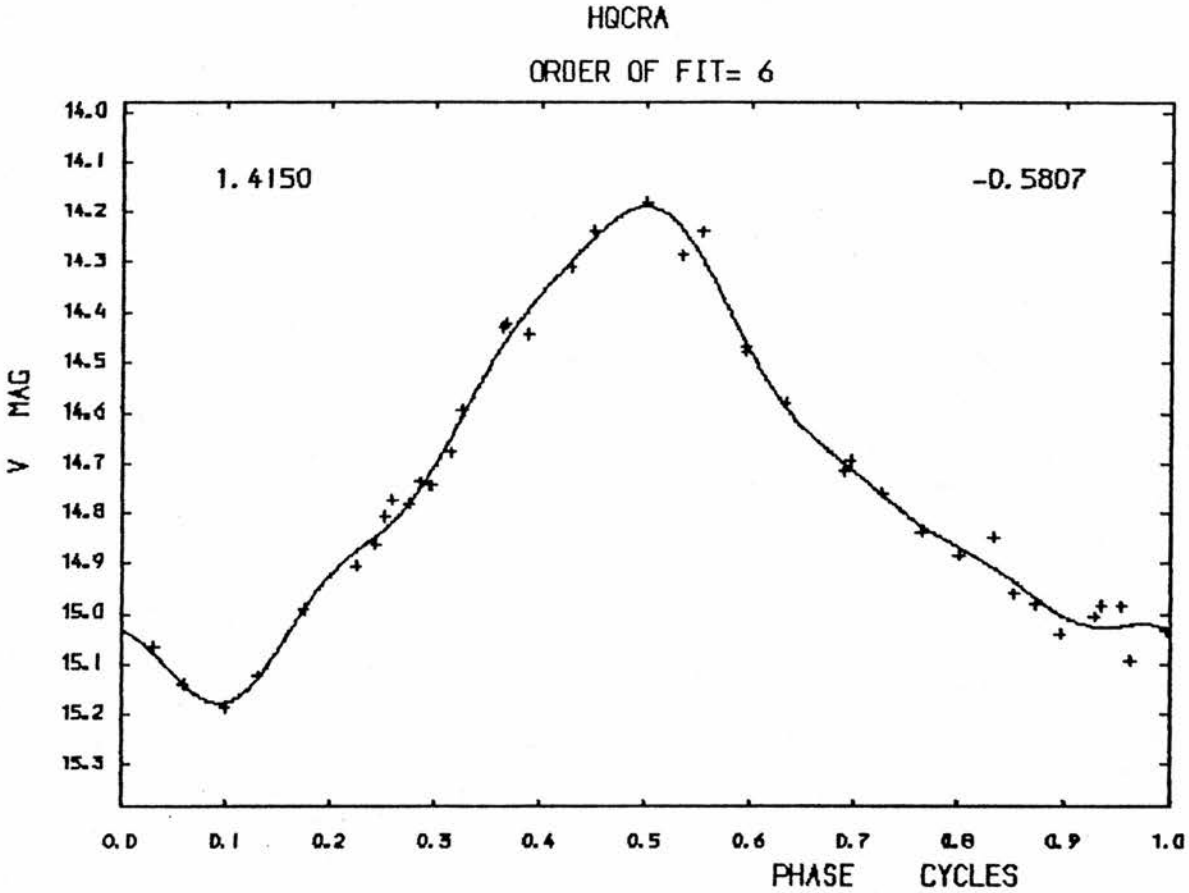

Fig. A2.5: Light Curve for V2022 Sgr.

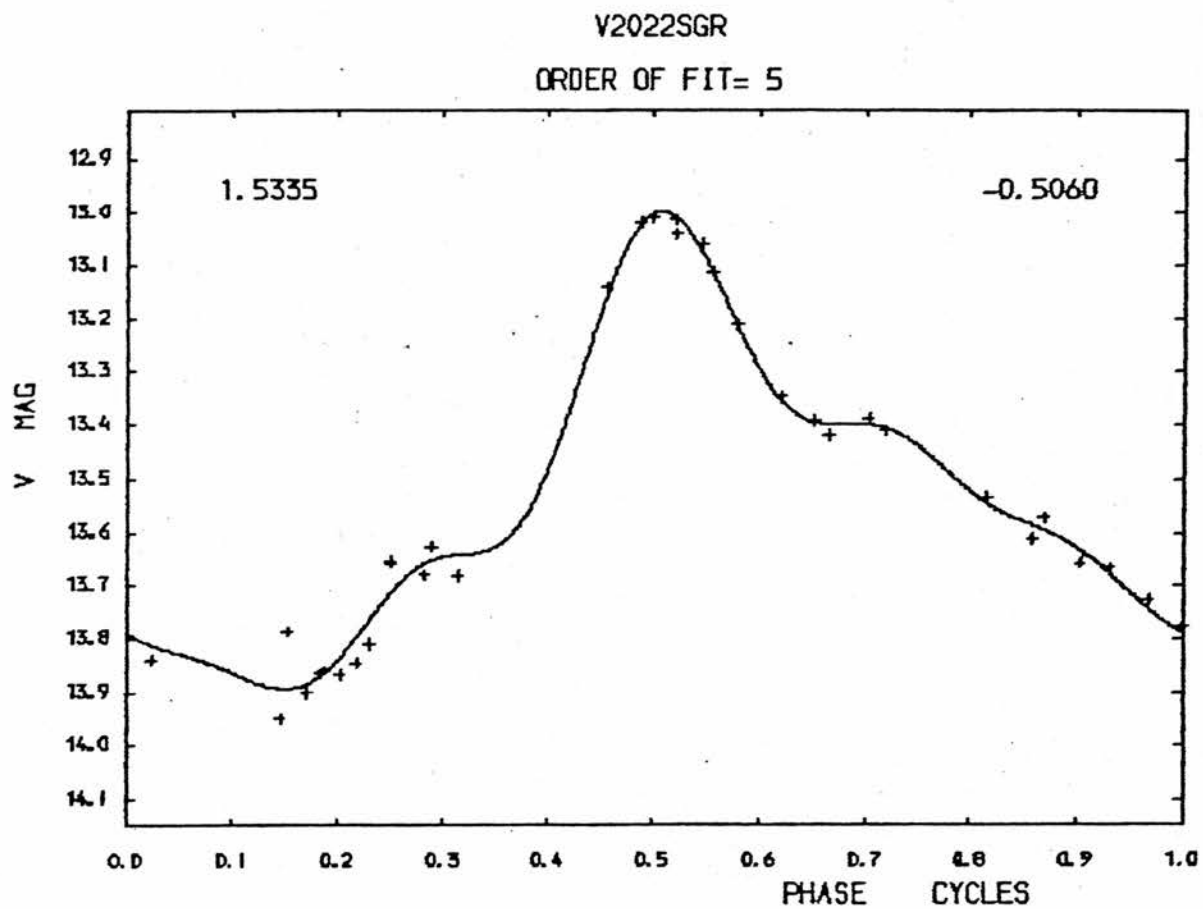

Fig. A2.6: Light Curve for V745 Oph.

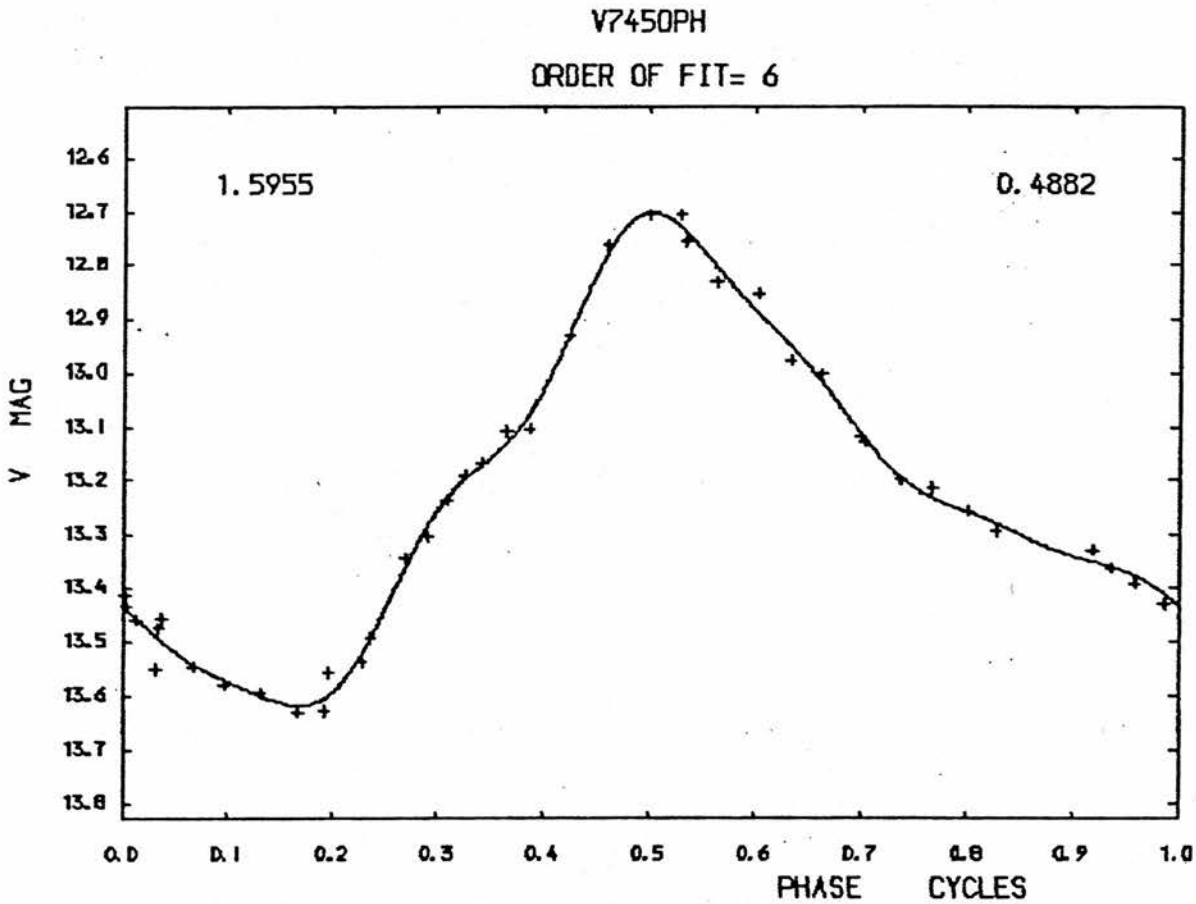

Fig. A2.7: Light Curve for V971 Aql.

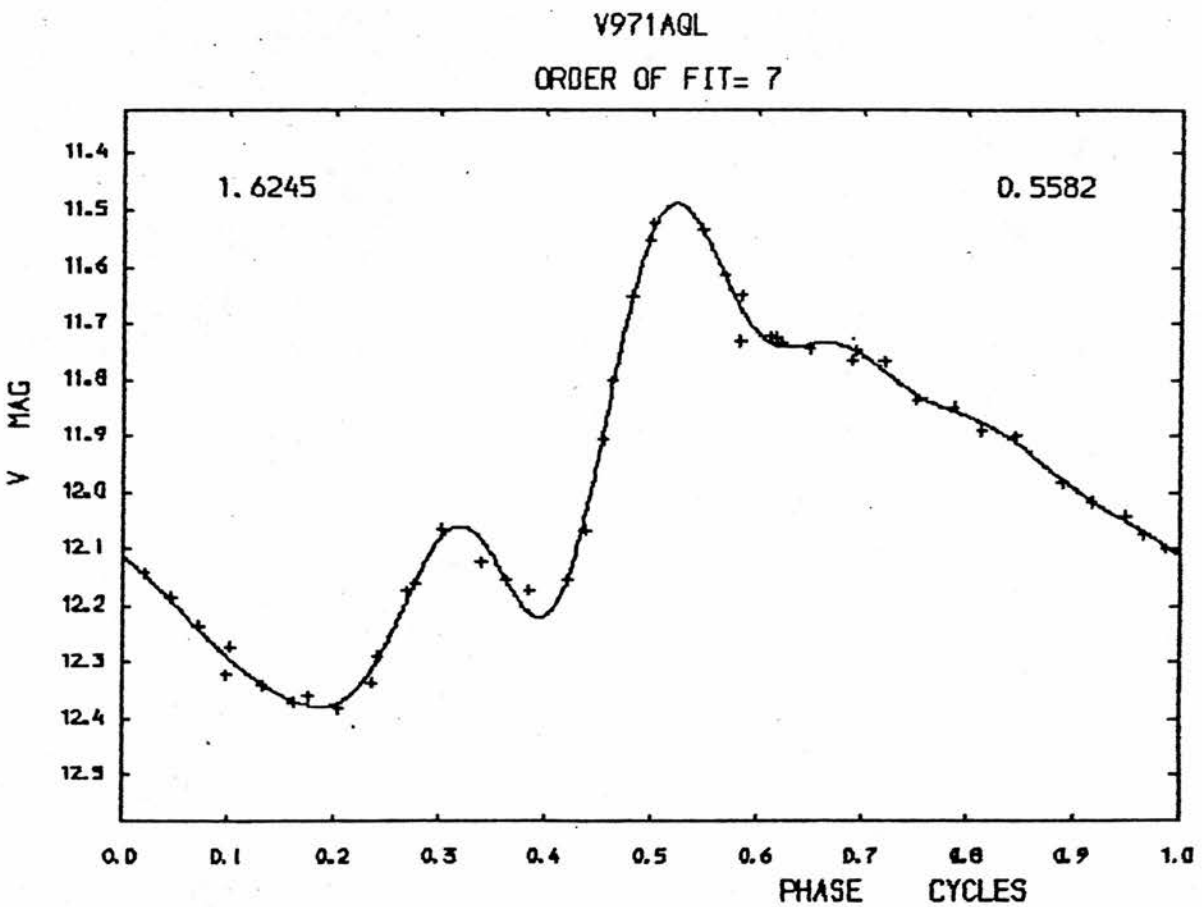

Fig. A2.8: Light Curve for DU Ara.

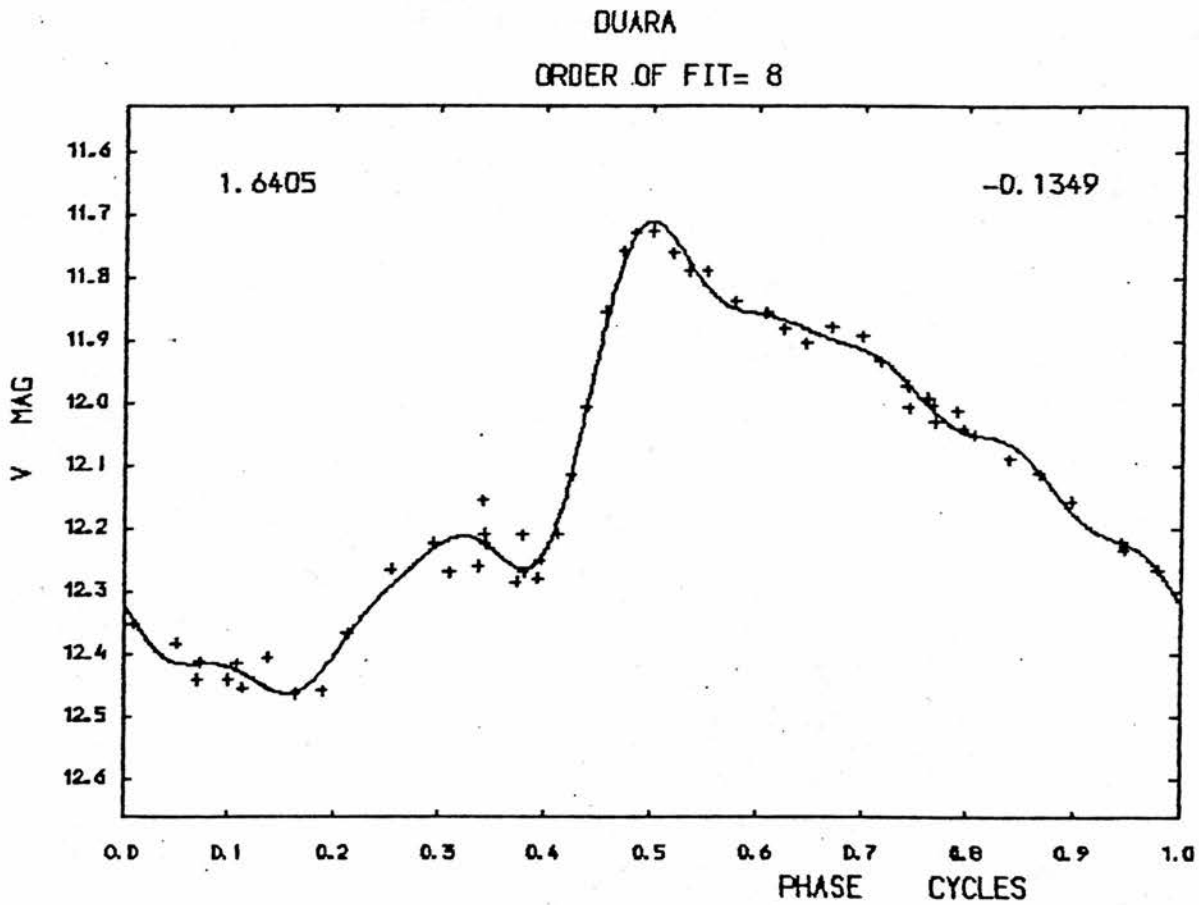

Fig. A2.9: Light Curve for VZ Aql.

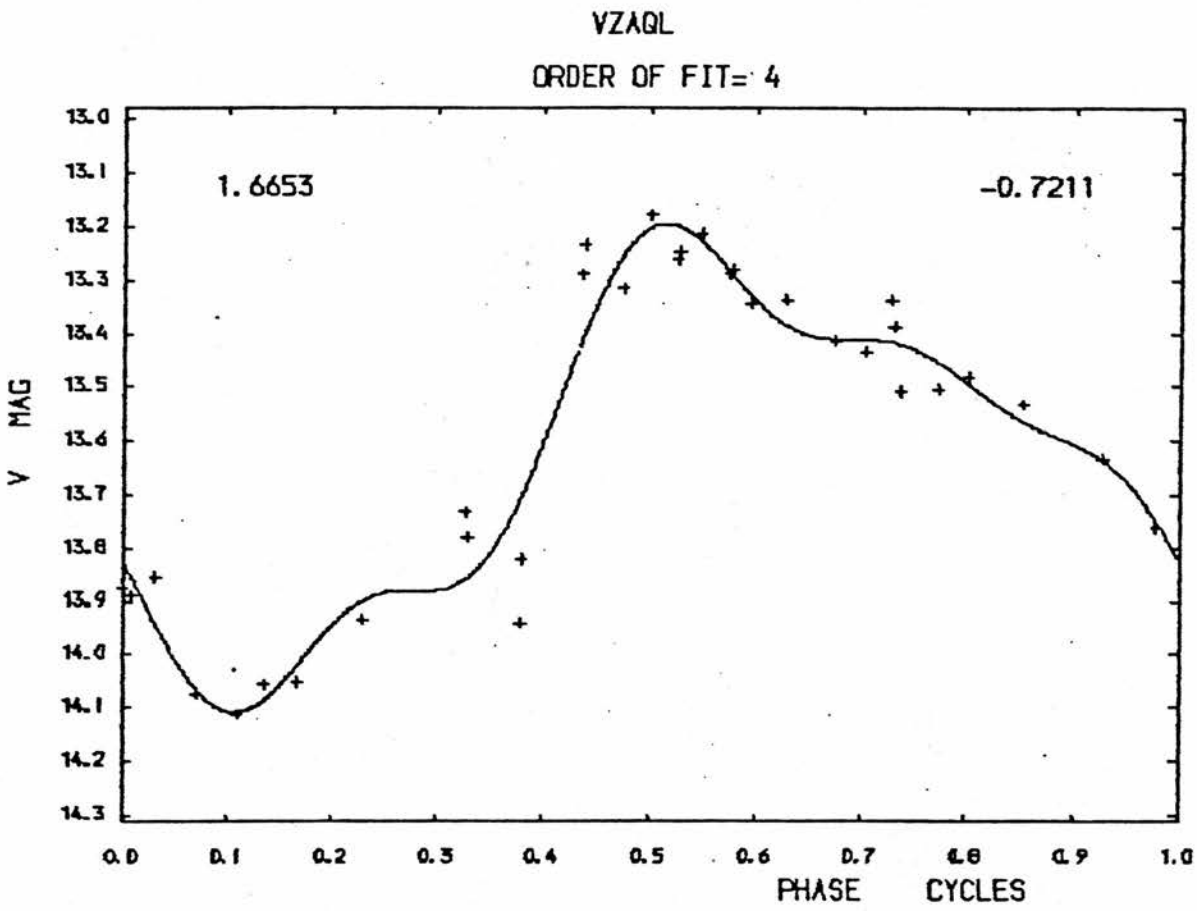

Fig. A2.10: Light Curve for V839 Sgr.

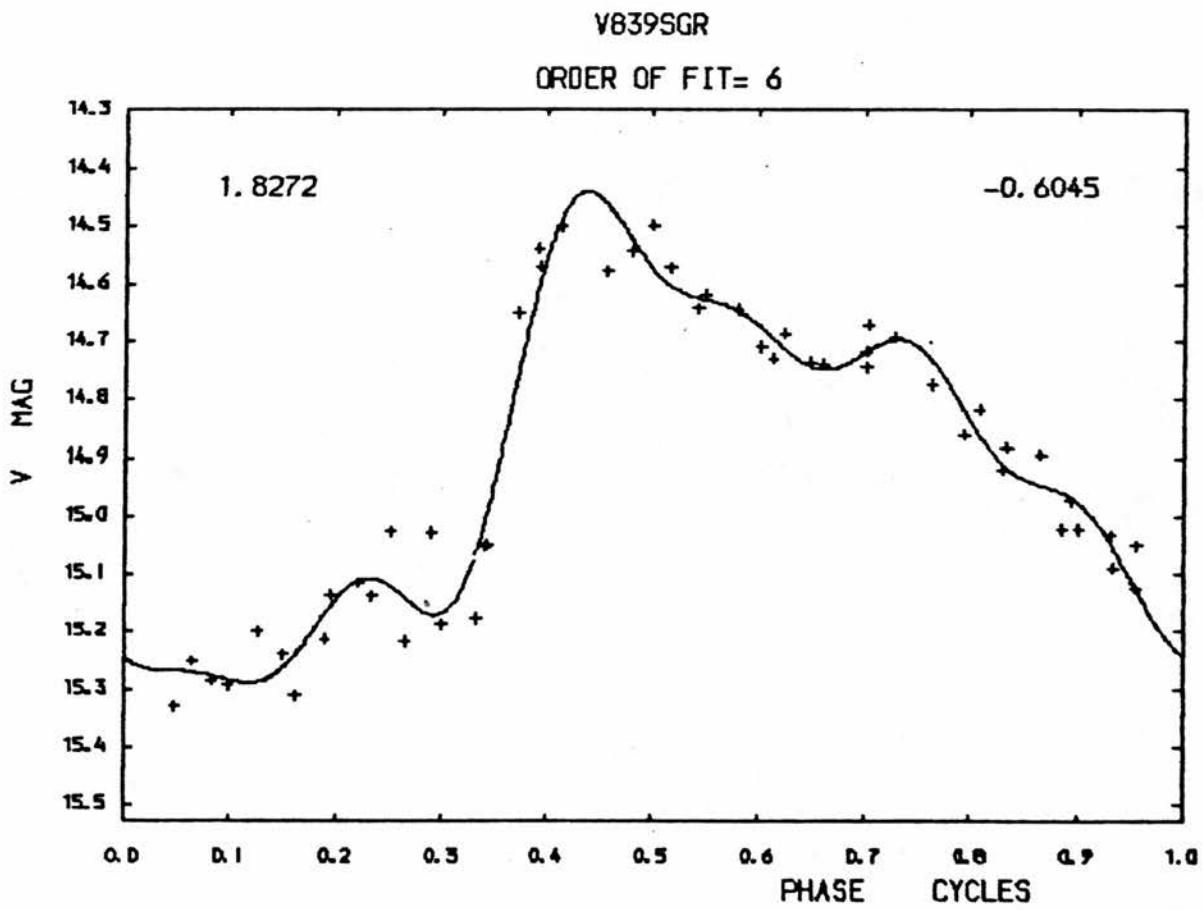

Fig. A2.11: Light Curve for EK Del.

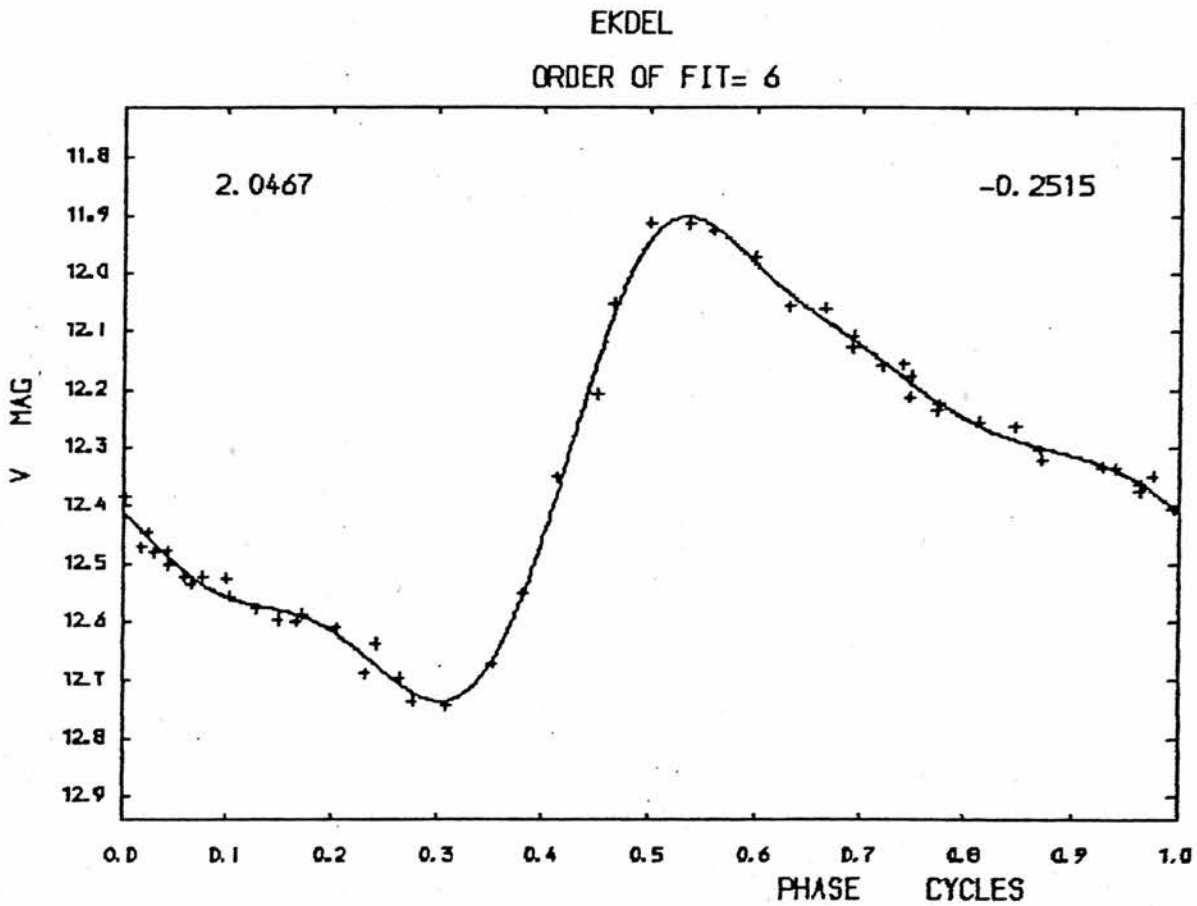

Fig. A2.12: Light Curve for UX Nor.

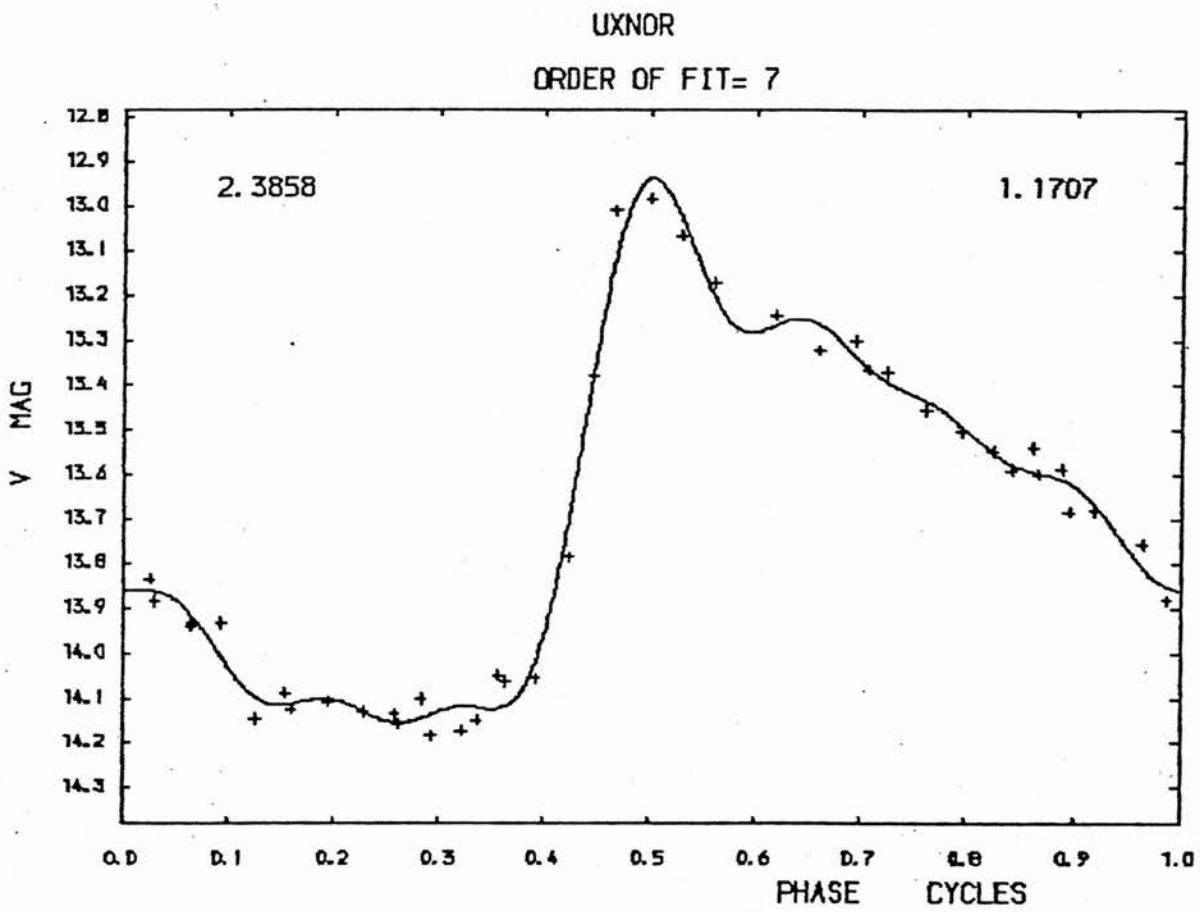

Fig. A2.13: Light Curve for V465 Oph.

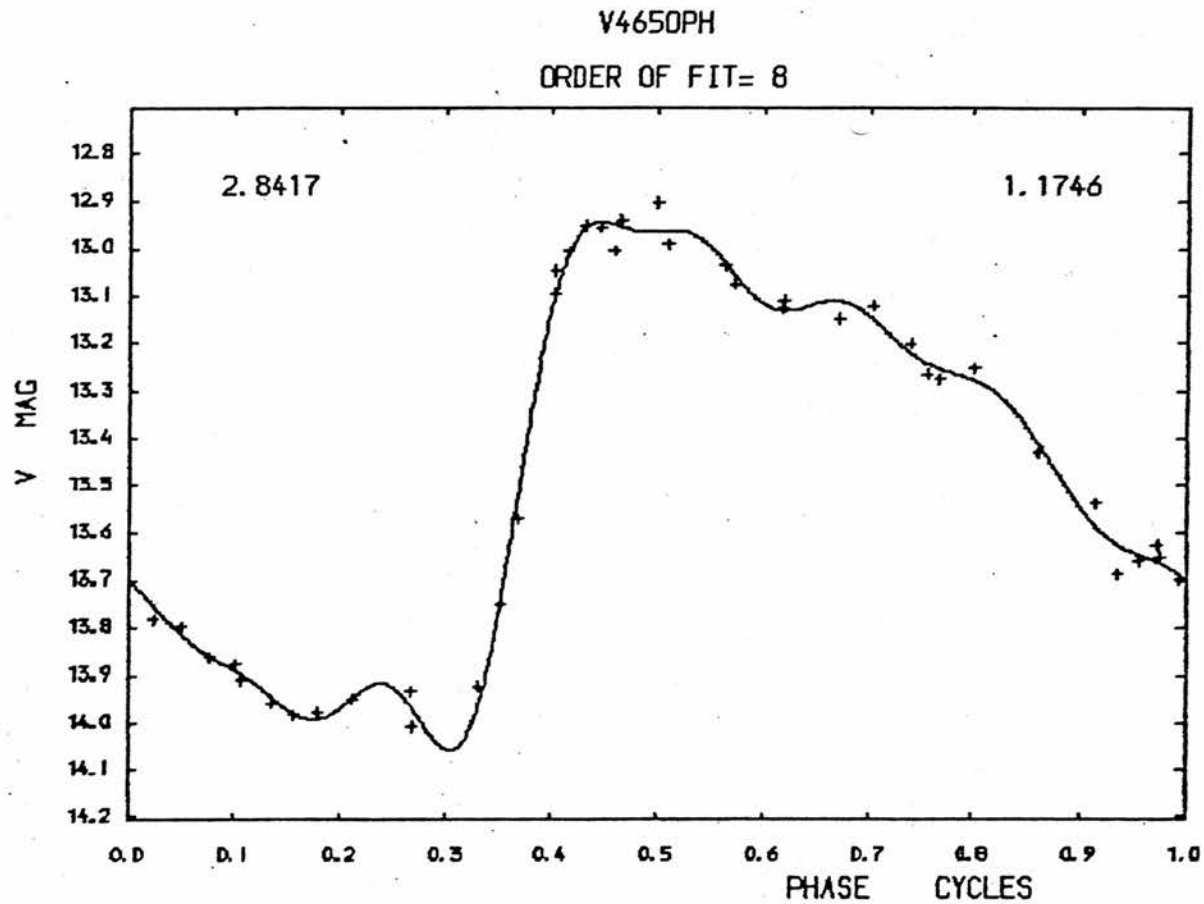

APPENDIX 3.

LIGHT CURVES FOR THE MODELS.

In this appendix, we present the light curves of eleven BL Herculis models. These light curves have been produced using the data provided by Carson and Stothers (1984a) and are described in RCRS. The names of the models associated with the following diagrams have also been provided by Carson and Stothers (1984a) and bear no relation to the stars of KD, as discussed in this thesis.

Fig. A3.1: Light Curve for BXD.

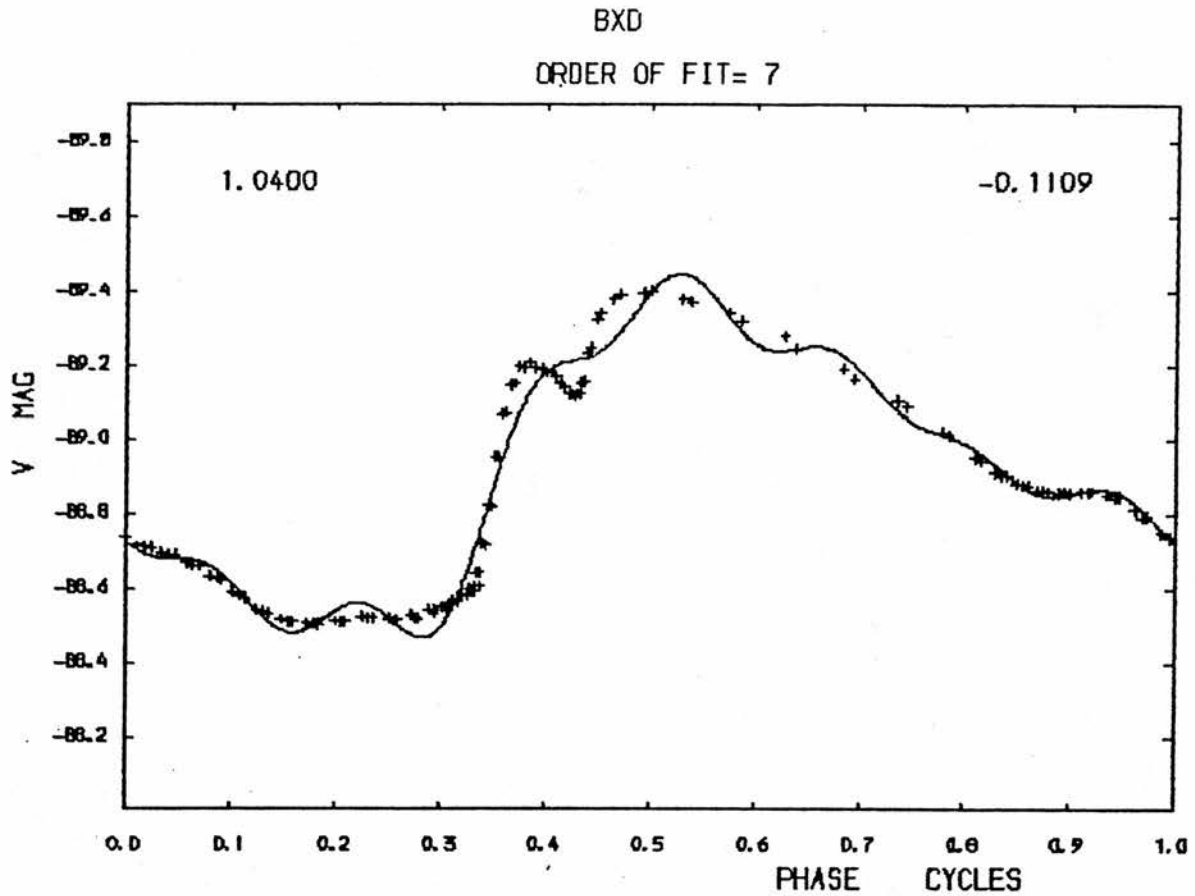

Fig. A3.2: Light Curve for BFS.

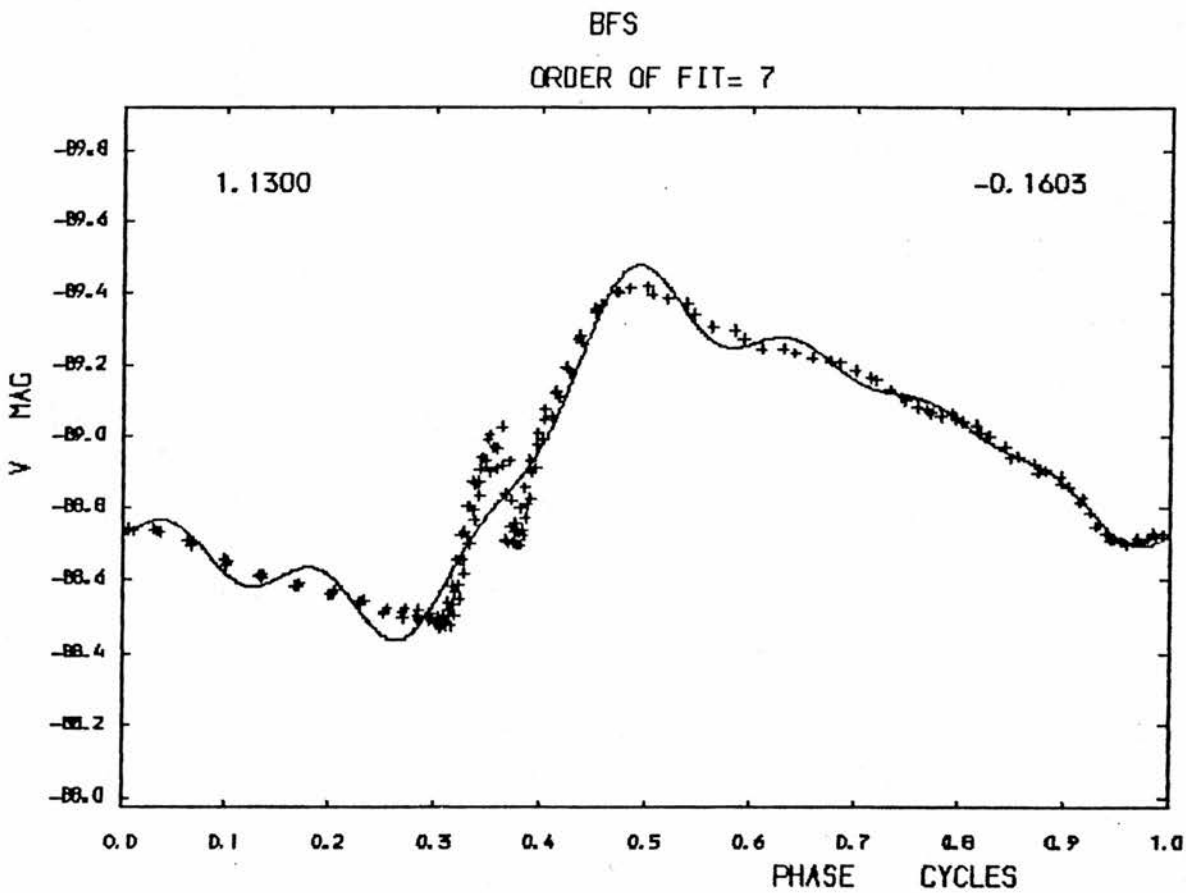

Fig. A3.3: Light Curve for XXZ.

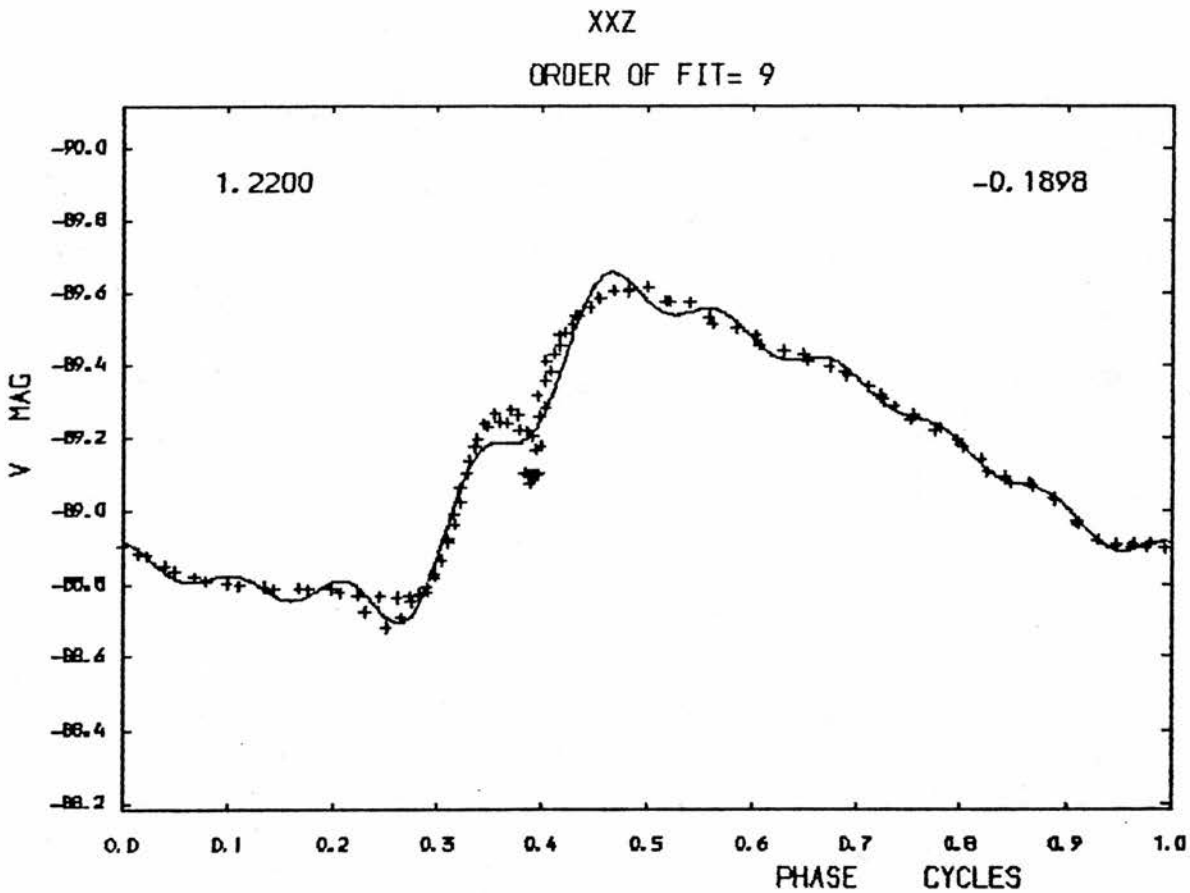

Fig. A3.4: Light Curve for CEH.

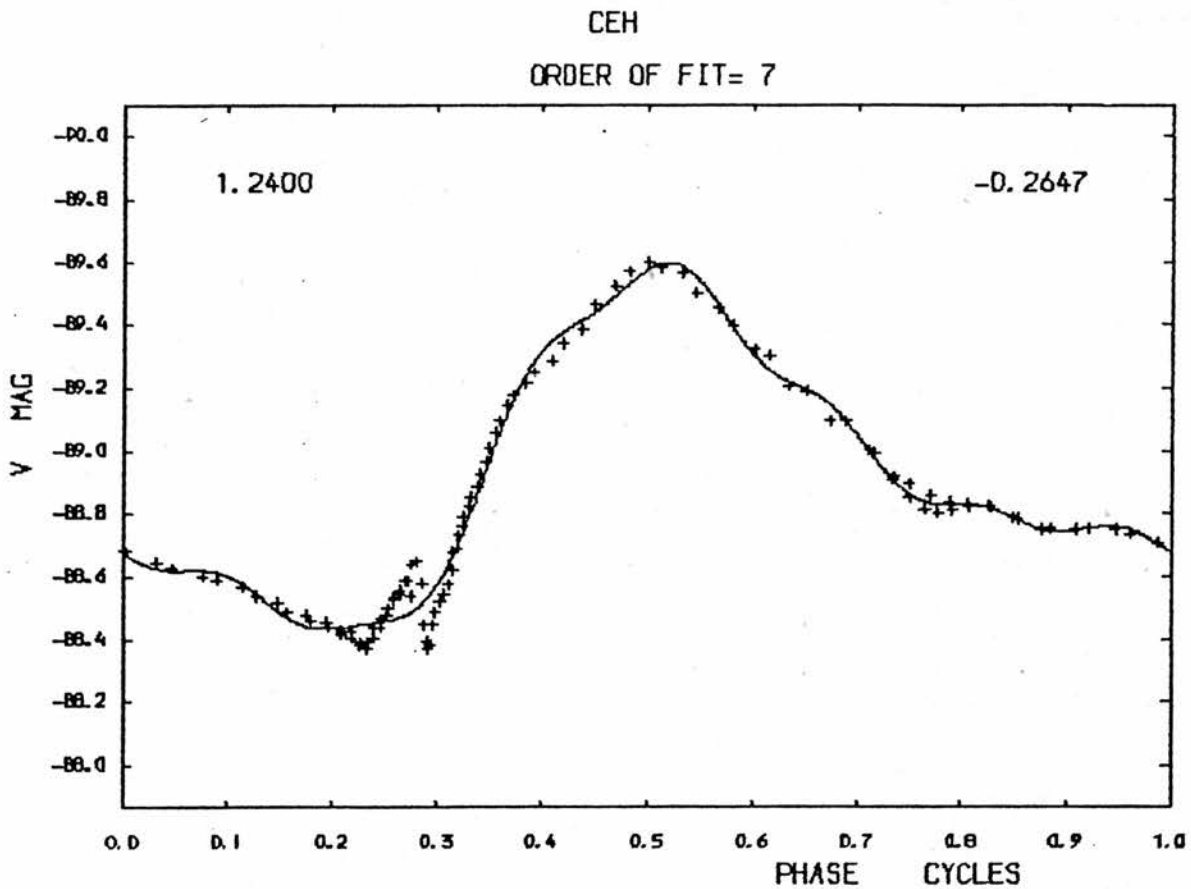

Fig. A3.5: Light Curve for SWT.

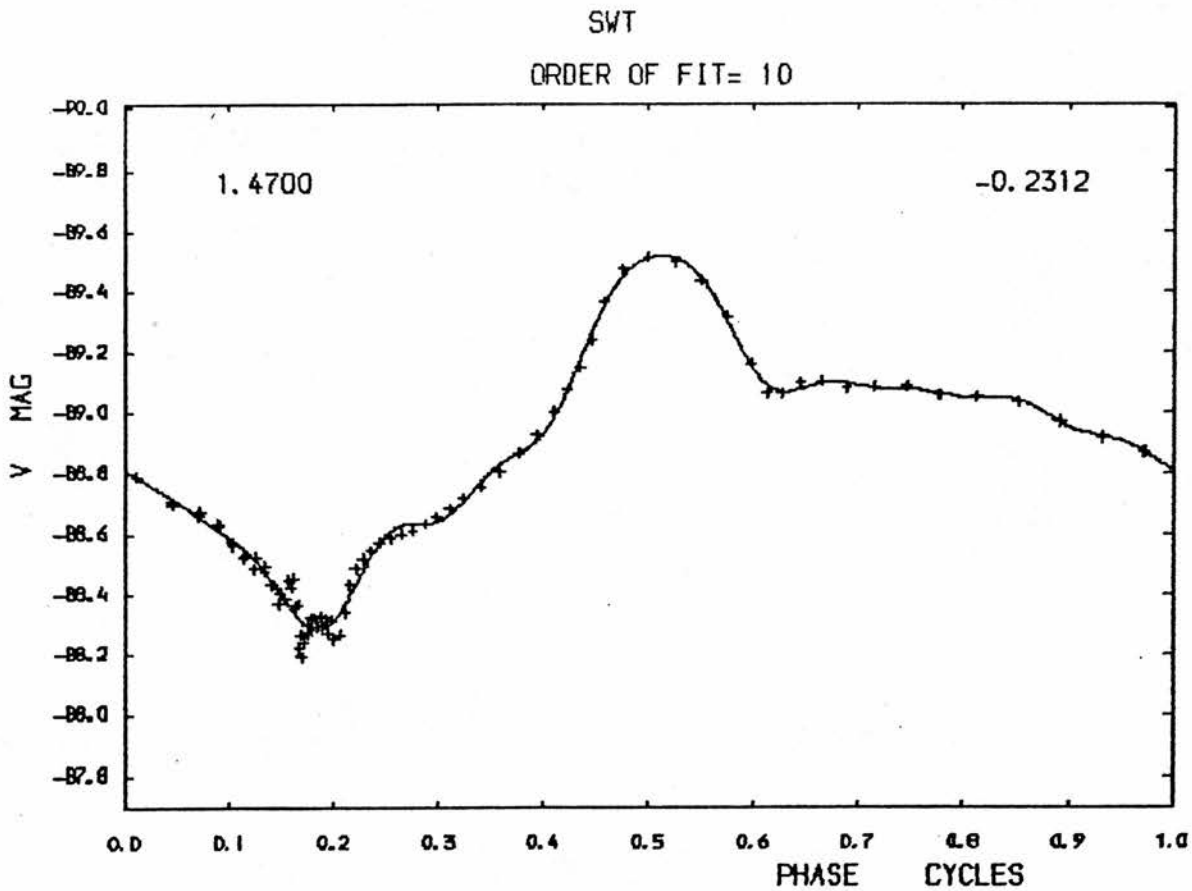

Fig. A3.6: Light Curve for 839.

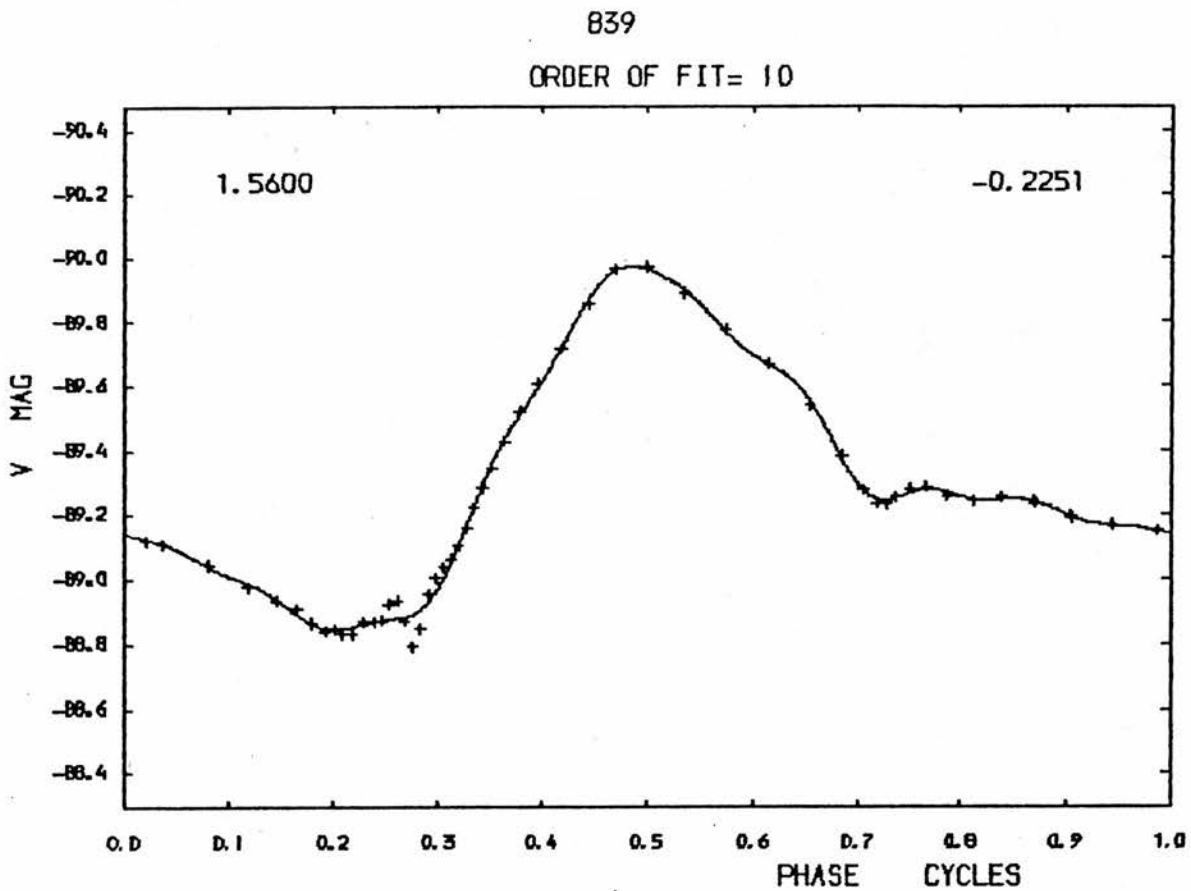

Fig. A3.7: Light Curve for 745.

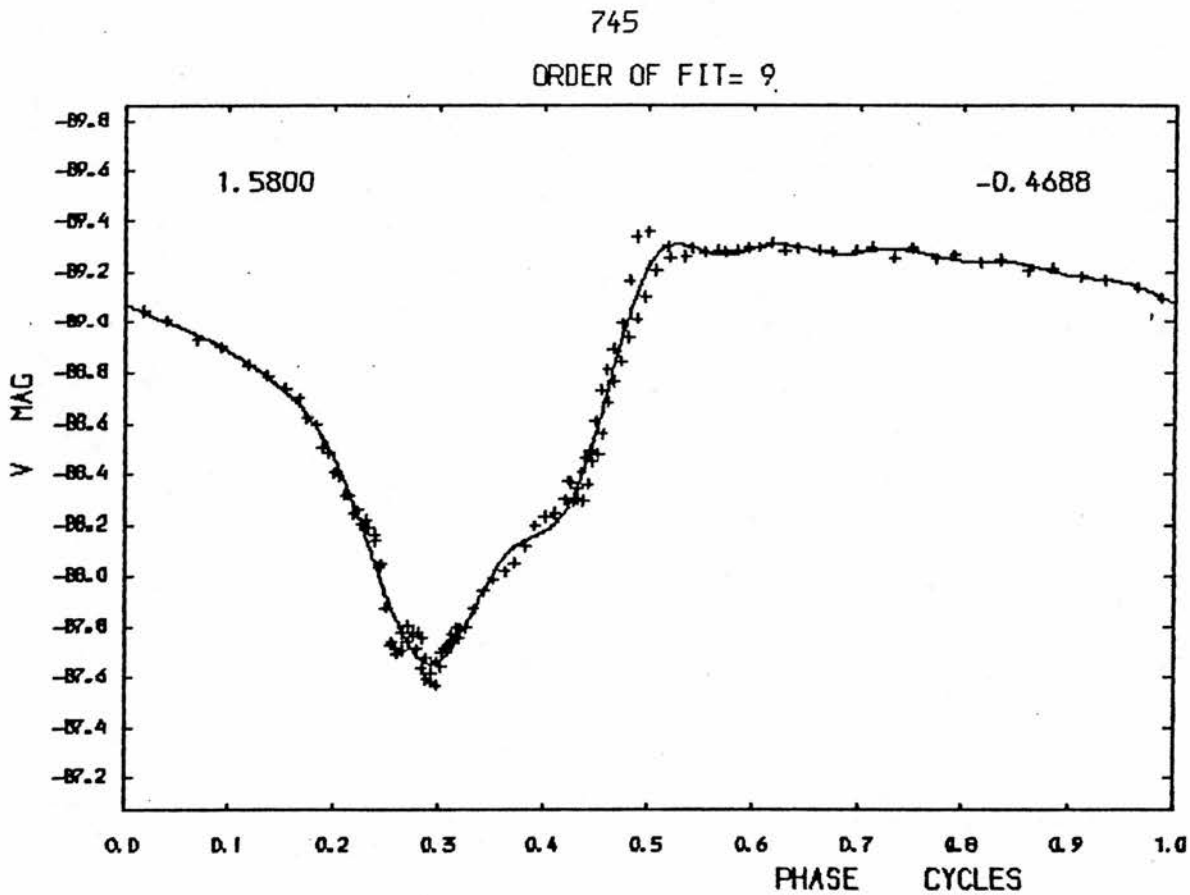

Fig. A3.8: Light Curve for NWL.

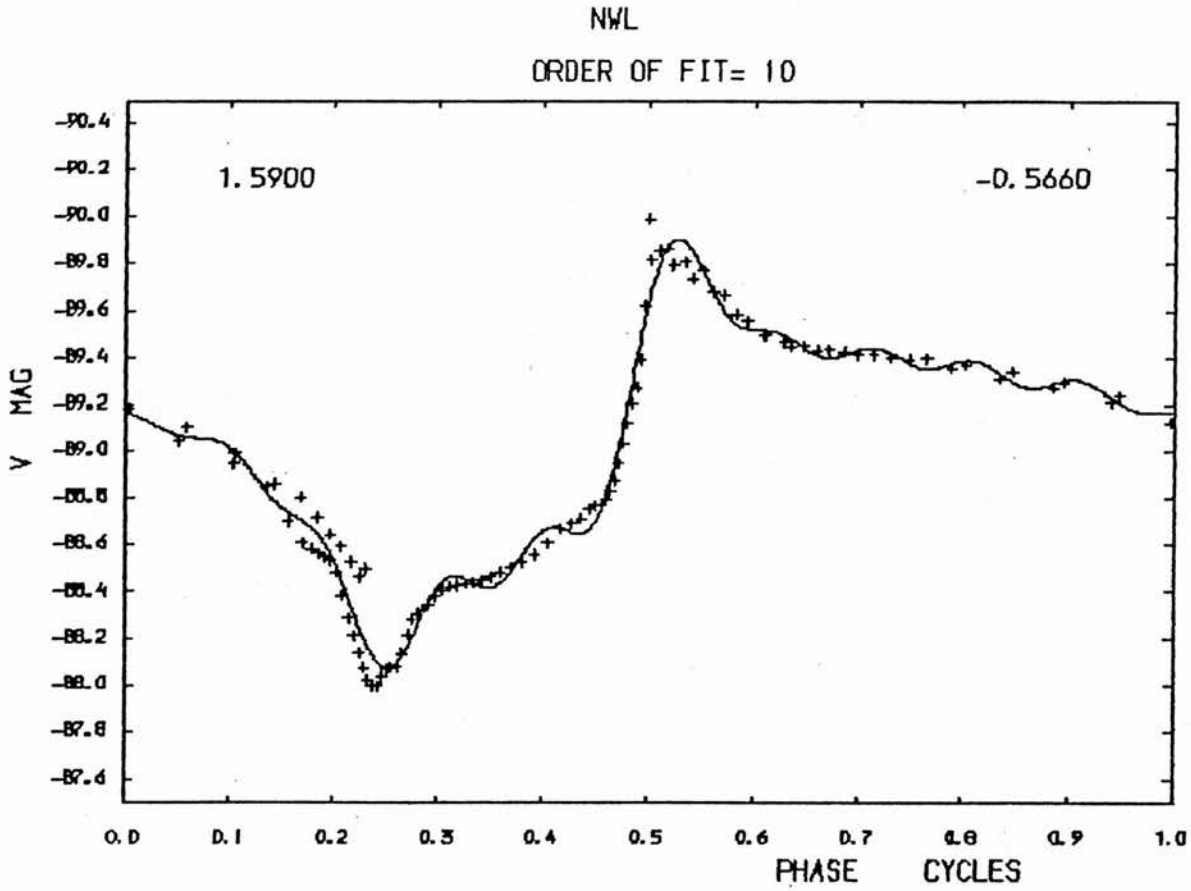

Fig. A3.9: Light Curve for VZA.

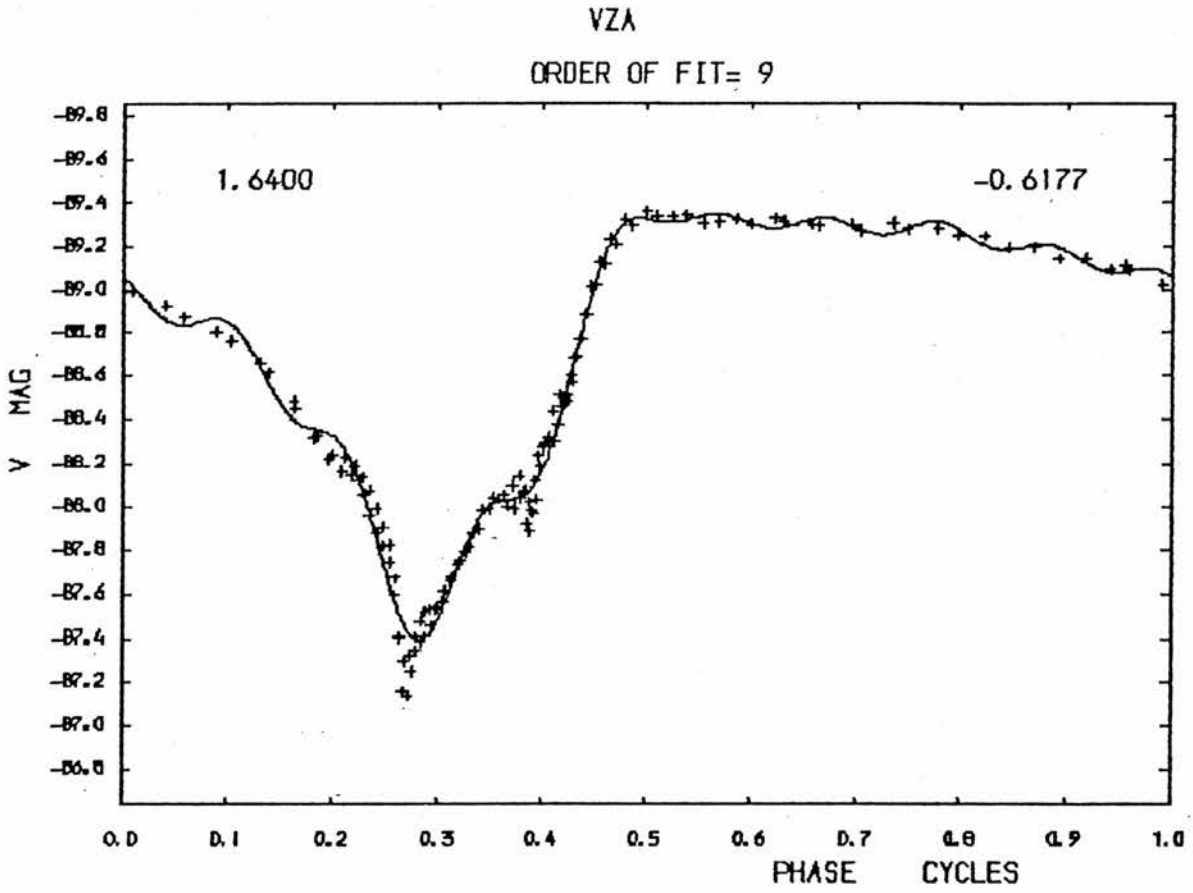

Fig. A3.10: Light Curve for UYE.

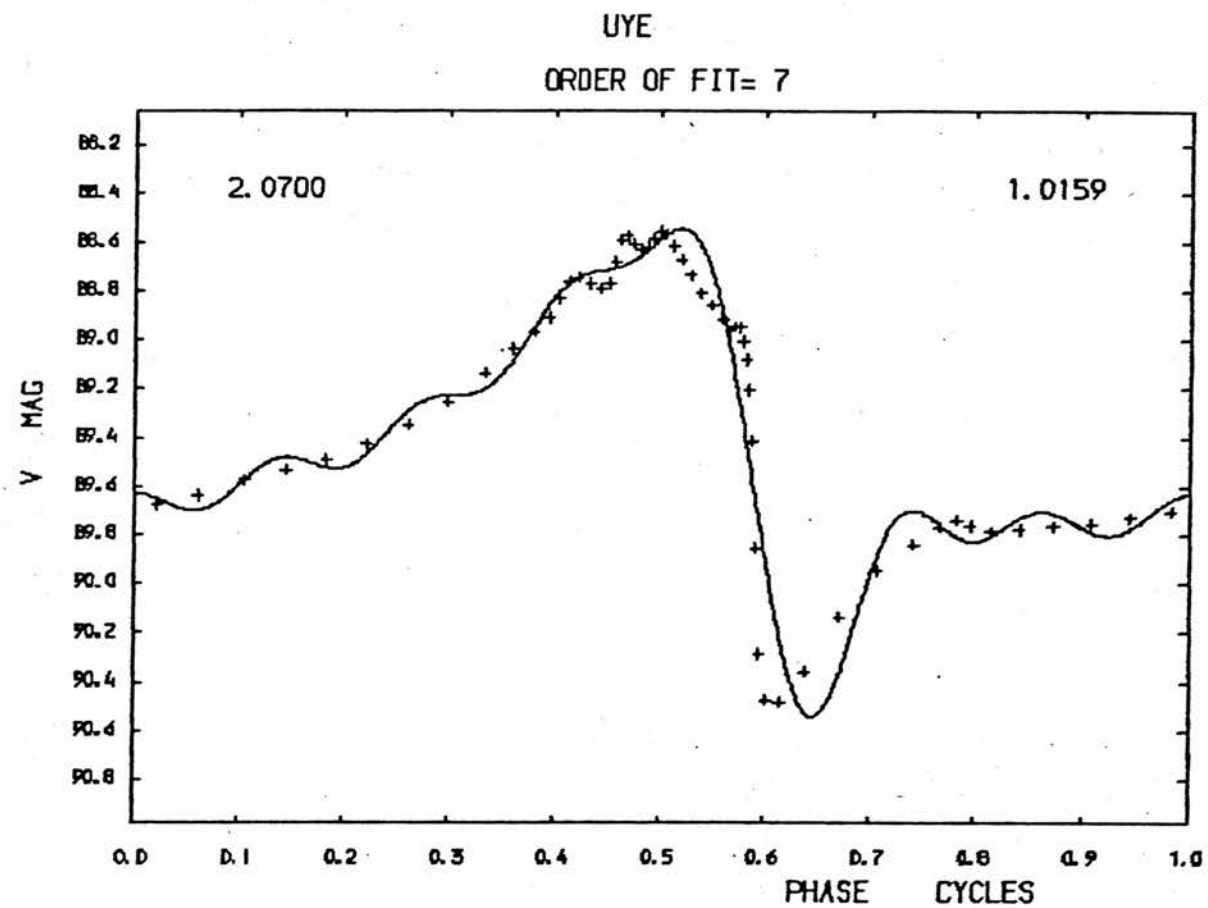

Fig. A3.11: Light Curve for YZC.

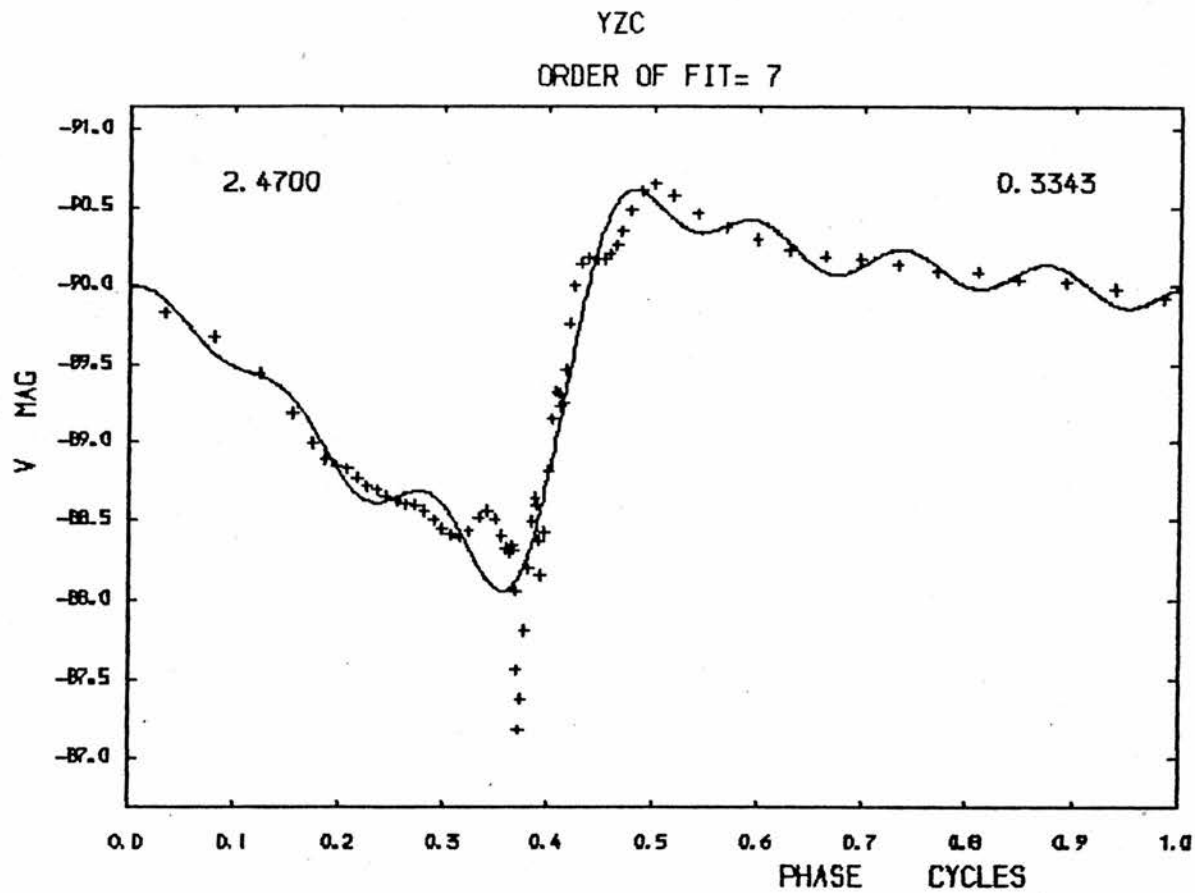

APPENDIX 4.

THE COMPUTER CODE.

This final appendix contains the computer code with which the author has Fourier analysed the data of KD and Carson and Stothers (1984a). The code has been explained fully in chapter 4 and further explanation is unnecessary.

```
C           A program which fits a Fourier series to an
C     array of data in the form of 'times' and 'magnitudes'.
C           It also computes periods of oscillation
C     or pulsation, using a power spectra or a Fouriergram
C           In this program, the following variables are
C     used :
C
C
C           G :    order of fit.
C           N :    rank of matrix (= 2G + 1)
C           I, I1, I1, I3 :    counting variables
C           T :    an array which contains the times of
C                  observations
C           F :    array containing the light data.
C           FC :   array containing the fit
C           P :    period
C           W :    angular frequency
C           PI :   3.1415926 (a double-precision number)
C           STAR : name of star ( 8 characters or less)
C           EPCH : epoch of observation
C           NOBS : number of observations
C           CEQ :  a character which holds the colour index
C           QW, QP, QF : character variables which contain
C                        the answer to a question
C           C :    array for errors in the solution of a
C                  set of simultaneous equations.
C           ERR :  standard deviation of fit
C           Z :    residuals F-FC
C           VMIN, VMAX :    minimum and maximum magnitudes
C                           in single precision
C           PHSE : phased data
C           PHI :  phase
C           AS :   amplitude
C           R1,j :  amplitude ratio A /A
C           PHI1,j :  phase difference
C           NF : number of frequency steps
C           FI, FF :  initial and final frequencies
C           DF :    frequency increment
C           FMEAN :  average magnitude
C           FTR, FTI :  real and imaginary parts of the
C                       Fourier transforms
C           ARG :    argument of above quantities
C           FREQ :   array of frequancies
C           PS :     power
C           EMIN, EMAX :  minimum and maximum errors in
C                         Fouriergram analysis
C
C
C           Declaration of Variables
C
      IMPLICIT REAL*8 (A-H,O-S,T-U,W-Z)
      IMPLICIT REAL*4 V
      CHARACTER STAR*32,QW*1,QN*1,CEQ(1)*12
      INTEGER ISTAR(8),ICEQ(1),G,XX
      DIMENSION T(1050),F(0:1050),FC(1050),A(50,50),B(50,50),
```

```
     *  E(1050)
        DIMENSION VPHSE(1050),R(50,50),AS(50),FHI(50),
     *  phic(50,50)
        DIMENSION VF1(1050),VFC1(1050),VPHSE1(1050),VF(1050)
        DIMENSION VFC(1050),C(50,50)
C
C               Input order of fit
C
        WRITE(6,10)
10      FORMAT(' ORDER OF FIT? ',$)
        READ(5,*)G
        N=2*G
        M=1
        I=0
        F(0)=0.0
        PRINT*,' '
C
C               Ask if pre-whitened data is to be computed and
C       analysed for periodicities.
C
        WRITE(6,20)
20      FORMAT(' Do you want to use pre-whitened data(y/n)? ',
     *  $)
22      READ(5,25)QW
25      FORMAT(A1)
        PRINT*,' '
        IF(QW.EQ.'Y'.OR.QW.EQ.'y')THEN
        PRINT*,' Input fundamental period '
        PRINT*,' '
        READ(5,*)P
        GOTO41
        ELSE IF(QW.NE.'N'.AND.QW.NE.'n')THEN
        PRINT*,' You must answer "y" or "n"'
        GOTO22
        ENDIF
C
C       Input Period
C
        WRITE(6,40)
40      FORMAT(' PERIOD? ',$)
        READ(5,*)P
41      PI=4.0*DATAN(1.D0)
        W=PI*2.D0/P
        PRINT*,' '
        WRITE(6,43)
43      FORMAT(' COLOUR INDEX (INPUT V,B-V OR U-B)? ',$)
44      READ(5,45)CEQ(1)
45      FORMAT(A12)
        IF(CEQ(1).NE.'V'.AND.CEQ(1).NE.'v'.AND.CEQ(1).NE.'B-V'.
     *  AND.CEQ(1)
     *  .NE.'b-v'.AND.CEQ(1).NE.'U-B'.AND.CEQ(1).NE.'u-b')THEN
        PRINT*,' You must answer "v", "b-v" or "u-b".'
        GOTO44
        ENDIF
        DECODE(12,46,CEQ)ICEQ(1)
```

```
111         46      FORMAT(3A4)
112                 PRINT*,' '
113         C               Read data from a file assigned to unit 4.
114         C       The data should contain the name of star; epoch; times
115         C       and magnitudes.
116         C
117                 WT=W
118                 READ(4,48)STAR
119         48      FORMAT(A32)
120                 DECODE(32,49,STAR)ISTAR
121         49      FORMAT(8A4)
122                 READ(4,*)EPCH
123                 T1=0.0
124                 I3=0
125                 NOBS=0
126                 DO50 I1=1,N+1
127                 DO50 I2=1,N+1
128                 A(I1,I2)=0.0
129                 B(I1,I2)=0.0
130         50      CONTINUE
131                 IF(CEQ(1).EQ.'V')GOTO70
132                 IF(CEQ(1).EQ.'B-V')GOTO60
133                 DO55 I=1,1050
134                 READ(4,*,END=80)T1,FV,FB,FU
135                 T(I)=T1-EPCH
136                 F(I)=FU
137                 VF(I)=F(I)
138         55      CONTINUE
139         60      DO65 I=1,1050
140                 READ(4,*,END=80)T1,FV,FB,FU
141                 T(I)=T1-EPCH
142                 F(I)=FB
143                 VF(I)=F(I)
144         65      CONTINUE
145         70      DO75 I=1,1050
146                 READ(4,*,END=80)T1,FV,FB,FU
147                 T(I)=T1-EPCH
148                 F(I)=FV
149                 VF(I)=F(I)
150         75      CONTINUE
151         80      NOBS=I-1
152         C
153         C               The coefficients of a Fourier series are
154         C       computed from a set of simultaneous equations.
155         C       COEFF computes the coefficients of these equations
156         C
157                 DO83 I3=1,NOBS
158                 CALL COEFF(T,F,N,G,I3,A,B,W,NOBS)
159         83      CONTINUE
160                 N=N+1
161         C
162         C               Solve simultaneous equations and return
163         C       coefficient of Fourier series to array A
164         C
165                 CALL SLINE(N,A,B,C)
```

```
C
C            Calculate a Fourier series using Foucalc
C
      CALL FOUCALC(ERR,N,G,NOBS,A,C,T,F,FC,Z,W)
      XX=7
87    WRITE(6,90)
90    FORMAT(' Do you want results from foufit printed at
     * terminal?',$)
      READ(5,95)QN
95    FORMAT(A1)
      IF(QN.EQ.'Y'.OR.QN.EQ.'y')THEN
      XX=XX-1
      GOTO97
      ELSE IF(QN.NE.'n'.AND.QN.NE.'N')THEN
      PRINT*,'YOU MUST ANSWER "Y" OR "N"'
      GOTO87
      ENDIF
      OPEN(UNIT=XX,NAME='FOR007.DAT',STATUS='NEW')
      PRINT*,' Results saved in for007.dat.'
97    PRINT*,' '
      PRINT*,' '
C            Print results (either in a file assigned to
C     unit 7 or at terminal
C
      WRITE(XX,110)STAR,ERR,F,W
110   FORMAT(1X,A8//' STD.DEVIATION= ',G11.6/' PERIOD= ',
     * G11.6/
     C ' ANG.FREQ.= ',G11.6)
      WRITE(XX,112)A(1,N)
112   FORMAT(//21X,'A0'/12X,G18.6/)
      DO120 I=1,G
      WRITE(XX,115)I,I
115   FORMAT(9X,'C',I2,18X,'S',I2)
      WRITE(XX,118)(A(1,2*I-1)),(A(1,2*I))
118   FORMAT(2(2X,G18.6)/)
      WRITE(XX,119)C(1,2*I2-1),C(1,2*I2)
119   FORMAT(' +/-',2(G18.6)//)
120   CONTINUE
      PRINT*,' '
      PRINT*,' '
      WRITE(XX,130)
130   FORMAT(11X,'I',11X,'F(I)',20X,'T')
      PRINT*,' '
      PRINT*,' '
      DO135 I=1,NOBS
      WRITE(XX,*)I,FC(I),T(I)
135   CONTINUE
      CALL COAMP(A,T,F,W,NOBS,G,XX)
C
C            Ask if a powerspectrum is required
C
      WRITE(6,137)
137   FORMAT(' Do you want to calculate the power spectra(y/n)
     * ?',$)
140   READ(5,145)QN
```

```
145     FORMAT(A1)
        PRINT*,' '
        IF(QN.EQ.'Y'.OR.QN.EQ.'y')GOTO146
        IF(QN.NE.'N'.AND.QN.NE.'n')THEN
        PRINT*,'You must answer "y" or "n".'
        GOTO140
        END IF
        GOTO150
C               Pre-whiten data at this stage if required
C
146     IF(QW.EQ.'Y'.OR.QW.EQ.'y')THEN
        DO147 I=1,NOBS
        F(I)=F(I)-FC(I)
        VF(I)=F(I)
147     CONTINUE
        ENDIF
        CALL POWSPEC(T,F,NOBS,N,PI,ISTAR)
C
C               Ask if a Fouriergram is required
C
150     WRITE(6,151)
151     FORMAT(' Do you want to calculate a fouriergram ',$)
152     READ(5,153)QF
153     FORMAT(A1)
        PRINT*,' '
        IF(QF.NE.'Y'.AND.QF.NE.'y'.AND.QF.NE.'N'.AND.QF.NE.'n')
     * THEN
        PRINT*,' You must answer y or n'
        GOTO152
        ELSE IF(QF.EQ.'N'.OR.QF.EQ.'n')THEN
        GOTO155
        ENDIF
C
C               If data hasn't been pre-whitened already, then
C       do so now
C
        IF((QP.EQ.'N'.OR.QP.EQ.'n').AND.(QW.EQ.'Y'.OR.QW.EQ.'y')
     * )THEN
        DO154 I=1,NOBS
        F(I)=F(I)-FC(I)
        VF(I)=F(I)
154     CONTINUE
        ENDIF
        CALL FOUGRAM(PI,ISTAR,T,F,N,M,G,NOBS)
        W=WT
C               Set up limits of axes in graphics routines and
C       phase the data
C
155     VMIN=VF(1)
        VMAX=VF(1)
        DO156 I=1,NOBS
        VMIN=AMIN1(VMIN,VF(I))
        VMAX=AMAX1(VMAX,VF(I))
        NP=T(I)/P
        DNP=NP
```

```
276                 VPHSE(I)=T(I)-DNP*P
277                 VFHSE(I)=VPHSE(I)/P
278           C             Centre the data with maximum light at phase 0.5
279           C
280                 IF(VMIN.EQ.VF(I))THEN
281                 VFHSMAX=VPHSE(I)-0.5
282                 VPHMAX=VPHSE(I)
283                 ENDIF
284                 VAV=VAV+VF(I)
285           156   CONTINUE
286                 VAV=VAV/NOBS
287                 DO157 I=1,NOBS
288                 VPHSE(I)=VPHSE(I)-VPHSMAX
289                 IF(VPHSE(I).LT.0.0)THEN
290                 VPHSE(I)=VPHSE(I)+1.0
291                 ELSE IF(VPHSE(I).GT.1.0)THEN
292                 VPHSE(I)=VPHSE(I)-1.0
293                 ENDIF
294           157   CONTINUE
295                 ADD=0.2
296                 IF(ABS(VMIN).LT.0.1)THEN
297                 ADD=0.02
298                 ELSE IF(ABS(VMIN).GT.80.0)THEN
299                 ADD=ADD+0.6
300                 ENDIF
301                 VMIN=VMIN-ADD
302                 VMAX=VMAX+ADD
303           C
304           C             Erase all output on the screen and select a
305           C       piece of graph paper
306           C
307                 CALL ERASE
308                 CALL PAPER(1)
309           C
310           C             Set up physical space according to size of
311           C       screen and mathememetical space onto which axes are
312           C       plotted
313           C
314                 CALL PSPACE(0.16,1.31,0.1,0.890)
315                 CALL MAP(0.0,1.0,VMAX,VMIN)
316                 CALL BORDER
317                 CALL SCALES
318           C
319           C             Alter space to allow titles and labels to be
320           C       plotted
321           C
322                 CALL PSPACE(0.05,1.31,0.02,1.0)
323                 CALL MAP(0.05,1.31,0.02,1.0)
324                 CALL CTRMAG(21)
325                 CALL CTRORI(90.0)
326                 CALL PCSCEN(0.05,0.51,ICEQ,4)
327                 CALL TCSCEN(' MAG',4)
328                 CALL CTRORI(0.0)
329                 CALL PCSCEN(1.0125,0.0205,'PHASE    CYCLES)',15)
330                 CALL PCSCEN(0.70,0.98,ISTAR,8)
```

```
331             CALL PCSCEN(0.73,0.92,'ORDER OF FIT=',14)
332             CALL TYPENI(G)
333             EPCH=(VPHMAX-0.5)*P
334             CALL POSITN(0.25,0.8)
335             CALL TYPENF(P,4)
336             CALL POSITN(1.1,0.8)
337             CALL TYPENF(EPCH,4)
338             CALL CTRMAG(18)
339             CALL PSPACE(0.16,1.31,0.1,0.89)
340             CALL MAP(0.0,1.0,VMAX,VMIN)
341             CALL POSITN(VPHSE(1),VF(1))
342       C
343       C             Plot characters at (VPHSE(I),VF(I) )
344       C
345             DO161 I=1,NOBS
346             CALL PLOTNC(VPHSE(I),VF(I),232)
347       161   CONTINUE
348       C
349       C             Draw a line through the points just plotted.
350       C     This will be the fit.
351       C
352             NOBS=1000
353             DO165 I=1,NOBS
354             VPHSE(I)=I*0.001
355             T(I)=VPHSE(I)*P
356             FC(I)=0.0
357       165   CONTINUE
358             Z=0.0
359             CALL FOUCALC(ERR,N,G,NOBS,A,C,T,F,FC,Z,W)
360             FCMIN=FC(1)
361             FCMAX=FC(1)
362             DO170 I=1,NOBS
363             VFC(I)=FC(I)
364             VPHSE(I)=VPHSE(I)-VPHSMAX
365             IF(VPHSE(I).LT.0.0)THEN
366             VPHSE(I)=VPHSE(I)+1.0
367             ELSE IF(VPHSE(I).GT.1.0)THEN
368             VPHSE(I)=VPHSE(I)-1.0
369             ENDIF
370             FCMAX=DMAX1(FC(I),FCMAX)
371             FCMIN=DMIN1(FC(I),FCMIN)
372             IF(FCMIN.EQ.FC(I))THEN
373             PHSEMIN=VPHSE(I)
374             ELSE IF(FCMAX.EQ.FC(I))THEN
375             PHSEMAX=VPHSE(I)
376             ENDIF
377       170   CONTINUE
378             AMP=ABS(FCMAX-FCMIN)
379             ASYMM=(PHSEMAX-PHSEMIN)/(1-PHSEMAX+PHSEMIN)
380             CALL POSITN(VPHSE(1),VFC(1))
381             DO175 I=1,NOBS
382             K=I
383             J=I
384             IF(VPHSE(J).GT.VPHSE(J+1))THEN
385             J=J+1
```

```
386                CALL POSITN(VPHSE(J),VFC(J))
387                ENDIF
388                CALL JOIN(VPHSE(I),VFC(I))
389          175   CONTINUE
390                CALL JOIN(VPHSE(J+1),VFC(J+1))
391          185   CALL GREND
392                CALL FRAME
393                WRITE(XX,190)AMP,FCMAX,FCMIN,ASYMM,VAV
394          190   FORMAT(1x,'Amplitude= ',g18.6/1x,'Maximum= ',g18.6/1x,
395               * 'Minimum= ',g18.6/1x,
396               * 'Asymmetry= ',g18.6/1x,
397               * 'Mean Light= ',g18.6)
398                STOP
399                END
400          C
401          C              Subroutine to compute coefficints of
402          C       simultaneous equations developed from a least squares
403          C       solution to the coefficients of a Fourier series
404          C
405                SUBROUTINE COEFF(T,F,N,G,I3,A,B,W,NOBS)
406                IMPLICIT REAL*8 (A-F,O-R,T-Z)
407                DIMENSION A(50,50),B(50,50),P(50,50),Q(50,50),T(1050),
408               * F(0:1050)
409                INTEGER G,H
410                DO50 I2=1,N
411                I1=1
412                DO50 J=1,G
413                DJ=J
414                P(I1,I2)=DCOS(DJ*W*T(I3))
415                Q(I1+1,I2)=DSIN(DJ*W*T(I3))
416                I1=I1+2
417          50    CONTINUE
418                S=0.0
419                DO55 H=1,N,2
420                I1=1
421                S=S+1.0
422                I2=H
423                DO54 J=1,N,2
424                A(I1,I2)=P(J,H)*DCOS(S*W*T(I3))+A(J,H)
425                A(I1+1,I2)=Q(J+1,H)*DCOS(S*W*T(I3))+A(J+1,H)
426                I1=I1+2
427          54    CONTINUE
428                B(I2,1)=F(I3)*DCOS(S*W*T(I3))+B(H,1)
429                A(N+1,I2)=DCOS(S*W*T(I3))+A(N+1,H)
430                A(I2,N+1)=A(N+1,I2)
431          55    CONTINUE
432                S=0.0
433                DO63 H=2,N,2
434                I2=H
435                I1=1
436                S=S+1.0
437                DO62 J=1,N,2
438                A(I1,I2)=P(J,H)*DSIN(S*W*T(I3))+A(J,H)
439                A(I1+1,I2)=Q(J+1,H)*DSIN(S*W*T(I3))+A(J+1,H)
440                I1=I1+2
```

```
441         62      CONTINUE
442                 B(I2,1)=F(I3)*DSIN(S*W*T(I3))+B(H,1)
443                 A(N+1,I2)=DSIN(S*W*T(I3))+A(N+1,H)
444                 A(I2,N+1)=A(N+1,I2)
445         63      CONTINUE
446                 B(N+1,1)=F(I3)+B(N+1,1)
447                 DNOBS=NOBS
448                 A(N+1,N+1)=NOBS
449                 RETURN
450                 END
451         C
452         C               Subroutine which solves the set of equalions
453         C       computed above. The solutions ar contained in the first
454         C       column in array A
455         C
456                 SUBROUTINE SLINE(N,A,B,C)
457                 IMPLICIT REAL*8 (A-F,O-U,W-Z)
458                 DIMENSION D(50,50),A(50,50),B(50,50),C(50,50)
459                 DO30 J=1,N
460                 DO20 I=1,N
461                 IF(I.EQ.J)GOTO20
462                 C(I,J)=-A(I,J)/A(J,J)
463                 DO20 K=1,N
464                 IF(K.EQ.J)THEN
465                 C(K,I)=A(K,I)/A(J,J)
466                 GOTO20
467                 ENDIF
468                 C(I,K)=A(I,K)-A(J,K)*A(I,J)/A(J,J)
469         20      CONTINUE
470                 C(J,J)=1/A(J,J)
471                 DO30 I=1,N
472                 DO30 K=1,N
473                 A(I,K)=C(I,K)
474                 D(I,K)=0.0
475         30      CONTINUE
476                 DO40 J=1,N
477                 DO40 I=1,N
478                 D(1,J)=B(I,1)*A(I,J)+D(1,J)
479         40      CONTINUE
480                 DO50 J=1,N
481                 A(1,J)=D(1,J)
482         50      CONTINUE
483                 END
484         C
485         C               Compute a Fourier series
486         C
487                 SUBROUTINE FOUCALC(ERR,N,G,NOBS,A,C,T,F,FC,Z,W)
488                 IMPLICIT REAL*8 (A-F,O-R,T-Z)
489                 INTEGER G,H,S
490                 DIMENSION A(50,50),B(50,50),T(1050),FC(1050),F(0:1050)
491                 DIMENSION E(1050),C(50,50),DC(50,50)
492                 ERROR=0.D0
493                 DO100 I3=1,NOBS
494         C
495         C               The series is computed in this loop for the
```

```
C       time T and frequency W
C
        DO90 I2=1,G
        DI2=I2
        FC(I3)=FC(I3)+A(1,2*I2-1)*DCOS(DI2*W*T(I3))+A(1,2*I2)*
     *  DSIN(DI2*W*T(I3))
90      CONTINUE
C
C               Add on the time-average mag. (m)
C
        FC(I3)=A(1,N)+FC(I3)
C
C               Compute the residuals Z and the standard
C       deviation between observations and fit
C
        Z=FC(I3)-F(I3)
        E(I3)=Z**2
        ERROR=E(I3)+ERROR
100     CONTINUE
        ERR=DSQRT(ERROR/(NOBS-N))
C
C               Compute error in coefficients of series ( C(I)
C       is the inverse of the matrix A computed in COEFF)
C
        DO110 I=1,N
        C(1,I)=DSQRT(C(I,I))*ERR
110     CONTINUE
        RETURN
        END
C
C               Compute phases PHI and amplitudes AS of series
C       Also, compute quantities Rii and PHIii, for i=1,2
C
        SUBROUTINE COAMP(A,T,F,W,NOBS,G,XX)
        IMPLICIT REAL*8 (A-F,O-R,T-Z)
        DIMENSION T(1050),F(0:1050),A(50,50),PHI(50),AC(50)
        DIMENSION AS(50),R(50,50),FC(50),FS(50),C(50,50)
        INTEGER G,H
        N=2*G
        PI=4.D0*DATAN(1.D0)
        DO10 I2=1,G
        X=A(1,2*I2)
        Y=A(1,2*I2-1)
        PHI(I2)=DATAN(-A(1,I2*2)/A(1,2*I2-1))
        AS(I2)=DSQRT(X**2+Y**2)
        PHIS=-X/DSQRT(X**2+Y**2)
        PHIC=Y/DSQRT(X**2+Y**2)
        IF(DTAN(PHI(I2)).GT.0.0.AND.PHIS.LT.0.0)THEN
        PHI(I2)=PHI(I2)+PI
        ELSE IF(PHIS.GT.0.0.AND.DTAN(PHI(I2)).LT.0.0)THEN
        PHI(I2)=PHI(I2)+PI
        ENDIF
        D=((Y*C(1,2*I2))**2.0+(X*C(1,2*I2))**2.0)/((X**2.0
     *  +Y**2.0)**2.0)
        D=DSQRT(D)
```

```
551                 Y1=Y**2.0
552                 X1=X**2.0
553                 C(1,2*I2-1)=DSQRT(((X*C(1,2*I2))**2.0+(Y*C(1,2*I2-1))
554               * **2.0)/(X1+Y1))
555                 C(1,2*I2)=D
556           10    CONTINUE
557                 R12=AS(2)/AS(1)
558                 PHI12=PHI(2)-2*PHI(1)
559                 R13=AS(3)/AS(1)
560                 PHI13=PHI(3)-3*PHI(1)
561                 PRINT*,' '
562                 PRINT*,' '
563                 DR21=DSQRT((C(1,3)/AS(1))**2.0+(C(1,1)*AS(2)/
564               * (AS(1)**2.0))**2.0)
565                 DR31=DSQRT((C(1,5)/AS(1))**2.0+(C(1,1)*AS(3)/
566               * (AS(1)**2.0)**2.0))
567                 DPHI21=DSQRT(4.0*C(1,2)**2.0+C(1,4)**2.0)
568                 DPHI31=DSQRT(9.0*C(1,2)**2.0+C(1,6)**2.0)
569                 DO80 I2=1,G
570                 WRITE(XX,50)I2,I2
571           50    FORMAT(10X,'A',I1,19X,'PHI',I1)
572                 WRITE(XX,55)AS(I2),PHI(I2)
573           55    FORMAT(2(3X,G18.6)/)
574                 WRITE(XX,83)C(1,2*I2-1),C(1,2*I2)
575           83    FORMAT(' +/-',2(G18.6)//)
576           80    CONTINUE
577                 WRITE(XX,85)R21,PHI21,DR21,DPHI21
578           85    FORMAT(2(G18.6)/,' +/-',2(G18.6))
579                 WRITE(XX,86)R31,PHI31,DR31,DPHI31
580           86    FORMAT(2(G18.6)/,' +/-',2(G18.6))
581                 RETURN
582                 END
583           C
584           C           Compute a power-spectrum from the Fourier
585           C     transform F_i = Sum { f(t_i)exp[ i2*vt_i ]}
586           C
587                 SUBROUTINE POWSPEC(T,F,NOBS,N,PI,ISTAR)
588                 IMPLICIT REAL*8 (A-F,O-Q,T-U,W-Z)
589                 INTEGER ISTAR(8)
590                 CHARACTER*1 PSR,PSG
591                 DIMENSION VPS(0:10000),PS(0:10000),VFREQ(10000)
592                 DIMENSION FREQ(10000),T(1050),F(0:1050),FA(1050)
593                 REAL*4 V
594           C
595           C           Compute a transform for the range of
596           C     frequencies FI to FF, incremented by DF
597           C           Maximum number of frequency steps is 10000
598           C
599                 WRITE(6,10)
600           10    FORMAT(' INPUT FREQ.INTERVAL',$)
601                 READ*,DF
602                 WRITE(6,20)
603           20    FORMAT(' INITIAL AND FINAL FREQ.',$)
604                 READ*,FI,FF
605                 NF=(FF-FI)/DF
```

```
606                 DO25 K=1,NOBS
607                 FSUM=FSUM+F(K)
608           25    CONTINUE
609                 AVF=FSUM/(NOBS)
610                 DO40 I=1,NF+2
611                 FTR=0.0
612                 FTI=0.0
613                 FREQ(I)=(I-1)*DF+FI
614                 ARG1=2.0*PI*FREQ(I)
615                 DO30 K=1,NOBS
616                 ARG=ARG1*T(K)
617                 FA(K)=F(K)-AVF
618                 FTR=FTR+FA(K)*DCOS(ARG)
619                 FTI=FTI+FA(K)*DSIN(ARG)
620           30    CONTINUE
621           C
622           C           Calculate power, given by ( Re(F_i) + Im(F_i) )
623           C     Also, normalise power
624           C
625                 PS(I)=(FTR**2+FTI**2)/((NOBS)**2)
626                 VPS(I)=PS(I)
627                 VFREQ(I)=FREQ(I)
628           40    CONTINUE
629                 XX=6
630                 PRINT*,'Do you want printout at terminal?'
631           42    READ(5,44)PSR
632           44    FORMAT(A1)
633                 IF(PSR.EQ.'N')THEN
634                 XX=XX+2
635                 PRINT*,'Data saved in for008'
636                 GOTO43
637                 ELSE IF(PSR.NE.'Y'.AND.PSR.NE.'N')THEN
638                 PRINT*,'You must answer y or n'
639                 GOTO42
640                 ENDIF
641           43    DO45 J=1,NF+2
642                 WRITE(XX,*)PS(J),FREQ(J)
643           45    CONTINUE
644                 PMIN=PS(1)
645                 PMAX=PS(1)
646                 DO50 I=1,NF+2
647                 PMAX=DMAX1(PMAX,PS(I))
648                 PMIN=DMIN1(PMIN,PS(I))
649           50    CONTINUE
650                 VPMIN=PMIN
651                 VPMAX=PMAX
652                 PRINT*,'Do you want to plot power spectra?'
653                 READ(5,55)PSG
654           55    FORMAT(A1)
655                 IF(PSG.EQ.'N')THEN
656                 GOTO70
657                 ENDIF
658           C
659           C           Plot power spectrum if required
660           C
```

```
661                 CALL PAPER(1)
662                 CALL PSPACE(0.16,1.31,0.1,0.92)
663                 CALL MAP(VFREQ(1),VFREQ(NF+2),VPMIN,VPMAX)
664                 CALL BORDER
665                 CALL SCALES
666                 CALL PSPACE(0.05,1.31,0.02,1.0)
667                 CALL MAP(0.05,1.31,0.02,1.0)
668                 CALL CTRMAG(21)
669                 CALL PCSCEN(1.0125,0.027,'FREQ.    CYCLES/DAY',19)
670                 CALL CTRORI(90.0)
671                 CALL PCSCEN(0.05,0.51,'POWER',5)
672                 CALL CTRORI(0.0)
673                 CALL CTRMAG(25)
674                 CALL PCSCEN(0.73,0.95,'POWER SPECTRUM FOR          ',28)
675                 CALL TCSEND(ISTAR,8)
676                 CALL CTRMAG(10)
677                 CALL PSPACE(0.16,1.31,0.1,0.92)
678                 CALL MAP(VFREQ(1),VFREQ(NF+2),VPMIN,VPMAX)
679                 CALL POSITN(VFREQ(1),VPS(1))
680                 DO60 I=2,NF+2
681                 CALL JOIN(VFREQ(I),VPS(I))
682           60    CONTINUE
683                 CALL FRAME
684                 CALL GREND
685           70    RETURN
686                 END
687           C
688           C               Compute a Fouriergram
689           C
690                 SUBROUTINE FOUGRAM(PI,ISTAR,T,F,N,M,G,NOBS)
691                 IMPLICIT REAL*8 (A-F,O-R,T-U,W-Z)
692                 INTEGER G,H,S
693                 REAL*4 V
694                 DIMENSION FREQ(1001),ERROR(1001),VFREQ(1001),VERR(1001)
695                 DIMENSION C(50,50),FC(1050),A(50,50),T(1050),F(0:1050)
696                 DIMENSION B(50,50)
697                 N=N-1
698           C
699           C               Compute a Fourier series for each frequency
700           C     in the range FI to FF, incremented by DF
701           C               Maximum number of frequency steps is 1000
702           C
703                 WRITE(6,35)
704           35    FORMAT(' FREQ.INTERVAL? ',$)
705                 READ(5,*)DF
706                 WRITE(6,40)
707           40    FORMAT(' INITIAL AND FINAL FREQ.? ',$)
708                 READ(5,*)FI,FF
709                 NF=(FF-FI)/DF
710                 DO120 I=1,NF+2
711                 FREQ(I)=(I-1)*DF+FI
712                 W=2.DO*FREQ(I)*PI
713                 ERR=0.DO
714                 Z=0.DO
715                 ERROR(I)=0.DO
```

```
716                 DO50 I1=1,50
717                 DO50 J1=1,50
718                 A(I1,J1)=0.D0
719                 B(I1,J1)=0.D0
720                 C(I1,J1)=0.D0
721           50    CONTINUE
722           C
723           C           Compute a Fourier series and it's standard
724           C     deviation
725           C
726                 DO60 I3=1,NOBS
727                 CALL COEFF(T,F,N,G,I3,A,B,W,NOBS)
728                 FC(I3)=0.D0
729           60    CONTINUE
730                 N=N+1
731                 CALL SLINE(N,A,B)
732                 CALL FOUCALC(ERR,N,G,NOBS,A,T,F,FC,Z,W)
733                 ERROR(I)=ERR
734                 WRITE(6,*)ERROR(I),1.D0/FREQ(I),FREQ(I)
735                 N=N-1
736           120   CONTINUE
737                 EMAX=ERROR(1)
738                 EMIN=ERROR(1)
739                 DO130 I=1,NF+2
740                 EMIN=DMIN1(EMIN,ERROR(I))
741                 EMAX=DMAX1(EMAX,ERROR(I))
742                 VERR(I)=ERROR(I)
743                 VFREQ(I)=FREQ(I)
744                 IF(ERROR(I).EQ.EMIN)THEN
745                 FMIN=FREQ(I)
746                 ENDIF
747           130   CONTINUE
748                 VEMIN=EMIN
749                 VEMAX=EMAX
750           C
751           C           Plot a Fouriergram of standard deviation
752           C     against error
753           C
754                 CALL PAPER(1)
755                 CALL PSPACE(0.16,1.3,0.1,0.9)
756                 CALL MAP(VFREQ(1),VFREQ(NF+2),VEMIN,VEMAX)
757                 CALL BORDER
758                 CALL SCALES
759                 CALL PSPACE(0.05,1.31,0.02,1.0)
760                 CALL MAP(0.05,1.31,0.02,1.0)
761                 CALL CTRORI(90.0)
762                 CALL CTRMAG(21)
763                 CALL PCSCEN(0.05,0.51,'ERROR',5)
764                 CALL CTRORI(0.0)
765                 CALL PCSCEN(1.0125,0.025,'FREQ.    CYCLES/DAY',19)
766                 CALL POSITN(0.545,0.98)
767                 CALL TYPENI(G)
768                 IF(G.EQ.1)THEN
769                 CALL TYPECS('ST ORDER FOURIERGRAM',20)
```

```
770                 ELSE IF(G.EQ.2)THEN
771                 CALL TYPECS('ND ORDER FOURIERGRAM',20)
772                 ELSE IF(G.EQ.3)THEN
773                 CALL TYPECS('RD ORDER FOURIERGRAM',20)
774                 ELSE IF(G.GE.4)THEN
775                 CALL TYPECS('TH ORDER FOURIERGRAM',20)
776                 ENDIF
777                 CALL POSITN(0.81,0.92)
778                 CALL TCSEND(ISTAR,8)
779                 CALL PSPACE(0.16,1.3,0.1,0.9)
780                 CALL MAP(VFREQ(1),VFREQ(NF+2),VEMIN,VEMAX)
781                 CALL CTRMAG(10)
782                 CALL POSITN(VFREQ(1),VERR(1))
783                 DO140 I=2,NF+2
784                 CALL JOIN(VFREQ(I),VERR(I))
785         140     CONTINUE
786                 CALL FRAME
787                 CALL GREND
788                 N=N+1
789                 RETURN
790                 END
```